

# IDŐJÁRÁS

QUARTERLY JOURNAL  
OF THE HUNGARIAN METEOROLOGICAL SERVICE

## CONTENTS

<i>Ádám Leelőssy, István Lagzi, and Róbert Mészáros: Spatial and temporal pattern of pollutants dispersed in the atmosphere from the Budapest Chemical Works industrial site .....</i>	101
<i>Katarzyna Piotrowicz, Dominika Ciaranek, and Izabela Guzik: Short-term variations in air temperature in Krakow (Poland) as an indicator of climate change in Central Europe .....</i>	117
<i>Helga Tóth, Brigitta Brajnovits, and Balázs Renczes: Statistical correction of the wind energy forecast at the Hungarian Meteorological Service .....</i>	137
<i>Tamás Illy: Near-surface wind speed changes in the 21st century based on the results of ALADIN-Climate regional climate model.....</i>	161
<i>Zoltán Tóth, Zoltán Nagy, and Balázs Szintai: Verification of global radiation fluxes forecasted by numerical weather prediction model AROME for Hungary .....</i>	189

# IDŐJÁRÁS

*Quarterly Journal of the Hungarian Meteorological Service*

*Editor-in-Chief*  
**LÁSZLÓ BOZÓ**

*Executive Editor*  
**MÁRTA T. PUSKÁS**

## EDITORIAL BOARD

- |                                       |  |
|---------------------------------------|--|
| ANTAL, E. (Budapest, Hungary)         | MIKA, J. (Eger, Hungary)                   |
| BARTHOLY, J. (Budapest, Hungary)      | MERSICH, I. (Budapest, Hungary)            |
| BATCHVAROVA, E. (Sofia, Bulgaria)     | MÖLLER, D. (Berlin, Germany)               |
| BRIMBLECOMBE, P. (Hong Kong, SAR)     | PINTO, J. (Res. Triangle Park, NC, U.S.A.) |
| CZELNAI, R. (Dörgicse, Hungary)       | PRÁGER, T. (Budapest, Hungary)             |
| DUNKEL, Z. (Budapest, Hungary)        | PROBÁLD, F. (Budapest, Hungary)            |
| FERENCZI, Z. (Budapest, Hungary)      | RADNÓTI, G. (Reading, U.K.)                |
| GERESDI, I. (Pécs, Hungary)           | S. BURÁNSZKI, M. (Budapest, Hungary)       |
| HASZPRA, L. (Budapest, Hungary)       | SZALAI, S. (Budapest, Hungary)             |
| HORVÁTH, Á. (Siófok, Hungary)         | SZEIDL, L. (Budapest, Hungary)             |
| HORVÁTH, L. (Budapest, Hungary)       | SZUNYOGH, I. (College Station, TX, U.S.A.) |
| HUNKÁR, M. (Keszthely, Hungary)       | TAR, K. (Debrecen, Hungary)                |
| LASZLO, I. (Camp Springs, MD, U.S.A.) | TÁNCZER, T. (Budapest, Hungary)            |
| MAJOR, G. (Budapest, Hungary)         | TOTH, Z. (Camp Springs, MD, U.S.A.)        |
| MÉSZÁROS, E. (Veszprém, Hungary)      | VALI, G. (Laramie, WY, U.S.A.)             |
| MÉSZÁROS, R. (Budapest, Hungary)      | WEIDINGER, T. (Budapest, Hungary)          |

*Editorial Office: Kitaibel P.u. 1, H-1024 Budapest, Hungary*  
*P.O. Box 38, H-1525 Budapest, Hungary*  
*E-mail: journal.idojaras@met.hu*  
*Fax: (36-1) 346-4669*

---

**Indexed and abstracted in Science Citation Index Expanded™ and  
Journal Citation Reports/Science Edition**

**Covered in the abstract and citation database SCOPUS®**

**Included in EBSCO's databases**

---

*Subscription by mail:*  
**IDŐJÁRÁS, P.O. Box 38, H-1525 Budapest, Hungary**  
*E-mail: journal.idojaras@met.hu*

## **Spatial and temporal pattern of pollutants dispersed in the atmosphere from the Budapest Chemical Works industrial site**

**Ádám Leelőssy<sup>1</sup>, István Lagzi<sup>2</sup>, and Róbert Mészáros<sup>1\*</sup>**

*<sup>1</sup>Eötvös Loránd University, Department of Meteorology,  
Pázmány Péter sétány 1/A, 1117 Budapest, Hungary*

*<sup>2</sup>Budapest University of Technology and Economics, Institute of Physics,  
Budafoki út 8, 1111 Budapest, Hungary*

*\*Corresponding author E-mail: mrobi@nimbus.elte.hu*

*(Manuscript received in final form July 25, 2016)*

**Abstract**— In April 2015, a serious industrial pollution gained large public interest in Budapest, the capital city of Hungary. An abandoned industrial site of the former Budapest Chemical Works company was found to contain 2000–3000 tonnes of leaking industrial waste and dangerous chemicals. As the former factory is located in a densely populated urban environment, serious public health concerns have risen. The pollution has been transported for several years from the industrial site to the neighboring areas by two ways: with groundwater transport and in the atmosphere.

This study attempts to estimate the main characteristics of atmospheric transport of pollutants originating from the Budapest Chemical Works site. The 13-year long dispersion pattern is investigated using a Gaussian dispersion model, taking into account the strong weather dependence of emission rates through deflation and evaporation. The very limited information of the amount, composition, and temporal evolution of the leaking chemicals makes it impossible to provide emission estimates; however, the spatial distribution and temporal characteristics of the pollution can be investigated.

Weather-dependent emission rate was found to be the dominant factor of the pollution, counteracted by the atmospheric stability. Largest concentrations were present in the spring and summer and during the day, while nighttime emissions were generally weak. The main direction of the dispersion was towards the south-east, however, deflating and evaporating materials showed largely different results.

*Key-words:* air pollution, industrial emission, Gaussian dispersion model

## 1. Introduction

On April 7, 2015, a short public visit was organized to the abandoned industrial site of the Budapest Chemical Works (Budapesti Vegyiművek) company in Budapest, Hungary. The visit revealed that a large amount of dangerous material was stored in leaked barrels in the open air, including carcinogenic pesticides, aromatic hydrocarbons, and isopropanol. As the company had gone bankrupt in 2007 with a confused ownership background, the responsibility has been subject of debates and a legal case. To avoid further pollution and a potential fire, authorities have decontaminated the site by January 2016 (Hevesi, 2016).

The site of the Budapest Chemical Works is located in the south-eastern part of Budapest, on a flat terrain covering an area of 0.15 km<sup>2</sup>. It is surrounded by warehouses, other factories, and a railyard from the northern and western directions (Fig. 1). The Danube river flows 1.6 km to the west. To the northeast, a residential area is located approximately 1 km away from the site with a busy road laying in between. To the southern and south-eastern directions, a densely populated residential area lies. The factory and the residential area is divided by an approximately 200 m wide wooded gap.

Due to the complex business and legal background, very few information has become available on the amount and chemical composition of the waste and the pollution in the nearby areas, as well as on the temporal period of the release. The company went bankrupt in 2007, however, an environmental inspection report had already warned of serious threats around the site in 2003 (Dura, 2003). Despite the early warning on potential threats, no measurements are known until 2015, when groundwater and dust analysis was performed by independent laboratories (Greenpeace, 2015; Wessling, 2015).



Fig. 1. The area of the Budapest Chemical Works (red shape) and DDT/DDD detections in soil and dust samples (red circles) (Greenpeace, 2015; Wessling, 2015). The industrial areas to the north and west are divided by a narrow band of vegetation from residential districts to the south-southeast. Background map © OpenStreetMap contributors, CC-BY-SA.

The largest environmental concern within the industrial site is clearly the groundwater pollution. Water samples were polluted above threshold with DDT (dichlorodiphenyltrichloroethane), PAHs (polycyclic aromatic hydrocarbons), benzene, and several other components (Wessling, 2015). However, groundwater pollution is localized to a small area ranging a few hundred meters around the site, and groundwater transport is directed towards the Danube river avoiding residential areas (Dura, 2003; Wessling, 2015). Chemical composition of soil and groundwater pollution in samples taken 600–800 m from the site (Fig. 1) suggested that DDT was rather transported in the atmosphere, and not by groundwater (Wessling, 2015).

Atmospheric transport of dust and gases is a great concern for residential areas. It can cover a distance of tens of kilometres, thus affecting several thousand people. Therefore, the investigation of atmospheric dispersion patterns is of key importance. As there was no direct release to the atmosphere, the emission occurred in two ways: by deflation of the polluted dust, and by the evaporation of liquid materials. The former is primarily responsible for the DDT pollution, and the latter is more important in case of aromatic hydrocarbons. Unfortunately, there is no data on the exact amount and chemical composition of the stored materials, and there is no further chance to retrieve this information as the site has been decontaminated. In the lack of any reliable information, no emission estimate is attempted; however, a sensitivity map can be produced using an atmospheric dispersion model to estimate the spatial distribution of the pollution taking into account the weather-dependent emission rate.

The aim of this study is to provide an estimate on the long-term spatial and temporal distribution of airborne pollution originating from the Budapest Chemical Works site. The concentration pattern is investigated as a combination of three factors: wind direction, atmospheric stability and emission rate. Two types of pollutants are differentiated: deflated dust and evaporated gases. Spatial distribution is given for both types, concerning the strongly different emission characteristics.

## ***2. Estimation of dust emission***

The major threat from the Budapest Chemical Works site affecting residential areas is the atmospheric transport of dust polluted with DDT. DDT is a pesticide that has been invented in 1948 to prevent insect-related diseases such as malaria and typhus. Despite its remarkable efficiency in disease control, DDT has been shown to have serious environmental effects due to its persistency and bioaccumulation. DDT also affects human health, interfering with the hormone system and causing neuropsychological dysfunction and adverse birth outcomes (Rogan and Chen, 2005; Beard, 2006). Furthermore, as it had been suspected for decades, the relation of DDT to breast cancer was finally proved in 2015 (Soto

and *Sonnenschein*, 2015). Hungary was one of the first countries to ban DDT in 1968. However, it is still detectable in the environment in a very low concentration. A recent survey found DDT and its decomposition products in 2 of 10 urban dust samples in the downtown of Budapest (*Simon*, 2012). A dust analysis survey around the Budapest Chemical Works site was conducted by Greenpeace on October 7, 2015. Although DDT was found only in 1 of 11 samples, its decomposition products, DDD (dichlorodiphenyldichloroethane) and DDE (dichlorodiphenyldichloroethylene) were present in 10 of 11 samples (*Greenpeace*, 2015) (*Fig. 1*). Other chemical tracers proved that the polluted dust originated from the Budapest Chemical Works site, supporting the assumption of a former study that the DDT detected in soil samples originated from dust and not from groundwater transport (*Greenpeace*, 2015; *Wessling*, 2015).

Dust flux from the uncovered ground to the atmosphere can be estimated based on the wind velocity and turbulence characteristics. A widely used approach is to estimate the  $Q$  dust emission flux as a cubic function of the  $U^*$  friction velocity (*Gillette*, 1978; *Tegen et al.*, 1997; *Takemura et al.*, 2000; *Uno et al.*, 2001; *Xuan*, 2004):

$$Q = a(U^* - U_T^*)U^{*2}, \quad (1)$$

where  $a$  is an empirical constant. If the friction velocity is below the  $U_T^*$  threshold friction velocity, no dust emission is assumed. The threshold friction velocity is dependent on the particle size and density. By an intercomparison of several parameterizations, the threshold friction velocity was found to be between approximately 0.2 and 0.8 m/s for soil dust particles between 10 and 1000  $\mu\text{m}$  (*Martcorena and Bergametti*, 1995). Smaller particles are more difficult to mobilize with threshold friction velocities reaching 2 m/s. The methods for dust flux estimation were mostly developed for large-scale emissions from deserts and bare soils. In an urban environment, strong microscale turbulence increases dust flux in two ways: (1) it decreases the effective threshold velocity, as turbulent fluctuations can locally generate significantly higher wind speeds than the mean wind; and (2) it increases the dust flux at any given wind speed with a more efficient turbulent upward transport of particles (*Xuan*, 2004). A correction factor proposed by *Xuan* (2004) was applied for the threshold friction velocity to incorporate this effect:

$$U_{T,corr}^* = \frac{U_T^*}{\sqrt{1 + 2\alpha \sqrt{\frac{\sigma_u^2}{U} + \alpha^2 \frac{\sigma_u^2}{U}}}}, \quad (2)$$

where  $U$  is the mean wind speed,  $\sigma_u$  is the standard deviation of the horizontal wind fluctuation, and  $\alpha$  is an empirical constant estimated as  $2.5 \text{ s}^{0.5}\text{m}^{-0.5}$  (Xuan, 2004).

Another important factor affecting dust emission flux is the moisture content of the surface. Most of the polluted dust laid in the area of the industrial site on solid surfaces, therefore, a conservative approach of rapidly drying dust was assumed, and dust emission flux was set to zero only during precipitation events and when snow covered the ground.

### 3. Estimation of evaporation

In the site of the Budapest Chemical Works, several hundred tons of organic solvents were stored in leaked containers. Vapor of isopropanol, benzene, and PAHs were released into the atmosphere, causing a characteristic odor in the neighboring area and posing a potential threat to human health. PAHs are carcinogenic organic compounds that are present in the atmosphere both in gaseous and aerosol form (Kim *et al.*, 2013). Unlike the rarely occurring DDT, both benzene and PAHs are frequent pollutants of the urban air, originating from fossil fuel burning. Although the lack of emission data and the large urban background pollution makes it impossible to provide concentration estimates, the temporal variation of the evaporation and, therefore, the spatial distribution of long-term pollution can be simulated. Assuming that the ambient air is far from saturation, the  $Q_E$  evaporation flux is estimated as the product of the saturation concentration, the  $U^*$  friction velocity, and a  $j$  mass transfer coefficient (Brighton, 1985). Using the Clausius–Clapeyron relation to obtain the saturation concentration, the following form yields:

$$Q_E = Aj \frac{U^*}{T} \exp\left(\frac{-L_m}{RT}\right), \quad (3)$$

where  $A$  is a material-dependent constant,  $T$  is the skin temperature of the fluid,  $L_m$  is the molar latent heat constant of vaporization, and  $R$  is the universal gas constant. In our study, the molar latent heat constant of benzene (34 kJ/mol) was applied and the skin temperature was approximated with the air temperature.

### 4. Atmospheric dispersion model

Over complex urban environment, the atmospheric dispersion can be best simulated with computational fluid dynamics (CFD) models. However, these models require huge computational cost depending on the applied grid type (Rákai *et al.*, 2014). Therefore, in this study, due to the huge number of model runs, the atmospheric dispersion was simulated in the 6 km vicinity of the site

with a Gaussian atmospheric dispersion model, a widely used approach in local scale long-term air pollution studies (*Cimorelli et al.*, 2005; *Holmes and Morawska*, 2006; *Leelőssy et al.*, 2011, 2014; *Mészáros et al.*, 2012). Concentration was assumed to follow a normal distribution in the crosswind and vertical directions, centered around the downwind axis from the source point. The axis of the plume was gradually elevated from the surface to the median height of the mixing layer. The mixing efficiency, i.e. the standard deviation of the normal distribution was estimated based on the Monin–Obukhov length,  $L$ :

$$L = \frac{TU^{*2}}{kgT^*}, \quad (4)$$

where  $g$  is the acceleration of gravity,  $k$  is the von Karman constant, and  $T^*$  is the dynamic temperature, calculated as:

$$T_{day}^* = \frac{-H}{\rho c_p U^*}, \quad (5)$$

$$T_{night}^* = 0.09(1 - 0.5n^2), \quad (6)$$

where  $H$  is the sensible heat flux,  $\rho$  is the density of air,  $c_p$  is the isobaric heat capacity of dry air and  $n$  is the fractional cloud cover (*Cimorelli et al.*, 2005). The friction velocity is obtained as a function of the Monin–Obukhov length:

$$U^* = \frac{kU}{\ln \frac{z_{ref}}{z_0} + \Psi_m \left( \frac{z_{ref}}{L} \right) + \Psi_m \left( \frac{z_0}{L} \right)}, \quad (7)$$

where  $z_{ref}$  is the wind measurement height,  $z_0$  is the surface roughness (in our study, 10 m and 2 m, respectively), and  $\Psi_m$  is the Monin–Obukhov universal function (*Foken*, 2006). Eqs. (4–7) were solved iteratively until convergence. Turbulent wind fluctuations and the consequent standard deviation of the normally distributed concentration field were calculated following the way described in *Cimorelli et al.* (2005).

Meteorological data were obtained from the nearby meteorological station of the Hungarian Meteorological Service at Budapest-Pestszentlőrinc, located 6 km to the southeast from the Budapest Chemical Works site. Hourly synoptic observations and 12–24 hourly radiosonde profiles were used to produce input data for the dispersion model in each hour of the 13-year long period between 2003 and 2015. Mixing layer height was assumed as the lowest altitude where virtual potential temperature exceeded the surface value (*Seidel et al.*, 2010). The temporal period was selected to cover the years from the first report of the pollution (*Dura*, 2003) until the decontamination (*Hevesi*, 2016). Although the emission might have started several years before 2003, the 13-year long period is assumed to be long enough to indicate general dispersion patterns. Missing

data (hours without synoptic observation or no radiosonde profile within 24 hours) occurred in 4.3% of the total period. After excluding missing data, dispersion results for 109,052 hours were evaluated to estimate the long-term load of the neighboring area. In each hour, plumes from 12 equally distributed point sources were superposed to represent the source area. Model results were evaluated on a rectangular grid with 100 m resolution. Without emission data, only the spatial distribution of the pollution can be examined through long-term sensitivity of receptor points. The surface sensitivity maps have been normalized to have a sum of one. Long-term average concentrations are assumed to be proportional to the given sensitivities.

## 5. Results

Dust emission was estimated at each hour from Eqs. (1)–(2), that show large sensitivity on the value of the  $U_T^*$  threshold friction velocity. In the main simulation run,  $U_T^*$  was conservatively set to 0.2 m/s. However, results have also been calculated with the more optimistic assumption of 0.8 m/s threshold friction velocity to obtain more focused information on the large wind speed (high dust emission) situations. For comparison, all dust results were normalized with the same value yielding a sum of one in the 13-year mean result of the main case. In the 13-year dataset, 19.6% of the observations provided friction velocities below 0.2 m/s and 15.6% above 0.8 m/s.

Dust sensitivity maps (*Fig. 2*) show a clear domination of dust transport towards the south-eastern direction. Although north-westerly wind is the dominant direction in Budapest (*Fig. 3a*), this result cannot be explained by the simple wind direction statistic that would yield much more isotropic dispersion field with a more southward dominance (*Fig. 3b*). This underlines that dust emission rate is the dominant factor in the dispersion model. While the sensitivities certainly decrease at larger threshold friction velocities, the difference is small, and the general dispersion pattern is very similar. This result can be surprising considering the fact that 64.8% of the observations fell between the 0.2 and 0.8 m/s threshold friction velocities. However, 80% of the total dust emission in the most conservative 0.2 m/s threshold friction velocity setup can be attributed to the observations where friction velocity also exceeded 0.8 m/s. More extremely, 3,750 strong-wind cases of the hourly observations, only 3% of the 13-year period caused 32% of the total dust emission.

The strong southwestward dispersion of dust is due to only a relatively few cases with strong winds that are typically related to cold fronts approaching from the northwest (*Fig. 3a*). The results correspond with the fact that the dust samples to the south and west of the site showed the largest DDD concentrations, however, the samples were not representative (*Greenpeace, 2015*). DDD detection in the dust to the west of the site is not explained by this

model. It could be caused by a short-period strong wind event (i.e., a gust front) from the eastern direction, as easterly winds are relatively frequent in the area (Fig. 3a). Another theory is to contribute this detection to water origin as the sample site lies in the main path of groundwater transport from the factory to the Danube.

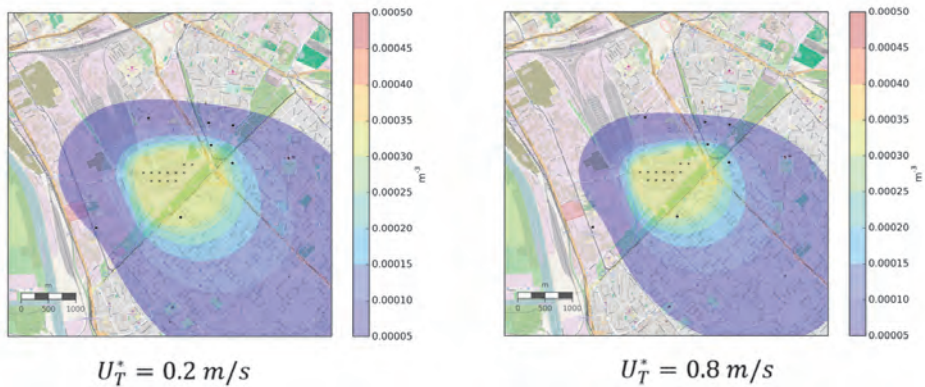


Fig. 2. 13-year mean dust normalized concentrations (sensitivities) at 2 m level, assuming 0.2 and 0.8 m/s threshold friction velocity. Black crosses indicate the source points, and black dots show the DDD detections in soil or dust samples. Background map © [OpenStreetMap](#) contributors, [CC-BY-SA](#)

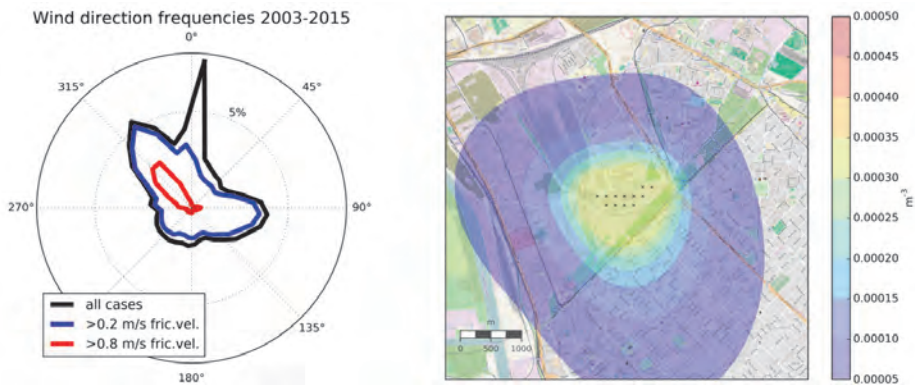
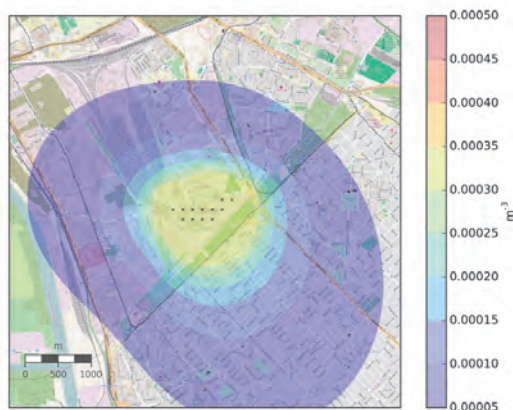


Fig. 3. Left: frequency distribution of wind directions in Budapest-Pestszentlőrinc between 2003–2015 in cases with larger than 0.0, 0.2, and 0.8 m/s threshold friction velocities. Right: reference 13-year mean dust normalized concentrations at 2 m level, assuming constant emission rate. Black crosses indicate the source points. With the consideration of weather-dependent emission rates, this spatial distribution is largely modified (cf. Fig.2. and Fig.4.). Background map © [OpenStreetMap](#) contributors, [CC-BY-SA](#)

The long-term spatial distribution of evaporating pollutants (*Fig. 4*) shows a different image. In this case, the emission rate is only a linear function of the friction velocity and an exponential function of temperature. A combination of these effects yields a south-eastward oriented plume that affects the eastward laying residential area less than the dust transport, but still more than the reference result with constant emission rate would imply. A clear northward direction is also observable related to rare, but extremely warm episodes caused by southerly winds (*Fig. 4*).



*Fig. 4.* 13-year mean normalized concentrations (sensitivities) of evaporating pollutants at 2m level. Background map © [OpenStreetMap](#) contributors, [CC-BY-SA](#)

The annual cycle of dust emission flux clearly follows the climatological characteristics of wind velocities, showing a well-defined spring maximum and fall/winter minimum (*Fig. 5*). Annual cycle of evaporation flux has a summer maximum and winter minimum following the temperature cycle. However, evaporation is stronger in the spring than in the autumn due to the generally stronger winds. For similar reasons, the daily cycle of emissions also shows a daytime maximum and a night minimum, according to the temperature and wind speed cycles (*Fig. 5*).

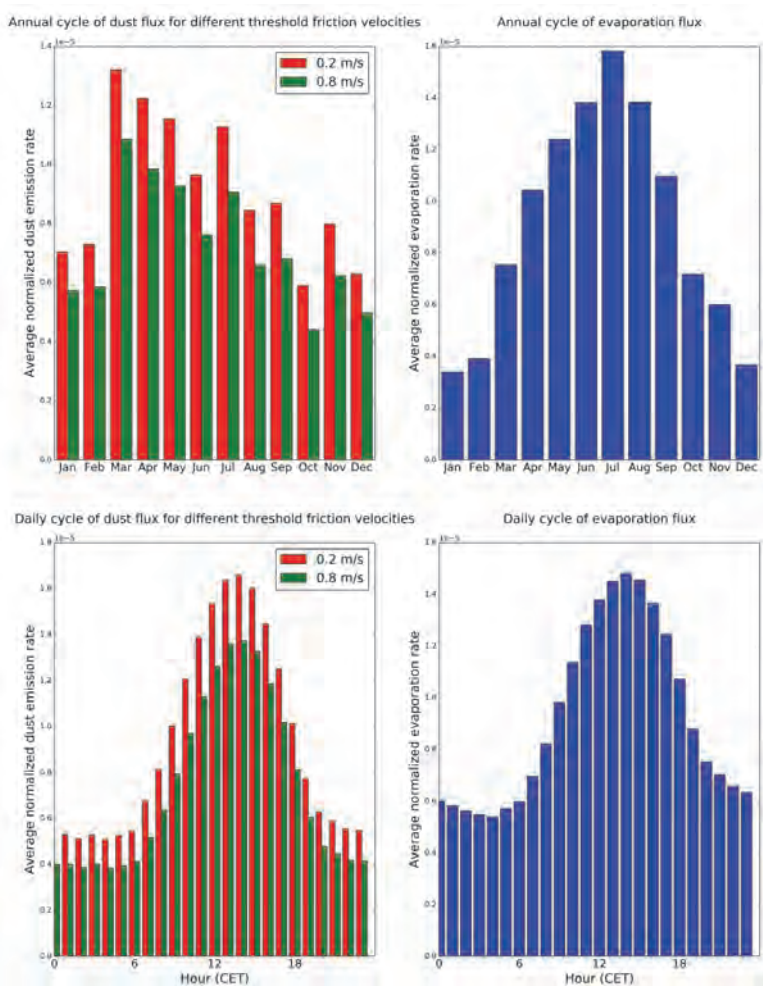


Fig. 5. Annual and daily cycle of normalized dust emission flux at different threshold friction velocities (left) and evaporation flux (right). Strong daytime and spring-summer maximum is observable in both cases.

The interaction of emission and dispersion processes can be interpreted as a favorable relationship to decrease surface air pollution. The emission is small or zero under atmospheric conditions with weak winds and cold nighttime inversions when surface concentrations would become the largest relative to the source term. On the contrary, high emission rate due to warm surface temperatures and strong winds is coupled with efficient turbulent mixing that ensures low surface concentrations relative to the source rate. In the counteraction of emission rate and mixing efficiency, the former factor seems to

be dominant, yielding summertime and daytime pollution maximum (Figs. 6–7). Nights, in general, show very limited emission rate, and thus, negligible pollution compared to daytime cases (Fig. 7). This temporal pattern is the opposite of what is generally experienced in urban air pollution statistics, and points out the importance of correct representation of emission characteristics. The increased risk by the spring-summer and daytime concentration maximum is the high exposure as people spend more time in the open air, and houses are more frequently ventilated. The relatively rare occurrence of significant emission events, however, provides a good chance of prevention in similar cases in the future, based on weather forecasts warning of strong, dry winds, especially if they are accompanied by high temperatures.

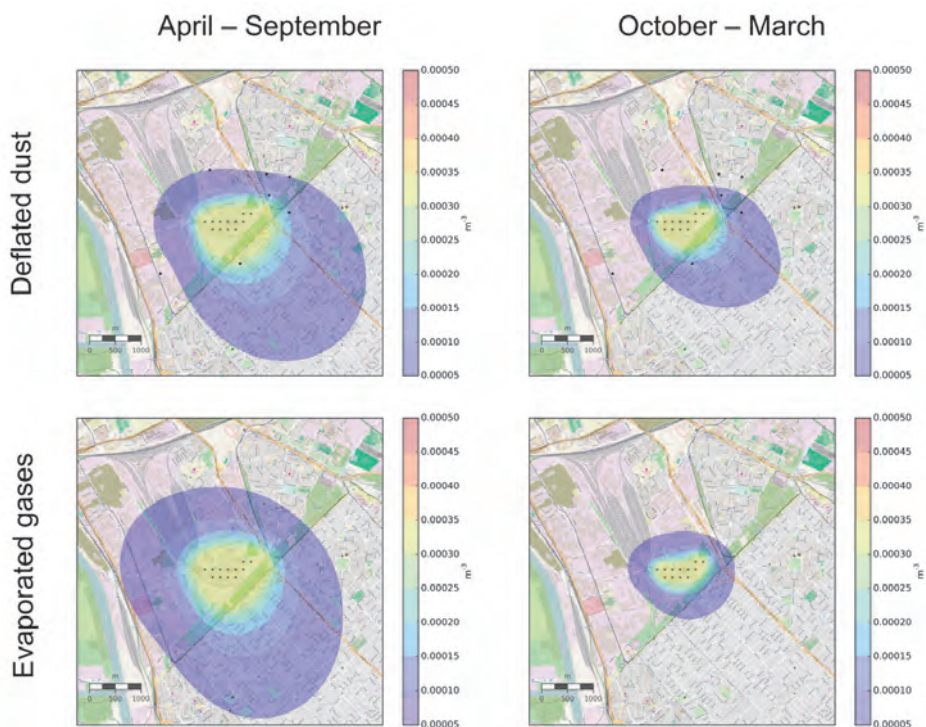
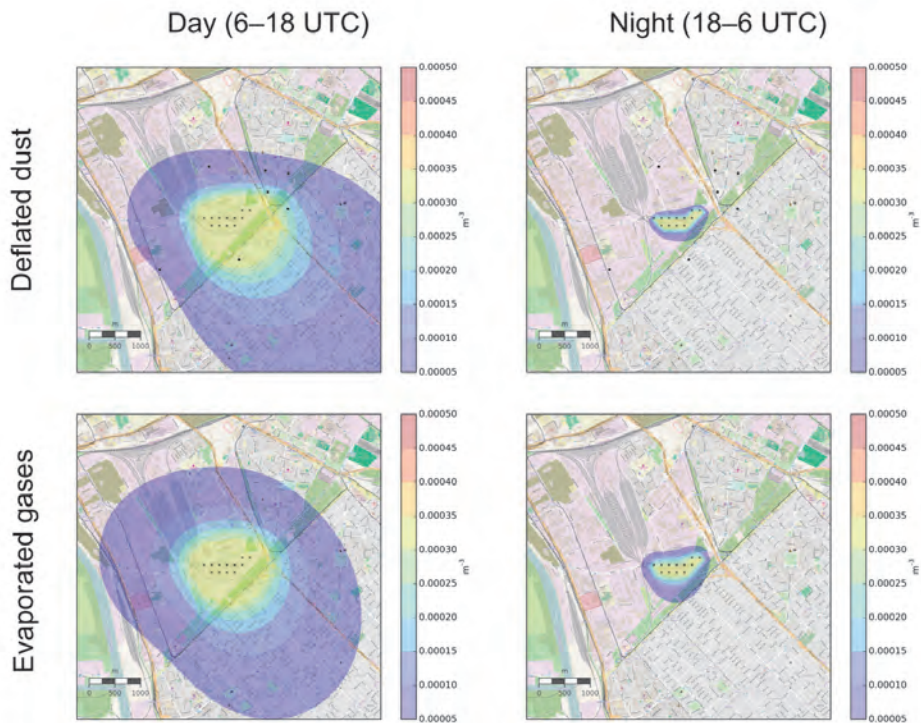


Fig. 6. 13-year mean normalized concentrations of the summer and winter half-years for deflated and evaporated pollutants. The dust pollution of the winter half-year is largely attributable to that of March. Background map © [OpenStreetMap](#) contributors, [CC-BY-SA](#)



*Fig. 7.* 13-year mean normalized concentrations of the daytime and nighttime half-days for deflated and evaporated pollutants. Despite the typically lower mixing heights, nighttime concentrations are small due to the decreased emission rate. Background map © [OpenStreetMap](#) contributors, [CC-BY-SA](#)

While the weather-dependent emission rate seems to be the ultimately dominant factor of the pollution, uncertainties and unrepresented effects can alter the results of this model simulation. Most importantly, the moisture content of the dust is an important factor in dust emission estimation. We have conservatively assumed a rapidly drying dust with zero emission only during precipitation, an approximation that seems to be acceptable for the thin dust layer laying on a solid surface. However, emission by strong winds only a few hours after intensive precipitation can still be decreased. This effect would probably decrease the domination of the south-eastern direction as situations with heavy precipitation followed by strong wind are typically related to northerly flows behind cold fronts.

The meteorological observatory is located only 6 km away from the industrial site, in a similar urban-domestic environment and on flat terrain, therefore, its data is assumed to be representative for the release site. However, microscale flow around the buildings can significantly alter dispersion patterns

in the vicinity of the source area, an effect that was partly taken into account by a correction factor. However, as it is generally true for Gaussian dispersion models, results must be carefully interpreted, and their accuracy is limited in a few hundred meters range from the source.

## 6. Conclusion

The long-term pollution originating from an abandoned industrial site in Budapest, Hungary has been studied with weather-dependent emission rates. In the lack of information on the actual amount of released material, sensitivities have been calculated to examine the spatial distribution and temporal cycle of pollutants. Deflation rate was assumed as a cubic function of the friction velocity, while evaporation rate was estimated as a linear function of friction velocity and an exponential function of temperature. Long-term dispersion of pollutants has been investigated through the 13-year period between 2003 and 2015, using a Gaussian dispersion model based on hourly observations and 12–24 hourly radiosonde data from a meteorological observatory located 6 km to the southeast from the release location.

In case of the dust release, relatively few occurrences of strong winds dominated the long-term dispersion pattern, yielding a distinct south-eastward transport of the plume. The sensitivity of results on a critical parameter of the emission model, the threshold friction velocity, has proved to be small despite the fact that the uncertainty range of the parameter covered almost two thirds of the observations. The spring and daytime maximum of emission rate has been found to be the dominant factor of the dispersion, counteracted by the efficient dilution of intensive turbulent mixing. For evaporated gases, the south-eastward and northward directions were the most affected due to a combination of wind direction distribution and the strongly temperature-dependent emission. Temporal cycle of evaporation closely followed the temperature cycle with summer and daytime maximum.

It has been shown that weather-dependent emissions can significantly alter the results of an air pollution model on local scale. Pollutants from deflation or evaporation origin showed largely different spatial distribution and temporal cycle than what the meteorological conditions and wind direction distribution would have suggested. The results can provide a basis for further measurements and health impact estimates to better assess the pollution risk from the Budapest Chemical Works.

**Acknowledgement:** The study was largely motivated by personal communications with *Zoltán Barcza*. Authors appreciate the efforts of civil groups and authorities to reveal the most possible information and to decontaminate the site. This work was supported by the National Research, Development and Innovation Office of Hungary (No. K109109 and No. K116506).

## References

- Beard, J., 2006: DDT and human health. *Sci. Total Environ.* 355, 78–89.
- Brighton, P.W.M., 1985: Evaporation from a plane liquid surface into a turbulent boundary layer. *J. Fluid Mech.* 159, 323–345.
- Cimorelli, A.J., Perry, S.G., Venkatram, A., Weil, J.C., Paine, R.J., Wilson, R.B., Lee, R.F., Peters, W.D., and Brode, R.W., 2005: AERMOD: A dispersion model for industrial source applications. Part I: General model formulation and boundary layer characterization. *J. Appl. Meteorol.* 44, 682–693.
- Dura, G., 2003: A Budapesti Vegyiművek Rt., Budapest, IX. ker. Illatos úti telepének vegyi szennyezettségéből eredő környezeti- és egészségkockázat részletes, mennyiségi felmérése. <http://kimittud.atlatszo.hu/request/4414/response/7383/attach/html/5/30%20128%202015%20mell%20klet.pdf.html>, accessed: 04/05/2016 (In Hungarian)
- Foken, T., 2006: 50 Years of the Monin–Obukhov Similarity Theory. *Boun.-Lay. Meteorol.* 119, 431–447.
- Gillette, D., 1978: A wind tunnel simulation of the erosion of soil: Effect of soil texture, sandblasting, wind speed, and soil consolidation on dust production. *Atmos. Environ.* 12, 1735–1743.
- Greenpeace, 2015: Porminták kémiai vizsgálata. Bálint Analitika Kft., Budapest. [www.greenpeace.org/hungary/hu/sajtokozpont/Lakott-teruleten-is-kimutathatoak-a-Budapesti-Vegyimuvek-szennyezi-a-Greenpeace-harompontos-kovetelese/](http://greenpeace.org/hungary/hu/sajtokozpont/Lakott-teruleten-is-kimutathatoak-a-Budapesti-Vegyimuvek-szennyezi-a-Greenpeace-harompontos-kovetelese/), accessed: 04/05/2016 (in Hungarian)
- Hevesi, F., 2016: SUCCESS: All toxic waste removed from Illatos Rd site of former Budapest Chemical Works. Greenpeace, [http://greenpeace.blog.hu/2016/01/15/success\\_all\\_toxic\\_waste\\_removed\\_from\\_illatos\\_rd\\_site\\_of\\_former\\_budapest\\_chemical\\_works](http://greenpeace.blog.hu/2016/01/15/success_all_toxic_waste_removed_from_illatos_rd_site_of_former_budapest_chemical_works), accessed: 05/04/2016.
- Holmes, N.S. and Morawska, L., 2006: A review of dispersion modelling and its application to the dispersion of particles: An overview of different dispersion models available. *Atmos. Environ.* 40, 5902–5928.
- Kim, K.-H., Jahan, S.A., Kabir, E., and Brown, R.J.C., 2013: A review of airborne polycyclic aromatic hydrocarbons (PAHs) and their human health effects. *Environ. Internat.* 60, 71–80.
- Leelőssy, Á., Jr, F.M., Izsák, F., Havasi, Á., Lagzi, I., and Mészáros, R., 2014: Dispersion modeling of air pollutants in the atmosphere: a review. *Cent. Eur. J. Geosci.* 6, 257–278.
- Leelőssy, Á., Mészáros, R., and Lagzi, I., 2011: Short and long term dispersion patterns of radionuclides in the atmosphere around the Fukushima Nuclear Power Plant. *J. Environ. Radioact.* 102, 1117–1121.
- Martcorena, B. and Bergametti, G., 1995: Modeling the atmospheric dust cycle: 1. Design of a soil-derived dust emission scheme. *J. Geophys. Res. Atmos.* 100, 16415–16430.
- Mészáros, R., Leelőssy, Á., Vincze, C., Szűcs, M., Kovács, T., and Lagzi, I., 2012: Estimation of the dispersion of an accidental release of radionuclides and toxic materials based on weather type classification. *Theor. Appl. Climatol.* 107, 375–387.
- Rákai, A., Kristóf, G., and Jörg, F., 2014: Sensitivity analysis of microscale obstacle resolving models for an idealized Central European city center, Michel-Stadt. *Időjárás* 118, 53–77.
- Rogan, W.J. and Chen, A., 2005: Health risks and benefits of bis(4-chlorophenyl)-1,1,1-trichloroethane (DDT). *The Lancet* 366, 763–773.
- Seidel, D.J., Ao, C.O., and Li, K., 2010: Estimating climatological planetary boundary layer heights from radiosonde observations: Comparison of methods and uncertainty analysis. *J. Geophys. Res.* 115, D16113.
- Simon, G., 2012: A Levegő Munkacsoport beltéri porszennyezettség vizsgálati eredményeinek értékelése. Levegő Munkacsoport, Budapest. (In Hungarian)
- Soto, A.M. and Sonnenschein, C., 2015: Endocrine disruptors: DDT, endocrine disruption and breast cancer. *Nat. Rev. Endocrinol.* 11, 507–508.
- Takemura, T., Okamoto, H., Maruyama, Y., Numaguti, A., Higurashi, A., and Nakajima, T., 2000: Global three-dimensional simulation of aerosol optical thickness distribution of various origins. *J. Geophys. Res.: Atmos.*, 105, 17853–17873.
- Tegen, I., Hollrig, P., Chin, M., Fung, I., Jacob, D., and Penner, J., 1997: Contribution of different aerosol species to the global aerosol extinction optical thickness: Estimates from model results. *J. Geophys. Res.: Atmos.* 102, 23895–23915.

- Uno, I., Amano, H., Emori, S., Kinoshita, K., Matsui, I., and Sugimoto, N., 2001: Trans-Pacific yellow sand transport observed in April 1998: A numerical simulation. J. Geophys. Res.: Atmos. 106, 18331–18344.*
- Wessling, 2015: Szakértői vélemény: Budapest IX. kerület talaj-, talajvíz-, felszíni víz vizsgálat. Wessling Hungary Kft., Budapest IX. kerület Ferencváros Önkormányzata, Budapest. [www.ferencvaros.hu/index0.php?name=hir\\_150915\\_BVM\\_SzakertVelemeny](http://www.ferencvaros.hu/index0.php?name=hir_150915_BVM_SzakertVelemeny), accessed: 04/05/2016 Budapest.*
- Xuan, J., 2004: Turbulence factors for threshold velocity and emission rate of atmospheric mineral dust. Atmos. Environ. 38, 1777–1783.*



## **Short-term variations in air temperature in Krakow (Poland) as an indicator of climate change in Central Europe**

**Katarzyna Piotrowicz\*, Dominika Ciaranek, and Izabela Guzik**

*Department of Climatology, Institute of Geography and Spatial Management,  
Jagiellonian University in Krakow,  
Gronostajowa 7, 30-387 Krakow, Poland*

*\*Corresponding author E-mail: k.piotrowicz@uj.edu.pl*

*(Manuscript received in final form August 1, 2016)*

**Abstract**—The paper discusses the long-term variability of maximum (Tmax) and minimum (Tmin) air temperature variations, both occurring from one day to the next and over several consecutive days (3-4), in Krakow (Poland, Central Europe) from 1826 to 2015 (i.e., over a period of 190 years). The authors analyzed the seasonal variability of short-term variations in air temperature, looking at the most significant changes ( $\pm 10$  °C), as well as at their dynamics and trends over the analyzed multi-annual period. A clear decrease has been observed both in the values of short-term Tmax and Tmin variations and in the number of cases with their significant fluctuations. The decrease has been gradual, without clear abrupt changes to the overall trend. The greatest short-term variations in temperature were most frequent in the cooler half-year, being smaller and less frequent in the summer months. If the observed trend persists, in the upcoming years we can expect a further decrease in the dynamics of variations in thermal conditions, i.e., short-term variations in temperature may more frequently be small, i.e.,  $\pm 0.1$ – $4.0$  °C. However, it is worth noting that Tmax more frequently increased from one day to the next and over several consecutive days, while Tmin more frequently decreased. The reasons for the analyzed changes remain unclear. It seems that natural factors, mainly including the advection of air masses, have a significant impact on short-term variations in air temperature, coupled with local factors, which have been strengthened by the human impact on the environment, including the urban heat island.

*Key-words:* Air temperature, short-term variations, day-to-day temperature variation, Central Europe, Poland

## 1. Introduction

Long-term air temperature variability analysis is among the essential research topics in contemporary climatology (Brunetti *et al.*, 2000; Moberg and Jones, 2005; Lorenc, 2007). To analyze relevant data, the authors of this paper have relied on weather data series of various lengths from a single weather station or from several different sites, as well as on grid-point values which enable the analyzed data to be interpolated to large areas. A reliable assessment of the variability and trends in thermal conditions is only possible on the basis of very long and homogenous instrumental record series (Moberg *et al.*, 2000). However, few such datasets are available in Europe, and where they do exist (Jones *et al.*, 2002), they most often represent the climate conditions prevalent in large urban agglomerations. Such data series include records from the historic weather station in Krakow, where weather data was first recorded in 1792, while daily values have been uninterruptedly tracked since 1826. This dataset has been repeatedly used in studies of long-term climate variability and compared against records from elsewhere in Europe and especially from Central European sites (e.g., Trepínska; 1990, Piotrowicz, 2010).

Most climate change studies point to a very clear rise in global temperatures, especially since the 1970s (Kozuchowski *et al.*, 2000; Wibig and Głowicki, 2002). Although far from exhibiting a regular spatial or temporal pattern, such variations have been used by many authors to prove that each consecutive decade has become warmer than the preceding one (Frich *et al.*, 2002; Klein Tank and Können, 2003; Moberg and Jones, 2005). An increase in temperature can be seen not only in mean annual values, but also in seasonal data. Researchers most often point out a clear increase in temperature in the winter season, which can also be observed, albeit less frequently, in summer (Rebetez, 2001; Gough, 2008). In the 20th century, it was in winter that the highest increase in temperature was recorded, e.g. in Central and Eastern Europe it reached 0.35 °C/10 years (Brázdil *et al.*, 1996; Jones *et al.*, 2002; Wibig and Głowicki, 2002). For spring and autumn, different and sometimes contradictory results have been obtained regarding temperature increases, depending on the study area and the length of the analyzed record (Frich *et al.*, 2002; Klein Tank *et al.*, 2002; IPCC, 2007, 2014). However, according to Alexander *et al.* (2006), the rise in temperature can be observed in all seasons of the year. The changes are clearer from March to May and less distinct from September to November. It is also worth emphasizing that variations in minimum temperatures are usually greater than those in maximum temperatures (Rebetez, 2001).

The dynamics of temperature variations in various regions of the world is yet to be analyzed. Some authors have pointed to an increasing frequency of abrupt temperature shifts in recent decades, while others claim that global warming manifests itself in the “attenuation” of temperature fluctuations, i.e.,

greater temperature stability over time (Rebetez, 2001; Ciaranek and Piotrowicz, 2014).

Air temperature variability in short time intervals provides insights into climate dynamics, but it is also relevant for practical reasons (Tam and Gough, 2012). Sudden rises and falls in temperature, both occurring from one day to the next and over several consecutive days (3–4), have a negative impact on human health and wellbeing, and may be detrimental to various sectors of the economy, including agriculture, transport, and construction. Very significant temperature drops in spring can cause winterkill or black ice, while warm spells before snow cover melts pose a risk of flooding (Fortuniak *et al.*, 2004).

In climatology literature, most papers on short-term variations in temperature focus on day-to-day fluctuations (Kossowska-Cezak, 1987; Tam *et al.*, 2015). In Poland, in the early 20th century, Merecki (1903) claimed that substantial variations in temperature are caused by atmospheric circulation and local factors. Central European climate is dominated by small (2–3 °C) day-to-day variations in temperature throughout the year. In extreme cases, however, such fluctuations may even exceed  $\pm 10\text{--}15$  °C (Kossowska-Cezak, 1987). They most frequently occur in winter and are related to the advection of both warm and cold air masses. The authors have not only analyzed the impact of atmospheric circulation (Kossowska-Cezak, 2003), but also that of urbanization and the urban heat island (UHI), on day-to-day temperature changes (Tam *et al.*, 2015).

In this paper, the authors decided to look at the nature of variations in temperature occurring from one day to the next and over several (3–4) consecutive days during the last 190 years (1826–2015) in Krakow (Southern Poland). Are short-term variations in temperature increasing or decreasing due to the clear overall increase in temperature values? What dynamics and trends can be identified? Consideration was also given to seasonal variability of short-term changes in temperature, including the most significant fluctuations.

## ***2. Data and methods***

The paper is based on data concerning the daily values of maximum (Tmax) and minimum (Tmin) air temperature at the historic weather station in Krakow ( $\varphi=50^{\circ}04'N$ ,  $\lambda=19^{\circ}58'E$ ,  $h=220$  m a.s.l.). It represents one of the longest weather data records in Europe. It is homogenous and very much representative of the area of Central Europe located below 600 m a.s.l. (Trepńska, 1997).

Authors of papers on day-to-day temperature changes have used both mean daily temperature values and Tmax and Tmin in their research. In this paper, only extreme temperatures were taken into consideration due to the numerous modifications introduced over time in the methods of calculation of the daily mean values. The authors also agree with Kossowska-Cezak (1987), who

claimed that Tmax and Tmin describe actual variations, while the mean daily temperature values may only be treated as indicators which, however, fail to reflect the actual day-to-day temperature increases or decreases.

Short-term temperature changes were calculated as the difference ( $\Delta$ ) between the values recorded on the next and on the preceding day ( $\Delta T = T_2 - T_1$ ; day-to-day) and additionally over three ( $\Delta T_{3-1} = T_3 - T_1$ ) and four ( $\Delta T_{4-1} = T_4 - T_1$ ) days. These calculations took account of both the absolute values the changes and of the actual values – decreases (–) and increases (+) in temperature in the analyzed cases.

Following the approach adopted by other researches (*Kossowska-Cezak, 1987; Tam and Gough, 2012*), the authors defined “significant” temperature changes as cases where the values of the calculated differences were above 10 °C or below –10 °C.

Without doubt, the increase in temperature in Krakow since 1826 has been driven not only by natural factors (atmospheric circulation) but also by human impact. Special caution was therefore exercised when analysing the causes of the observed variations. The changes occurring over time were compared to the history of the city’s development (its surface area, population size, and industrial development).

A statistical analysis of relevant trends was performed using the nonparametric Mann-Kendall test (*Kendall, 1975*). The variations were deemed statistically significant when they were smaller than 5%.

The analysis also included cases where the day-to-day temperature difference had the same mathematical sign, i.e., it was positive or negative, on consecutive days. The persistence of such phenomena, defined as series of days with day-to-day increases or decreases in temperature, was determined. In terms of length, one-day long, short (2–4 days), medium (5–9 days), and long ( $\geq 10$  days) sequences of days were identified. Their number in each analyzed year was calculated. The fewer of them occurred, the longer they were in a given year, i.e., the temperature more frequently changed in a single direction, i.e., rose or fell, from one day to the next.

### ***3. Essential characteristics of short-term variations in air temperature***

Regarding the short-term variations in Tmax taken into account in the analyzed multi-annual period, increases were slightly more frequent than decreases, while the opposite was true for Tmin. It more frequently decreased than increased, both on a day-to-day basis and over three or four consecutive days (*Table 1*). Cases where no temperature changes were recorded, were accounted for between 1.1% and 2.3%. As the measurement error for the analyzed meteorological element amounts to 0.1 °C, the analysis also took account of cases where  $\Delta T$  amounted  $\pm 0.1$  °C ( $\Delta T = \pm 0.1$  °C). The frequency of occurrence

of such cases is shown in *Table 1*. They were most numerous for day-to-day variations in Tmin (5.6%), and least numerous for Tmax changes over four days (2.6%).

*Table 1.* Essential characteristics of short-term variations in maximum and minimum air temperature in Krakow in the period 1826–2015

Short-term variations	Maximum temperature			Minimum temperature		
	Freq. (%)	mean	$\sigma$	Freq. (%)	mean	$\sigma$
$\Delta T_{2-1} > 0.0^\circ\text{C}$	50.8	2.5	2.0	46.1	2.3	2.1
$\Delta T_{2-1} < 0.0^\circ\text{C}$	47.3	-2.7	2.3	51.6	-2.1	1.7
$\Delta T_{2-1} = 0.0^\circ\text{C}$	1.9	-	-	2.3	-	-
$\Delta T_{2-1} = \pm 0.1^\circ\text{C}$	4.5	-	-	5.6	-	-
$\Delta T_{3-1} > 0.0^\circ\text{C}$	50.4	3.5	2.7	48.4	3.0	2.7
$\Delta T_{3-1} < 0.0^\circ\text{C}$	48.4	-3.7	3.0	50.0	-2.9	2.4
$\Delta T_{3-1} = 0.0^\circ\text{C}$	1.2	-	-	1.6	-	-
$\Delta T_{3-1} = \pm 0.1^\circ\text{C}$	3.0	-	-	3.7	-	-
$\Delta T_{4-1} > 0.0^\circ\text{C}$	49.9	4.1	3.1	49.2	3.4	3.0
$\Delta T_{4-1} < 0.0^\circ\text{C}$	49.0	-4.2	3.2	49.4	-3.4	2.8
$\Delta T_{4-1} = 0.0^\circ\text{C}$	1.1	-	-	1.4	-	-
$\Delta T_{4-1} = \pm 0.1^\circ\text{C}$	2.6	-	-	3.4	-	-

The mean multi-annual values of differences in temperature and standard deviation ( $\sigma$ ) indicate that small changes of  $\pm 2-4^\circ\text{C}$  were the most abundant (*Table 1*). In the case of Tmin,  $\pm 4^\circ\text{C}$  changes were a little more frequent ( $>70\%$ ), while they were the least numerous for Tmax variations over 4 days ( $>58\%$ ).

Clear patterns can be seen in terms of short-term variations in temperature during the year (*Fig. 1*). An analysis of changes to Tmax shows that the greatest mean monthly values of the differences occurred in April and May, while the same was true for Tmin in winter (Dec-Feb). Higher values were recorded for variations over a period of four days ( $\Delta T_{4-1} = T_4 - T_1$ ), and the lowest values were recorded for day-to-day changes ( $\Delta T_{2-1} = T_2 - T_1$ ). However, in general, the pattern of the mean monthly values of the analyzed differences is more varied than for Tmin, with smaller ones recorded in summer (Jun-Aug). The differences between the mean monthly values of Tmax variations are clearly smaller.

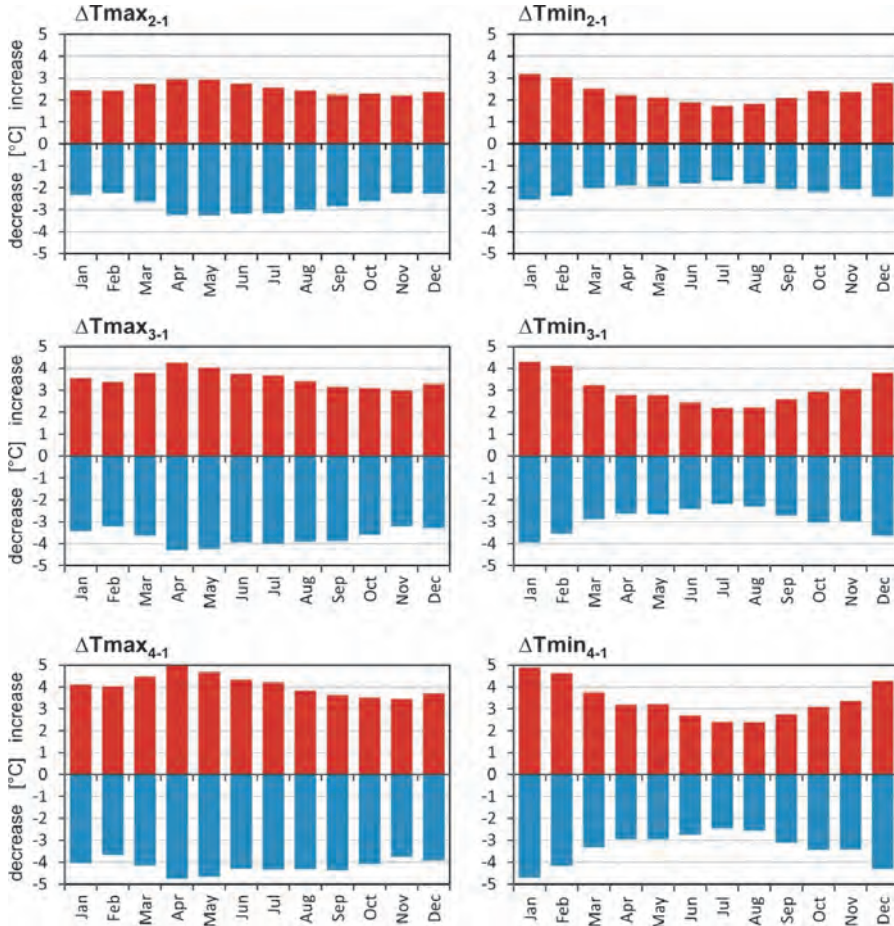


Fig. 1. Mean monthly values, increases and decreases in maximum and minimum air temperature of day-to-day ( $\Delta T_{2-1}$ ), over three ( $\Delta T_{3-1}$ ), and four ( $\Delta T_{4-1}$ ) days in Krakow in the period 1826–2015.

The above-described analysis was complemented by the identification of patterns in the annual variability of cases with no variation, i.e.,  $\Delta T = \pm 0.1^\circ\text{C}$  (Fig. 2). An average of ca. 8% of such cases per month was recorded. For Tmax, they mainly occurred in winter and particularly in December (more than 10% of all days). Tmin most frequently remained the same in summer (Jun–Aug). However, it is worth noting that no day-to-day Tmin changes were recorded with equal frequency in spring (Mar–Apr), September–November, and December (more than 8% of all cases).

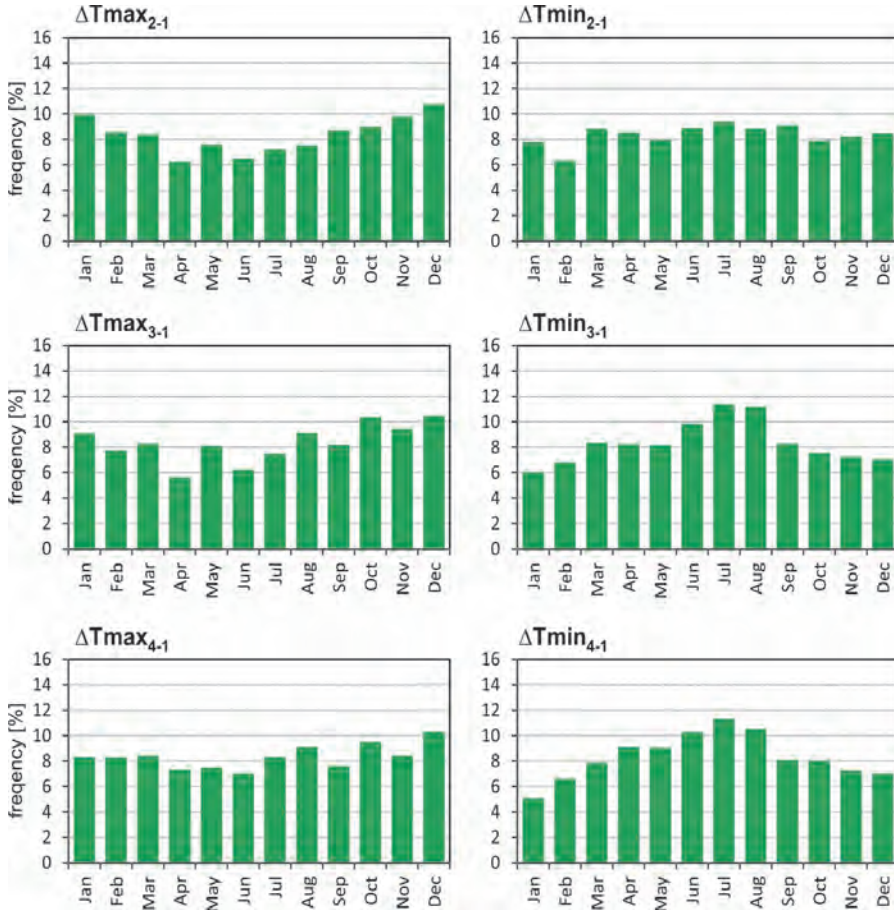


Fig. 2. Frequency of cases with no short-term variations in air temperature ( $\Delta T = \pm 0.1$  °C) of day-to-day ( $\Delta T_{2-1}$ ), over three ( $\Delta T_{3-1}$ ) and four ( $\Delta T_{4-1}$ ) days in Krakow in the period 1826–2015.

#### 4. Multi-annual variability of short-term variations in air temperature

The mean annual values of Tmax and Tmin of increases and decreases in the analyzed period spanning 190 years have been shown in Fig. 3. All trends indicate a decrease in the values of short-term variations in temperature, and they are statistically significant at the level of 0.05. The most significant changes in the analyzed period were recorded for Tmin, especially regarding its decreases over three and four consecutive days (Fig. 3). Somewhat lower values of short-term temperature variations could be seen at the turn of the 20th century (1886–1905) and around 1970–1976.

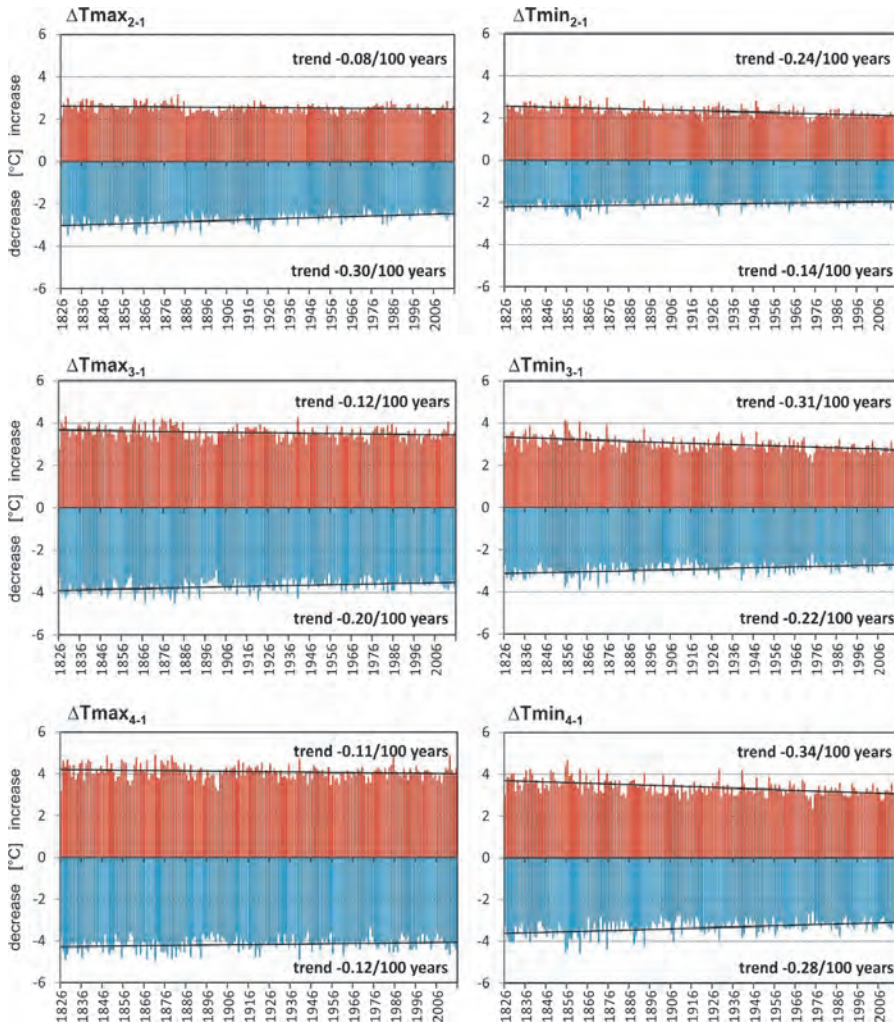


Fig. 3. Multi-annual variability and trends of increases and decreases in maximum and minimum air temperature of day-to-day ( $\Delta T_{2-1}$ ), over three ( $\Delta T_{3-1}$ ), and four ( $\Delta T_{4-1}$ ) days in Krakow in the period 1826–2015.

The long-term variability of the number of cases with no changes in temperature ( $\Delta T = \pm 0.1 \text{ }^\circ\text{C}$ ) did not exhibit a clear trend (Fig. 4). The only statistically significant trend which suggests a decrease in the number of the analyzed cases was observed for day-to-day variations in Tmax (1.05/100 years).

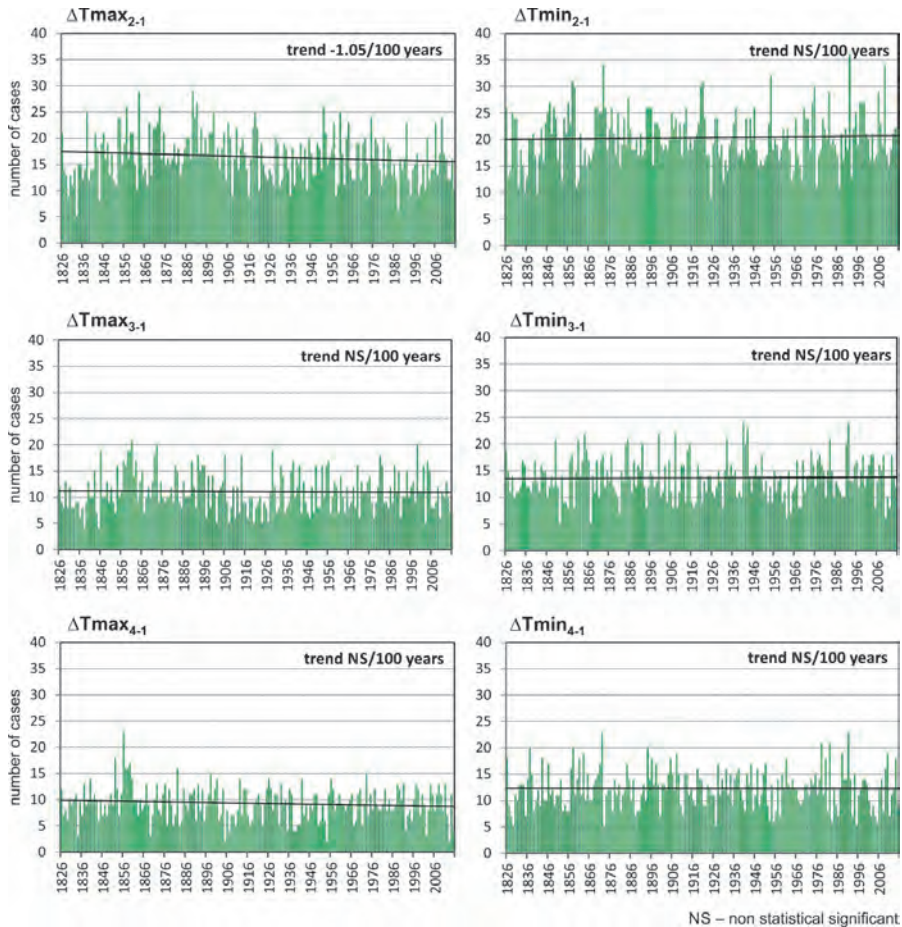
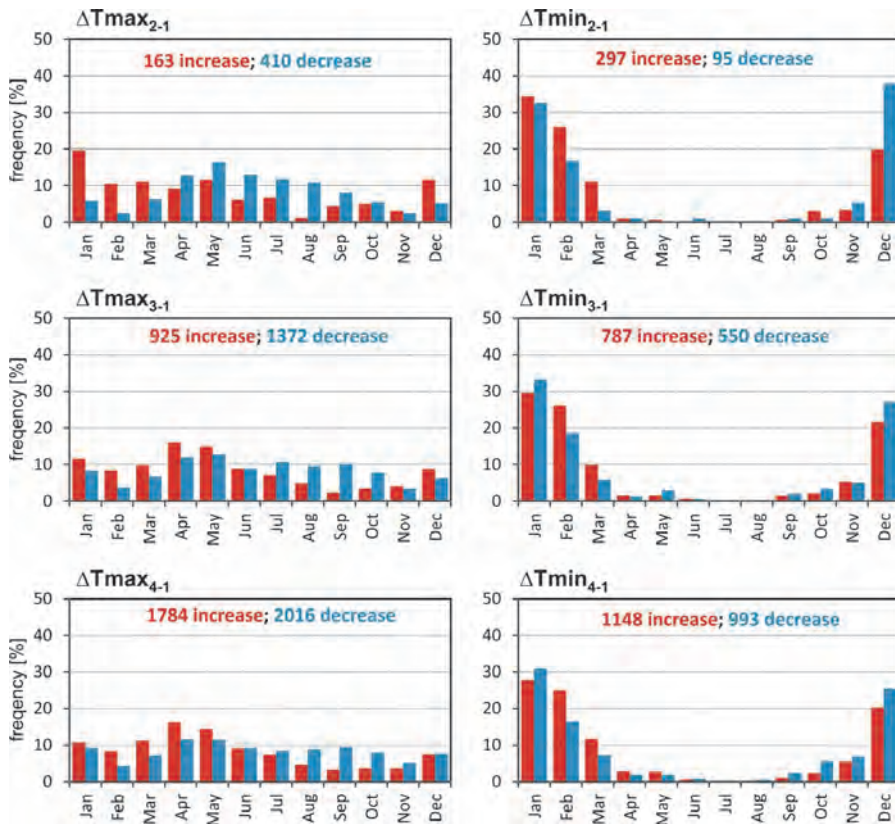


Fig. 4. Multi-annual variability and trends of no-variation ( $\Delta T = \pm 0.1$  °C) in maximum and minimum air temperature of day-to-day ( $\Delta T_{2-1}$ ), over three ( $\Delta T_{3-1}$ ), and four ( $\Delta T_{4-1}$ ) days in Krakow in the period 1826–2015.

### 5. Significant ( $> \pm 10$ °C) short-term variations in air temperature

Regarding to day-to-day variation, significant decreases in Tmax were more numerous (410 cases) than in Tmin (95), whereas the opposite was true for significant increases – they were more numerous in the case of Tmin (297 cases) than for Tmax (163). During the year, a clear difference is visible between the frequency of occurrence of significant variations in Tmin in winter (Dec-Feb) and March, and in the remaining months of the year (Fig. 5). More than 90% of

such cases (91.2% of increases, 90.5% of decreases) occurred in those four months. Day-to-day abrupt changes in Tmax occurred with a similar frequency in all seasons, with significant increases being much more frequent in spring (31.9%) and winter (34.4%), and significant decreases prevailing in spring (35.4%) and summer (35.4%). Significant variations in temperature over three and four days, as compared to day-to-day changes, only differed in terms of the number of cases, as they were much more frequent. However, their frequency of occurrence over the year was quite similar (*Fig. 5*).



*Fig. 5.* Frequency of occurrence of short-term variations of  $\geq \pm 10^\circ\text{C}$  in extreme temperatures in Krakow in the period 1826–2015.

The multi-annual trend of significant variations in temperature, including both increases and decreases, suggests that they are becoming smaller (*Fig. 6*).

In terms of day-to-day changes, there were significantly fewer cases of Tmax differing by  $-10\text{ }^{\circ}\text{C}$  (2.08/100 years) and Tmin by  $+10\text{ }^{\circ}\text{C}$  (1.47/100 years). Regarding the variations in Tmax over a slightly longer time interval (3–4 days), greater trends appeared in the case of differences exceeding  $-10\text{ }^{\circ}\text{C}$ , while regarding the Tmin, trends in both significant decreases and increases were quite significant (from 2.64 to 3.08/100 years).

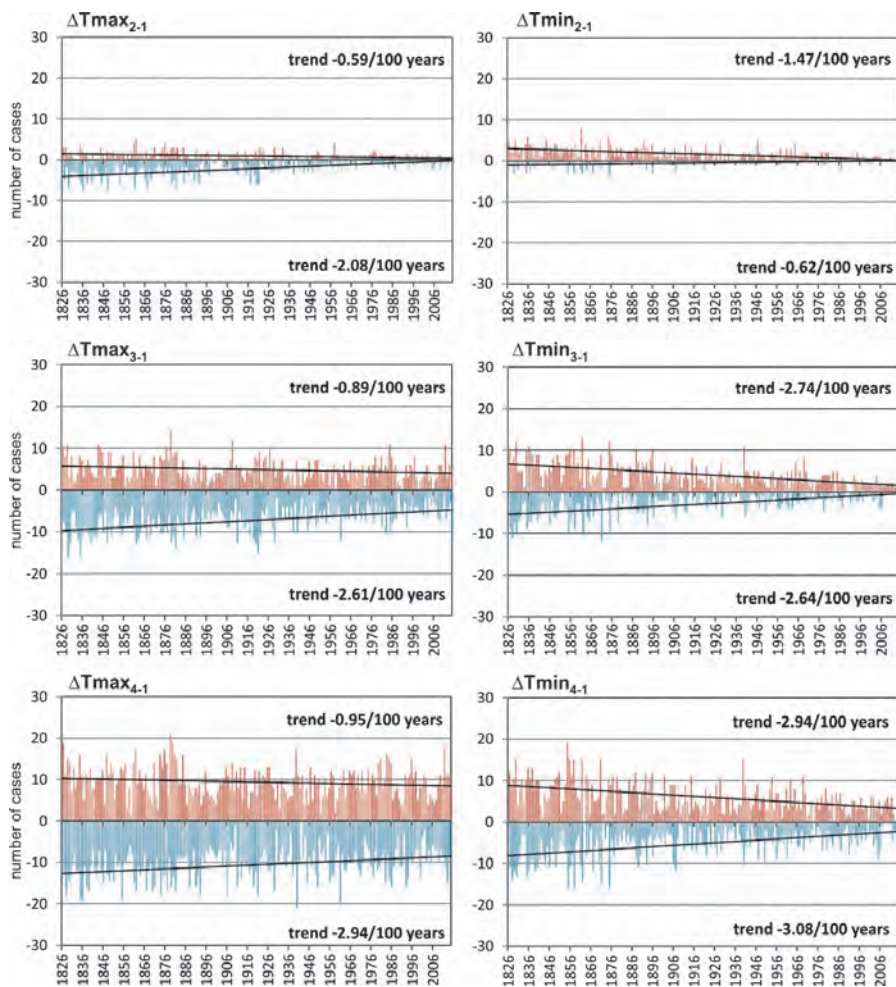


Fig. 6. Multi-annual variability and trends in significant maximum and minimum air temperature increases ( $>10\text{ }^{\circ}\text{C}$ ) and decreases ( $<-10\text{ }^{\circ}\text{C}$ ) in day-to-day ( $\Delta T_{2-1}$ ), over three ( $\Delta T_{3-1}$ ) and four ( $\Delta T_{4-1}$ ), consecutive days in Krakow in the period 1826–2015.

## ***6. Sequences of day-to-day variations in maximum and minimum air temperatures***

The variability of temperature in short time intervals can also be identified by analyzing sequences of days when the difference in temperature values was denoted with the same sign, i.e., when temperature decreased (-), increased (+), or remained stable, i.e.,  $\Delta T_{2-1} = \pm 0.1$  °C.

Most frequently, day-to-day temperature increases and decreases occurred in isolation, i.e., from one day to the next. Such cases accounted for between 46% and 54% of all cases (*Fig. 7*). In 43–49% of all cases, temperature increases and decreases persisted for 2–4 consecutive days. *Fig. 7* also shows that there were some cases where the same direction of change was recorded for up to 10–12 consecutive days. Such long sequences occurred in January, February, April, July, October, November, and December, i.e., in almost all seasons, but they were predominant in winter. Temperature increases and decreases were equally frequent in such series.

In 93% of all cases no variations in Tmax were recorded in one-day sequences (*Fig. 7*); however, such slight temperature fluctuations occurred in up to 4-day-long sequences. Therefore, also in this case, defining short-term variations in temperature as changes in temperature values occurring for up to four days turned out to be right.

The multi-annual variability of the analyzed sequences leads to the conclusion that in the case of day-to-day variations in Tmax, the average annual number of all sequences (regardless of their length) in which the temperature increased (91.5 sequences) and decreased (91.0) was almost the same (*Fig. 8*). The situation was similar for Tmin, although the number of cases was slightly higher. The respective values amounted to 94.3 and 95.2 (*Table 2*).

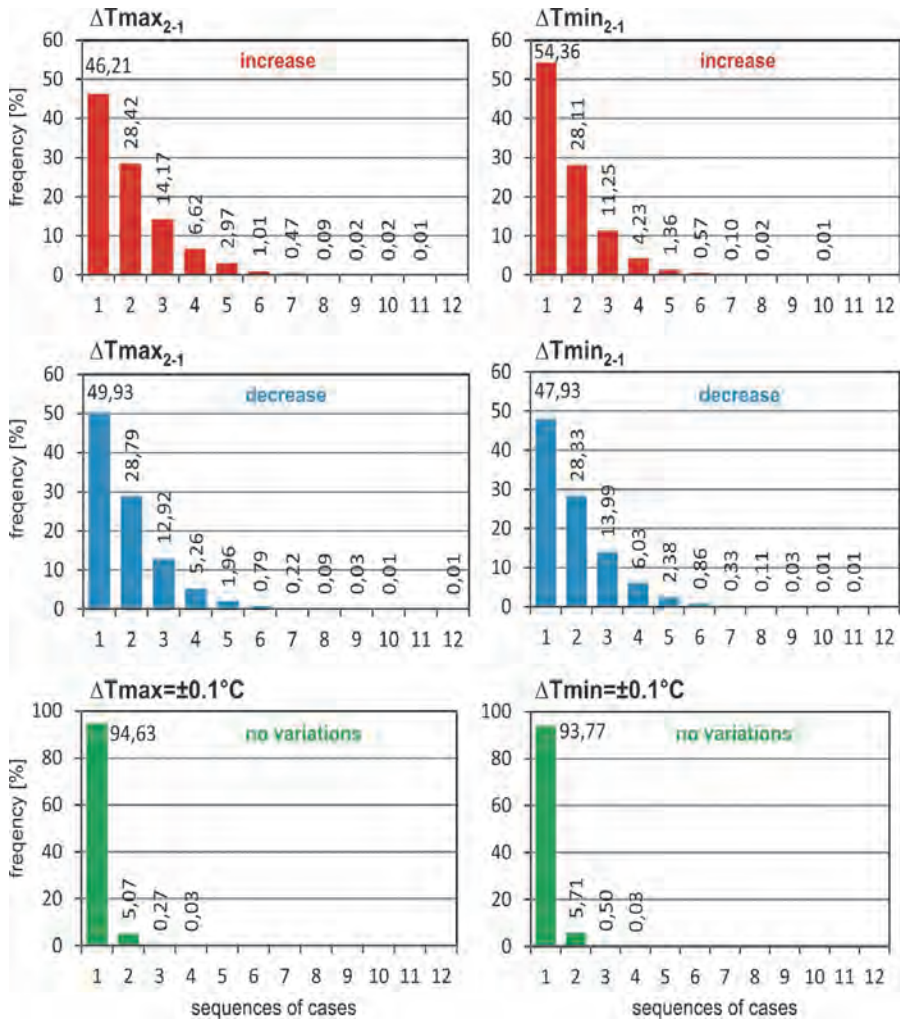


Fig. 7. Frequency of occurrence of sequences of days with day-to-day variations (and no-variations) in air temperature, broken down by length in Krakow in the period 1826–2015.

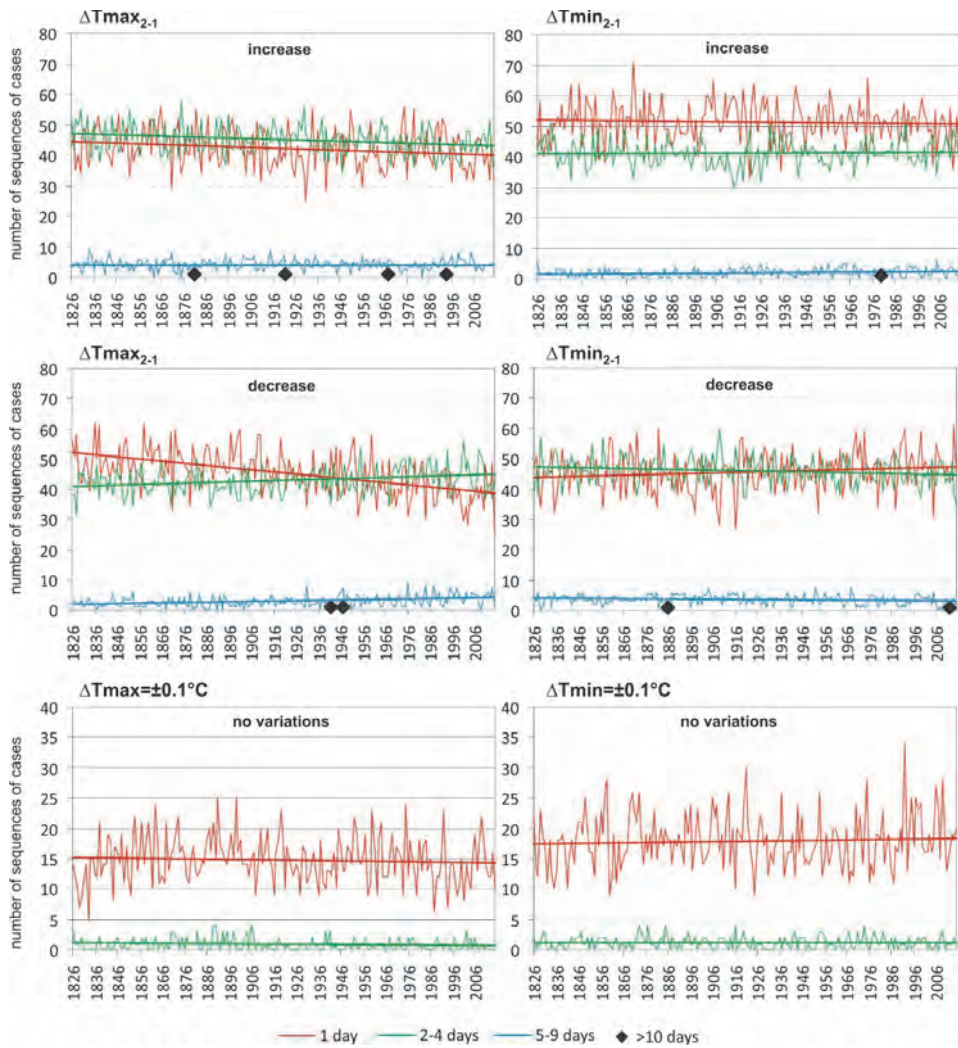


Fig. 8. Multi-annual variability of sequences of days with day-to-day variations (and no-variations) in air temperature, broken down by length in Krakow in the period 1826–2015.

*Table 2.* Average number of sequences of days with day-to-day variations (and no-variations) in air temperature, broken down by length and trends (trend/100 years) in Krakow in the period 1826–2015

Sequences	Tmax – increase		Tmin – increase	
	Mean number in the year	Trend/100 years	Mean number in the year	Trend/100 years
One-day	42.3	–2.18	51.2	NS
2–4 days	45.0	–2.18	41.1	NS
5–9 days	4.2	NS	1.9	+0.52
all	91.5	–4.33	94.3	NS
	Tmax – decrease		Tmin – decrease	
One-day	45.4	–6.90	45.6	+1.72
2–4 days	42.7	+2.11	46.0	–1.46
5–9 days	2.8	+1.18	3.6	–0.41
all	91.0	–3.61	95.2	NS
	Tmax – with no variations		Tmin – with no variations	
One-day	14.7	NS	17.9	NS
2–4 days	0.8	NS	1.2	NS
all	15.6	NS	19.1	NS

In the analyzed period, the overall number of all sequences in Tmax clearly decreased (*Table 2*). This was mainly due to a reduced number of 1-day sequences, as well as a reduced number of short sequences (2–4 days) in which temperature increased. Therefore, recently there have been fewer cases of alternating day-to-day increases and decreases of temperature. Thus, Tmax more frequently increases or decreases over several consecutive days.

In the case of Tmin, statistically significant trends, albeit small ones, were only noticed when the multi-annual variability of some sequences was analyzed (*Table 2*). Over the last 190 years in Krakow, Tmin has changed from one day to the next in quite similar sequences of days. On average during the year, the Tmin increases in one-day sequences were most numerous, while decreases were most frequent in 2–4 day sequences. The latter, however, exhibited a slight downward trend, and thus, one can still expect frequent day-to-day variation in the direction of change (increase and decrease) of Tmin (i.e., in one-day long sequences).

No clear trends in the multi-annual period were observed for the other previously analyzed parameter, i.e., the no-variation in temperature (*Table 2, Fig. 8*). On average during the year, such cases of no-variation are grouped in 15.6 (Tmax) and 19.1 (Tmin) sequences, and one-day long sequences are the most frequent.

## 7. Discussion

In the analyzed multi-annual period (1826–2015), there was a clear decrease both in the values of short-term T<sub>max</sub> and T<sub>min</sub> changes, and in the number of cases with significant changes ( $\pm 10$  °C). Similar conclusions were drawn by *Rebetez* (2001), who relied on data from Switzerland (Neuchatel and Davos), stating that an increase in temperature in the 20th century was accompanied by its reduced day-to-day variation. *Moberg et al.* (2000) point out that the day-to-day variations in temperature in England, Stockholm, Uppsala, and Saint Petersburg were 10% greater in the 19th century than between 1961 and 1990.

Analyses conducted by *Kossowska-Cezak* (1987, 1988, 2003) suggest that significant variations in temperature in Poland may co-occur with various types of atmospheric circulation. Moreover, the same type of circulation may lead to both a decrease and an increase in temperature. Rather than with changes in atmospheric circulation, short-term variations in temperature should then be linked to the advection of air masses and local conditions, such as the inflow of air from areas with contrasting thermal conditions (e.g., coastal areas), night-time temperature inversion near the ground, and adiabatic heating of air. Unfortunately, it is impossible to measure the strength of this relationship due to a lack of long-term data on the frequency of occurrence of particular air masses over Krakow. Undoubtedly, changes in temperature in the city are influenced by local conditions, such as land relief, and especially its location in the inversion valley of the Vistula River, the influence of foehn winds in the mountain range located ca. 100 km away, and the built-up urban land (urbanization), including the urban heat island (UHI).

In Krakow, more than half of all days of the year have an inverse temperature distribution, and in the case of T<sub>min</sub>, that frequency raises even up to 92% (*Matuszko et al.*, 2015). Inversions are especially intense in the cool half-year (Oct-Mar) and particularly in winter (Jan-Feb). At the same time, abrupt temperature increases may occur in connection with the occurrence of the foehn wind. Over the last 190 years (1826–2015), the impact of these factors did not demonstrate any significant changes. Increasing urbanization and the urban heat island may have a much greater influence on temperature and also on its short-term variation. The UHI phenomenon has been examined in detail in Krakow since the 1950s. Currently, the UHI extends over an area which is almost three times greater than it was in the mid-20th century, but its intensity is considered to reach an average of 1.2 °C and a maximum of 5–7 °C (*Lewińska*, 1996). Research into the impact of the city on day-to-day variations in temperature has been conducted by *Kossowska-Cezak* (1988) in Warsaw, *Olejniczak* (2003) in Krakow, and *Tam et al.* (2015) in USA and Canada. The authors observed lower T<sub>min</sub> variability in the city center, which resulted from the influence of urban built-up land. The effect is especially noticeable in the evening and at night, i.e., during the time when daily minimum temperature

values are most frequently recorded. Differences in day-to-day temperature variability in Krakow turned out to be quite small. For Tmin, they amounted to 0.7 °C on average, while for the daily mean and for Tmax they equalled to 0.3 °C (Olejniczak, 2003).

## 8. Conclusions

When discussing short-term variation in Tmax and Tmin in Krakow – which is representative of the wider area of Central Europe – the authors used relatively rarely applied methodology. Besides day-to-day variation in temperature, they also examined changes occurring over three or four consecutive days. The latter were taken into account due to the observed highest frequency of occurrence (over 95%) of day-to-day variations over 4-day-long periods. The analysis also included cases where there were no day-to-day variations in temperature.

An analysis of short-term variations in temperature in Krakow between 1826 and 2015, as well as of significant temperature increases and decreases ( $\pm 10$  °C) has found that both the size of such variations and the number of cases are decreasing. However, it is worth noting that Tmax more frequently increased from one day to the next and over several consecutive days, while Tmin more frequently decreased.

Significant short-term variations in temperature most frequently occur in the cooler half of the year, when the air masses over Poland are most thermally diverse and weather fronts are most frequent (Kossowski, 1970). In the summer months, such shifts are smaller and happen less frequently, while changes in cloud cover, which influence night-time radiation cooling, become a contributing factor (Moberg *et al.*, 2000). As a result, significant day-to-day variations in Tmax occur in summer.

Short-term variation in Tmax and Tmin decrease has been gradual over the entire analyzed long-term period, without clear and sudden changes to the overall trend. It seems that it was largely influenced by anthropogenic factors, such as increasing population size and urban sprawl, which in Krakow took place in several clear-cut stages. However, even when an entire new city district with a steel mill was erected in 1949–1954, the expansion did not result in abrupt changes to thermal conditions. Certainly, however, more detailed studies would be required to determine the impact of urbanization on thermal conditions using the values of day-to-day variations in temperature (and especially in Tmin). This has previously been pointed out by Kossowska-Cezak (1988). This, however, requires data from a pair of weather stations (one located in the city and another one outside the city) for a long period of time. Data from at least several large cities would be recommendable.

The causes of the analyzed changes in thermal conditions are still unclear and it is impossible to be certain whether they are permanent or a reversal of the

trend should be expected. It seems that short-term variations in temperature are largely influenced by natural factors – mainly by the advection of air masses and to a lesser extent by local conditions, which have been compounded by the human impact, including the urban heat island.

If this trend persists, in the upcoming years a further reduction in the dynamics of changes in thermal conditions can be expected, i.e., short-term variations in temperature may more often be only slight, i.e., around  $\pm 0.1$ – $4.0$  °C.

## References

- Alexander, L.V., Zhang, X., Peterson, T.C., Caesar, J., Gleason, B., Klein Tank, A.M.G., Haylock, M., Collins, D., Trewin, B., Rahimzadeh, F., Tagipour, A., Rupa Kumar, K., Revadekar, J., Griffiths, G., Vincent, L., Stephenson, D.B., Burn, J., Aguilar, E., Brunet, M., Taylor, M., New, M., Zhai, P., Rusticucci, M., and Vazquez-Aguirre, J.L. 2006: Global observed changes in daily climate extremes of temperature and precipitation. *J Geophys Res* 111, D05109.
- Brázdil, R., Budíková, M., Auer, I., Böhm, R., Cegnar, T., Faško, P., Lapin, M., Gajić-Čapka, M., Zaninović, K., Koleva, E., Niedźwiedz, T., Ustrnul, Z., Szalai, S., and Weber, R.O. 1996: Trends of maximum and minimum daily temperatures in Central and Southeastern Europe. *Int J Climatol* 16,765–782.
- Brunetti, M., Buffoni, L., Maugeri, M., and Nanni, T. 2000: Trends of minimum and maximum daily temperatures in Italy from 1865 to 1996. *Theor Appl Climatol* 66, 49–60.
- Ciaranek, D. and Piotrowicz, K. 2014: Stability of thermal conditions in Central Europe. In (Eds.: Kanakidou, M., Mihalopoulos, N., Nastos, P.), COMECAP, 12 International Conference of Meteorology, Climatology and Physics of the Atmosphere, 28-31 May 2014, Heraklion, University of Crete, Greece, 1, 198–203.
- Fortuniak, K., Klysiak, K., and Wibig, J. 2004: Międzydobowa zmienność temperatury powietrza w Łodzi. *Acta Univ Lodz* 89, 35–46 (in Polish, summary in English).
- Frich, P., Alexander, L.V., Della-Marta, P., Gleason, B., Haylock, M., Klein Tank, A.M.G., and Peterson, T. 2002: Observed coherent changes in climatic extremes during the second half of the twentieth century. *Clim Res* 19, 193–212.
- Gough, W.A. 2008: Theoretical considerations of day-to-day temperature variability applied to Toronto and Calgary, Canada data. *Theor Appl Climatol* 94, 97–105.
- IPCC, 2007: Climate change 2007: the physical science basis. Cambridge University Press, Cambridge.
- IPCC, 2014: Climate change 2014. Synthesis Report of the fifth assessment report of the Intergovernmental Panel on Climate Change. WMO.
- Jones, P.D., Briffa, K.R., Osborn, T.J., Moberg, A., and Bergström, H. 2002: Relations between circulation strength and the variability of growing-season and cold-season climate in northern and central Europe. *Holocene* 12, 643–656.
- Kendall, M.G. 1975: Rank correlation methods, 4th ed. Charles Griffin, London.
- Klein Tank, A.M.G., Wijngaard, J.B., Können, G.P., Böhm, R., Demarée, G., Gocheva, A., Mileta, M., Pashiardis, S., Hejkrlik, L., Kern-Hansen, C., Heino, R., Bessemoulin, P., Müller-Westermeier, G., Tzanakou, M., Szalai, S., Pálsdóttir, T., Fitzgerald, D., Rubin, S., Capaldo, M., Maugeri, M., Leitass, A., Bukantis, A., Aberfeld, R., Van Engelen, A.F.V., Forland, E., Miletus, M., Coelho, F., Mares, C., Razuvaev, V., Nieplova, E., Cegnar, T., Antonio López, J., Dahlström, B., Moberg, A., Kirchhofer, W., Ceylan, A., Pachaliuk, O., Alexander, L.V., and Petrovic, P. 2002: Daily dataset of 20th-century surface air temperature and precipitation series for the European climate assessment. *Int J Climatol* 22, 1441–1453.

- Klein Tank, A.M.G., and Können, G.P. 2003: Trends in indices of daily temperature and precipitation extremes in Europe, 1946–1999. *J Climate* 16, 3665–3680.
- Kossowska-Cezak, U. 1987. Duże zmiany temperatury z dnia na dzień a cyrkulacja atmosferyczna. *Przeegl Geofiz* 32(3), 289–302 (in Polish).
- Kossowska-Cezak, U. 1988: Zmienność temperatury z dnia na dzień w warunkach miejskich. *Przeegl Geofiz* 33, 429–439 (in Polish).
- Kossowska-Cezak, U. 2003: Uwarunkowania cyrkulacyjne dużych zmian temperatury powietrza z dnia na dzień w Warszawie. *Prace Geograficzne PAN* 188, 33–52 (in Polish).
- Kossowski, J. 1970: Zmienność z dnia na dzień maksymalnej i minimalnej temperatury powietrza w Lublinie w latach 1951–1960. *Annales UMCS B* 25(6), 159–174 (in Polish).
- Kożuchowski, K., Degirmendžić, J., Fortuniak, K., and Wibig, J. 2000: Trends to change in seasonal aspects of the climate in Poland. *Geogr Polonica* 73, 7–24.
- Lewińska, J. 1996: Geneza i rozwój miejskiej wyspy ciepła w Krakowie oraz możliwości jej minimalizacji. *Folia Geogr ser Geogr-Phys* 26-27, 75–87 (in Polish).
- Lorenc, H. 2007: Zmienność i tendencje maksymalnej i minimalnej temperatury powietrza w Warszawie w okresie 1897–2002. *Wiad IMGW* 51 (4), 3–32 (in Polish).
- Matuszko, D., Piotrowicz, K., and Kowanetz, L. 2015: Klimat. In (Eds.: Baścik, M., Degórska, B.) Środowisko przyrodnicze Krakowa. Zasoby – Ochrona – Kształtowanie, 2nd edn. IGI GP UJ, Kraków, 81–108 (in Polish, summary in English).
- Merecki, R. 1903: Nieokresowa zmienność temperatury powietrza. *Kosmos* 28, Lwów (in Polish).
- Moberg, A., Jones, P.D., Barriendos, M., Bergström, H., Camuffo, D., Cocheo, C., Davies, T.D., Demarée, G., Martin-Vide, J., Maugeri, M., Rodriguez, R., and Verhoeve, T. 2000: Day to day temperature variability trends in 160- to 275-year-long European instrumental records. *J Geophys Res* 105, D18.
- Moberg, A., and Jones, P.D. 2005: Trends in indices for extremes in daily temperature and precipitation in Central and Western Europe analyzed 1901–1999. *Int J Climatol* 25, 1149–1171.
- Olejniczak, J. 2003: The day to day variability of air temperature in Cracow and its surroundings. *Prace Geograficzne IGI GP UJ* 112, 93–103.
- Piotrowicz, K. 2010: Seasonal differentiation of maximum and minimum air temperature in Cracow and Prague in the period 1836–2007. In: *The Polish Climate in the European Context: An Historical Overview*, 407–421.
- Rebetez, M. 2001: Changes in daily and nightly day-to-day temperature variability during the twentieth century for two stations in Switzerland. *Theor Appl Climatol* 69, 13–21.
- Tam, B.Y. and Gough, W.A. 2012: Examining past temperature variability in Moosonee, Thunder Bay, and Toronto, Ontario, Canada through a day-to-day variability framework. *Theor Appl Climatol* 110, 103–113.
- Tam, B.Y., Gough, W.A., and Mohsin, T. 2015: The impact of urbanization and the urban heat island effect on day to day temperature variation. *Urban Climate* 12, 1–10.
- Trepińska, J. 1990: Patterns of formation of air pressure and air temperature tendency in Europe (20th century). In (Ed. Brázdil, R.). *Climatic change in the historical and the instrumental periods*, Brno, 208–210.
- Trepińska, J. 1997: Wahania klimatu w Krakowie (1792–1995). IG UJ, Krakow, 1–204 (in Polish, summary in English).
- Wibig, J. and Głowicki, B. 2002: Trends of minimum and maximum temperature in Poland. *Clim Res* 20, 123–133.



# IDŐJÁRÁS

*Quarterly Journal of the Hungarian Meteorological Service  
Vol. 121, No. 2, April – June, 2017, pp. 137–160*

## **Statistical correction of the wind energy forecast at the Hungarian Meteorological Service**

**Helga Tóth<sup>1\*</sup>, Brigitta Brajnovits<sup>2</sup>, and Balázs Renczes<sup>3</sup>**

<sup>1</sup>*Hungarian Meteorological Service,  
Kitaibel Pál u. 1; H-1024 Budapest, Hungary  
E-mail: toth.h@met.hu,*

<sup>2</sup>*MAVIR Hungarian Independent Transmission System Operator Company Ltd.  
Anikó u. 4, H-1031 Budapest, Hungary  
E-mail: brajnovitsb@gmail.com*

<sup>3</sup>*Budapest University of Technology and Economics,  
Department of Measurement and Information Systems,  
Magyar tudósok körútja 2, H-1117 Budapest, Hungary  
E-mail: renczes@mit.bme.hu*

*\*Corresponding author*

*(Manuscript received in final form, March 10, 2017)*

**Abstract**— In order to efficiently integrate renewable energy sources – the production of which can be planned harder – in the energy grid, quite accurate forecasts are needed. Especially in Hungary, where energy storage is yet an unsolved problem. The limited ability of wind forecast means that the delivered power of the wind farms cannot be predicted with sufficient accuracy. This work focuses on the improvement of wind power forecast precision by using different statistical methods. In the first part of the paper, simple BIAS correction approaches and more complex ensemble based methods are applied to improve the power prediction for the whole country. The second part of the work focuses on enhancement of the wind power forecast of a single wind farm. While mostly only wind speed is taken into consideration for the calculation of the generated power, it is shown that air density is also an important factor in the equations. Autoregressive filtering is launched in order to show that wind speed and power forecasts can also be improved by this kind of statistical method.

*Key-words:* wind power, numerical weather prediction; statistical correction, quantile regression, analog ensembles, characteristic curves, fuzzy model, autoregressive filtering

Paper is based on the presentation delivered at Meteorological Scientific Days held on 19–20 Nov, 2015 entitled „Meteorological aspects of use of renewable energies”.

## 1. Introduction

Nowadays it is a crucial question to use renewable energy all over the world and to integrate it to the electricity network. Due to huge energy demand in the 20th century, the depletion of conventional energy sources (e.g., fossil oil, natural gas), and the increasing CO<sub>2</sub>-emission, wind energy, as renewable energy source, has become of increasing importance. In the last decades, the world's wind energy utilization exploded. While in 1996 only 6 GW built-in capacity was in operation, by 2015 this value has exceeded 433 GW, and the wind energy industry is set to grow by another 60 GW in 2016 (*Global Wind Energy Council*, 2016). The European Union is also committed to use renewable energy sources. The latest revised RES-E directive in 2016 sets out the EU target of at least 27% for the renewables in the final energy consumption by 2030 (*European Commission*, 2016). In 2014, 195.8 Mtoe (Million of tonnes of oil equivalent) renewable primary energy was produced in the EU-28 area. The share of the energy sources were the following: biomass and waste 63.1%, hydropower 16.5%, wind 11.1%, geothermal 3.2%, solar 6.1% (*Eurostat*, 2016). The Hungarian production was 2.05 Mtoe for renewable primary energy, and the share of the sources are: Biomass and waste 89.2%, Geothermal 6.3%, Wind 2.8%, Hydropower 1.3%, Solar 0.5% (*Eurostat*, 2016). In spite of many advantages, the users of 'green energy' are also facing several unresolved problems. Critics of wind power argue that the intermittent energy production of the turbines has a negative effect on the security of the power system. The limited ability of the forecast of wind eventuates that the delivered power of wind farms cannot be forecasted with sufficient accuracy. As a consequence, to ensure secure system operation, the energy supplied by wind should only have a limited proportion in the total electricity production. In the last few decades, fluctuations could easily be regulated, but since the wind energy has gained higher proportion in the power system, these uncertainties cannot be ignored any longer.

In Hungary, currently there is no scope for wind power expansion. In 2006, the Hungarian Energy and Public Utility Regulatory Authority limited the wind power capacity to 330 MW. This value seemed to be sufficient that time, but 329 MW was built in by 2011, so practically no more installation is possible at the moment. The current political and regulatory environment in Hungary does not allow installing new wind power plants. For capacity expansion, a more precise predictability of wind power would be elemental. Nowadays, several methods are being investigated in order to ensure this issue, such as the energy storage. By means of this, in case of oversupply, a battery can be charged, and the stored energy can be used, when undersupply occurs (*Hartmann*, 2012). Another area is the prediction of the generated wind power. Statistical data mining approach was applied for wind farm power prediction (*Kusiak*, 2009). Another possible way is to use numerical weather prediction (NWP) models. However, NWP models forecast the wind speed and direction values, the system operator needs wind power data. To overcome this problem, neural networks are generally

constructed (*Barbounis et. al*, 2006). Another approach is to calculate the characteristic curve between wind speed and wind power, by means of, e.g., the bin method or regression (*Llombart et. al*, 2005).

The production of wind energy strongly depends on weather, resulting that its planning is very difficult. It is an important task for the meteorologists to prepare the most accurate forecasts for the target users. The goal for the Hungarian Meteorological Service (OMSZ) is to adapt and develop algorithms connected to the calculation of power energy for wind, solar, and water resources. The operational usage is also important and expected.

This work focuses on the forecast of the wind power and on the improvement of its precision by using different methods. In Hungary, the power production has to be given for two days ahead, and for this horizon, meteorological forecasts have certainly to be used to achieve the desired accuracy. The aim of this work is to ensure the possibly most accurate forecast using meteorological data.

In the first part of this work, statistical correction of wind power forecast is shown, which is summarized for all wind power stations in Hungary for the Hungarian Transmission System Operator Ltd (MAVIR). Simple BIAS correction approaches (*Sweeney and Lynch*, 2011), like short term rolling trend (STT), short term rolling bias (STB), composite forecast (COM) are applied to correct the wind power predictions, without real access.

Quantile regression (QR) and analog ensemble (AnEns) methods (*Alessandrini et al.*, 2014) were also applied to gain probabilistic information from a deterministic model. The expectation was that not only additional information can be generated, but the final result would mean a more accurate prediction than that obtained with a single model run.

The second part of the paper focuses on improving of the wind power forecast of a single wind farm. It is shown that not only wind speed, but also air density is an important influencing parameter of wind power production. Air density has already been taken into consideration in former works (*Rizwan et. al*, 2012; *Farkas*, 2011), calculating the characteristic curve from two separate inputs. In this work, the wind speed is normalized with the air density as suggested in *IEC 61400-12-1* (2005), so the characteristic curve is determined from one input parameter, keeping the model simpler. Results can also be improved by applying statistical methods, as autoregressive modeling (*Collomb*, 2009).

## 2. Data and methods

The kinetic energy of the wind, can be calculated by  $E$  formula:  $E = \frac{1}{2}mv^2$ , where  $m$  is the air mass,  $v$  is the wind speed. Assuming a constant wind speed, the quantity of air flowing through an area  $A$ , which is perpendicular to the wind direction can be given by:

$$A = \frac{m}{\rho vt}, \quad (1)$$

where  $\rho$  denotes the air density, and  $t$  is the time. The power is the time derivative of kinetic energy:

$$P_0 = \frac{dE}{dt} = \frac{E}{t} = \frac{1}{2} \rho A v^3. \quad (2)$$

For standard atmosphere (temperature of 273 K and pressure of 1013 hPa), the power can be calculated using the following equation:

$$\frac{P_0}{A} = 0.647 v^3. \quad (3)$$

From this equation, two consequences follow. First, wind has low power density compared to conventional energy sources. Thus, large turbine diameter is needed in order to get sufficiently high power density (*Hunyár et al.*, 2001). On the other hand, the equation is strongly non-linear, which may lead to significant error in the later prediction that is based on the wind speed. The first issue is further augmented by the Betz's law (*Betz*, 1966), i.e., the maximum amount of power supply  $P_w$  is:

$$(P_w)_{max} = \frac{16}{27} A \frac{\rho}{2} v^3 \quad (4)$$

However, real wind power plants cannot produce arbitrarily large power. On the other hand, under and above given wind speeds, no power can be obtained – these are called cut-in and cut-out speed, respectively. The characteristic curve is illustrated in *Fig. 1*.

Furthermore, wind speed varies with the height. This can be calculated by:

$$v_h = v_{10} \left( \frac{h}{h_{10}} \right)^n, \quad (5)$$

where  $v_{10}$  is the velocity at height  $h_{10} = 10 \text{ m}$ ,  $n$  is the so-called Hellmann exponent, which is different above dry land and sea, and also depends on the topography.

Meteorological forecasts do not provide the value of wind power, which is the most important parameter for system operator. Their outputs are wind speed, temperature, relative humidity, etc. However, these data can be used to determine the produced wind power.

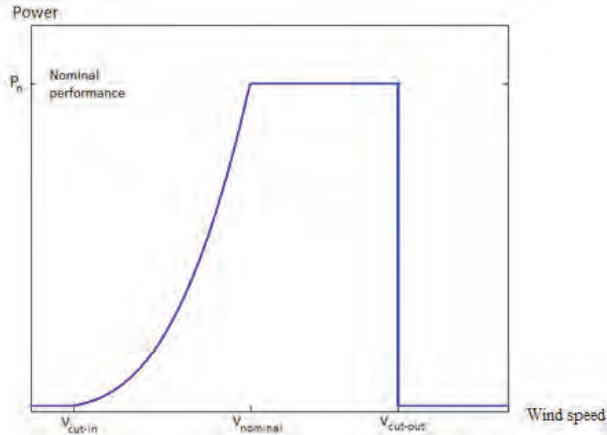


Fig. 1. Wind turbine performance as a function of wind speed (Hunyár et al, 2001).

The maximum obtainable power of wind turbines depends on several parameters (Eq. (4)). The most important of these is certainly the wind speed. Thus, mostly the wind power – wind speed ( $P-v$ ) characteristic curve is given by manufacturers. However, according to Eq. (2), also air density plays an important role. This effect will be investigated later.

In practice, the shape of a characteristic curve is slightly different from that of Fig. 1, since it is sigmoid-shaped – curves for different turbines are given in Fig. 2. Furthermore, real power curves are significantly different from those of given by manufacturers, so determination of the real characteristic curve is crucial in order to give precise schedule.

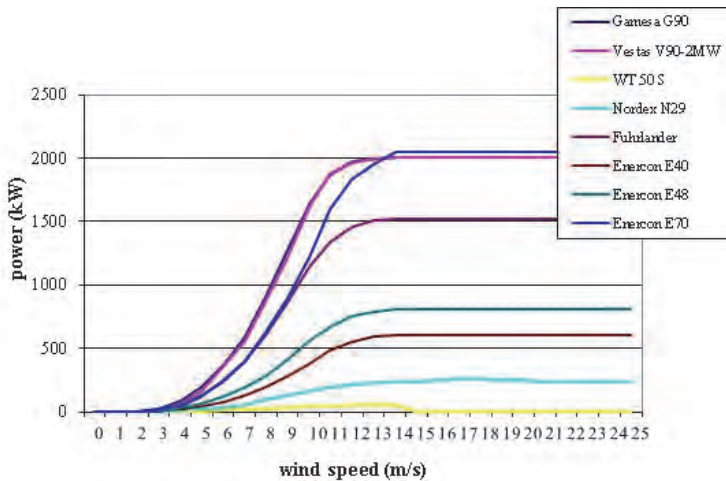


Fig. 2. Characteristic curves of different turbines.

To calculate power using the characteristic curves, wind speed forecast is needed on the hub height. The wind speed forecasts are provided by the AROME non-hydrostatic numerical weather prediction model (Szintai *et al.*, 2015) with 2.5 km horizontal and 15 minutes temporal resolution over the Carpathian domain (Fig. 3).

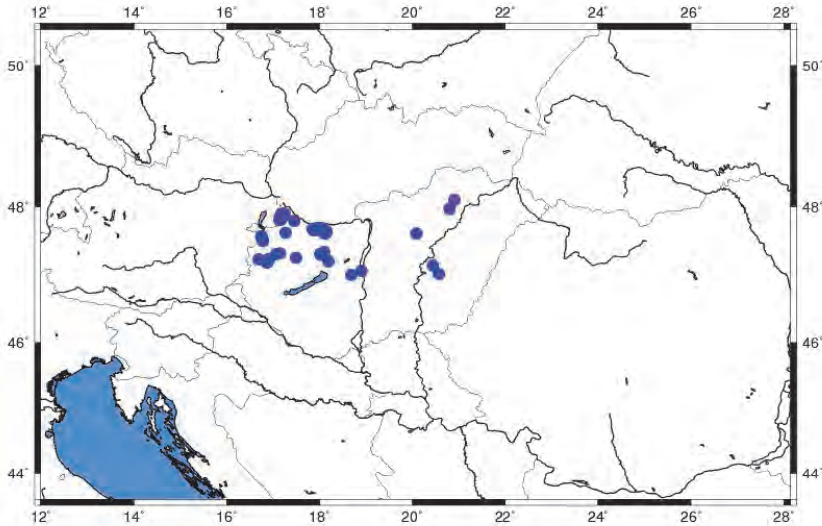


Fig. 3. Domain of the AROME model as run operationally at OMSZ. Blue dots are wind power plants in Hungary.

The predicted wind speed is vertically interpolated to hub height, and horizontally to turbine position. From the individual wind speed values, power productions are calculated with a simple transformation of the characteristic curves. MAVIR gets the summarized power estimation of the 172 Hungarian tubes (Fig. 3 and Table 1). Most of the wind power stations belong to 2 MW installed capacity and locate in the north western part of the country.

Forecasts are valid for +3–39 hours with 15 min temporal resolution, and are prepared 4 times a day (00 UTC, 06 UTC, 12 UTC, and 18 UTC). The system operator is able to use the latest wind power estimations for the planning in the next hours/day, and he/she is able to control the uncertainties of the wind power depending on the weather conditions (Fig. 4).

Table 1. Most important parameters of wind farms in Hungary (MEH, 2015)

Type of wind turbine	Number of pieces	Nominal capacity of turbine [MW]	Rotor height [m]
Enercon E40	7	0.6	78
Enercon E48	5	0.8	75
Enercon E70	5	2.0	100
Fuhrlander MD77	2	1.5	100
Gamesa G90	91	2.0	100
Nordex N29	1	0.3	50
Repower MM 82	12	2.0	100
Vestas V27	1	0.23	32
Vestas V52	1	0.8	86
Vestas V90 – 1.8 MW	2	1.8	105
Vestas V90 – 2 MW	36	2.0	100–105
Vestas V90 – 3 MW	8	3.0	100
WT 50 S	1	0.05	24

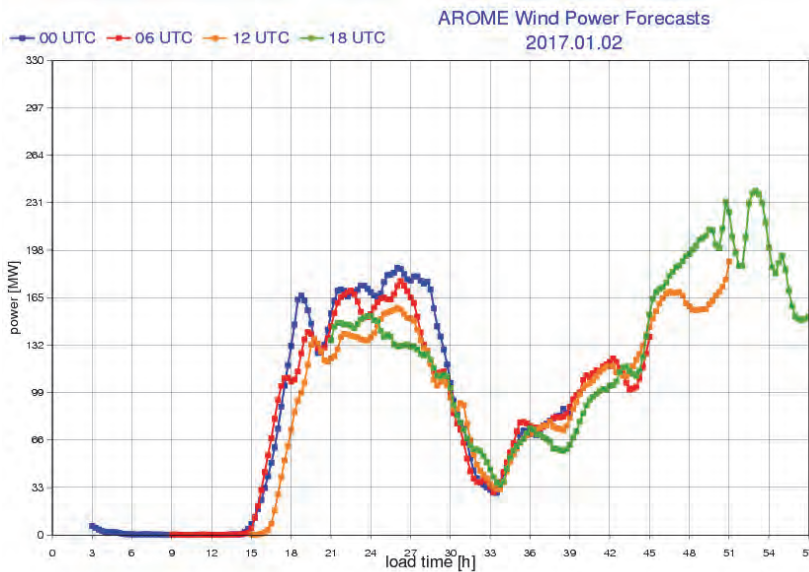


Fig. 4. AROME wind power forecast for Hungary (blue: 00 UTC, red: 06 UTC, orange: 12 UTC, green: 18 UTC forecasts).

MAVIR expects that the power forecasts should be as precise as it is possible, and the mean absolute error (MAPE) should not exceed 5%:

$$MAPE = \frac{1}{n} \sum_1^n \left| \frac{P_{me} - P_{mo}}{P_{me}} \right| * 100 \% , \quad (6)$$

where  $P_{me}$  means the power measurement and  $P_{mo}$  denotes the modeled value. In real purposes this expectation is unrealistic, e.g., the value of  $MAPE$  was 53% in the summer of 2015. Mean relative error (*modeled-measured*) histogram in Fig. 5 shows that the model significantly overestimates the wind power. In 30 % of the cases, the error reaches 100 %. This result seems scary, but most of the forecasted and measured data are relatively small, so the errors are not so large (Fig. 6).

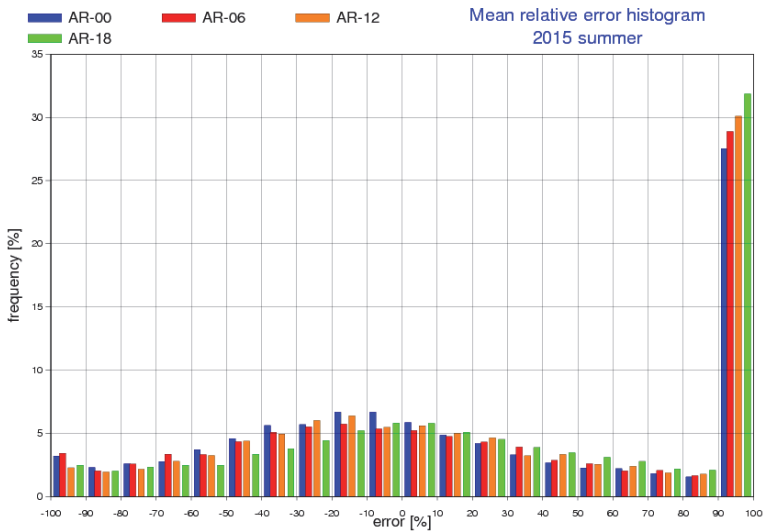


Fig. 5. Mean relative errors of AROME wind power forecast for Hungary for summer, 2015 (blue: 00 UTC, red: 06 UTC, orange: 12 UTC, green: 18 UTC forecasts).

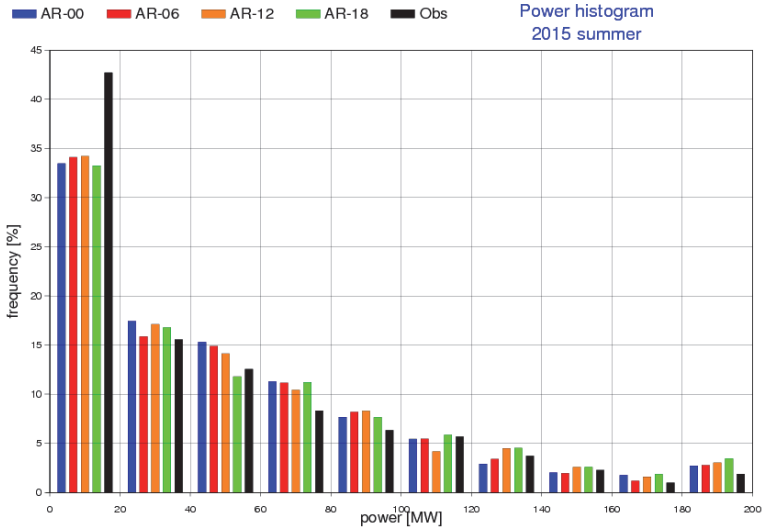


Fig. 6. Forecasted and measured power values for Hungary for summer, 2015 (blue: 00 UTC, red: 06 UTC, orange: 12 UTC, green: 18 UTC forecasts, black: measured).

Wind is a very fluctuating meteorological parameter. Thus, the power also changes rapidly due to the cubic relationship between the two variables (Eq. (2)). Unfortunately, this kind of issue affects also the results of BIAS corrections.

### 2.1. Statistical corrections of wind power forecasts

First of all, simple BIAS correction methods were applied on the summarized wind power forecast valid for the whole country. The power measurements are also available only for the whole country. This makes any kind of statistical correction work less accurate. Some model output statistics were provided with 100 days training period to improve the forecast skill.

Short-term rolling trend (STT) correction calculates the average errors for every time step over the previous 28 days (Sweeney and Lynch, 2011). Then the method corrects the raw forecast values with the computed ones at every time steps. Short-term rolling bias (STB) computes the average error of the previous 3 days, and corrects the original forecasts with this single value. Composite method (COM) is given by the sum of weighted STT, STB, and simple BIAS corrections.

Secondly, quantile regression (QR) and analog ensemble (AnEns) were applied to get probability information based on deterministic forecast using statistical approach. QR was provided to generate a set of the wind power predictors. 19-member ensemble forecasts were based on the AROME model from quantile 0.05 to 1 by step 0.05. QR can be carried out for a random variable  $Y$  as follows:

$$Q(\tau) = \beta_0(\tau) + \beta_1(\tau)x_1 + \beta_2(\tau)x_2 + \dots + \beta_p(\tau)x_p, \quad (7)$$

where  $x_p$  are the  $p$  known regressors,  $\beta_p(\tau)$  are the coefficients for the  $\tau$ th quantile and  $\tau$  is the probability of finding values of  $Y$  below  $Q(\tau)$ . The coefficients for each quantile might be gained throughout a learning period. In our case, the total dataset is one-year-long (July 2012 – August 2013), therefore both the training period and the test period are half-year-long. Similarly to the work in *Alessandrini et al.* (2014), wind speed, wind direction, and forecast leadtime had been used as predictors, testing which can probably be neglected. Thus, four setups have been tried, in two of them forecast leadtime was used as predictor (wind speed and leadtime, then wind speed, wind direction, and leadtime as predictors). The coefficients for each quantile had been trained, and for the other two setups (wind speed, and wind speed and wind direction as predictors) not only each quantile but every leadtime had their own coefficients.

The analog ensemble technique is based on the work of *Alessandrini et al.* (2014). It was originally applied for ensemble forecasts, but can also be used with deterministic forecasts (*Delle Monache et al.*, 2012). The method, as its name suggests, searches for the closest  $N$  analogues to each forecast leadtime's prediction in the training period. These  $N$  members are the ensemble members for the given leadtime. In our case, the program searches for analogous wind speeds and wind directions in the training period, and extracts the corresponding power measurement. The general metric used to search for the best analogue for the current forecast is as follows:

$$\|F_{t'}, A_{t'}\| = \sum_{i=1}^{N_v} \frac{w_i}{\sigma_{f_i}} \sqrt{\sum_{j=-\tilde{t}}^{\tilde{t}} (F_{i,t-j} - A_{i,t+j})^2}, \quad (8)$$

where  $F_{t'}$  is the forecast that we search the  $A_{t'}$  analogue for in the past at time  $t'$ .  $N_v$  is the number of physical variables and  $w_i$  are their weights, while  $\sigma_{f_i}$  is the standard deviation of the past forecasts of the given variable for the selected location (*Alessandrini et al.*, 2014). As the number of ensemble members should be the square root of the number of training days, we chose the first 15 analogues, gaining a 15-member EPS.

## 2.2. Corrections of a single wind farm data

### 2.2.1. Fitting the $P$ - $v$ curve with fuzzy model

Measured data of two turbines (600 kW E40 and 2 MW E70) are available from May 2010 to June 2011, containing wind speed, wind direction, and wind power with the time resolution of 10 minutes. For fitting of the  $P$ - $v$  characteristic curve, a cluster estimation method is applied (Chiu, 1994). This method can deal with more input parameters, so not only wind speed, but, e.g., wind direction can be handled. In this work, however, only wind speed is considered as input in order to keep our model as simple as possible.

The model assumes that in the investigated multi-dimensional function, different groups can be created that behave similarly. For wind turbines, at low speeds the output power is zero, and at high speeds (but lower than the cut-out speed) it equals to the nominal performance of the turbine. The center of these groups can be calculated, and these centers characterize the groups accurately. The applied fuzzy method implements the principle of Sugeno and Tanaka, 1992. In this case, the model will be able to describe a complex behavior with only a few rules. Using this approach, the characteristic curve fitting can be executed.

### 2.2.2. Consideration of air density

Most power forecasting methods take only wind speed into consideration. However, Eq. (4) clearly shows that the maximum obtainable performance is the linear function of air density. Certainly, the most important parameter is the wind speed, but only a few percent of improvement can be crucial for the system operator (who wants to ensure system stability) and the turbine operator (whose aim is to minimize the regulatory surcharge to be paid).

Fig. 7 shows the effect of air density on the produced power. Usually the higher the air density, the higher the generated power (at the same wind speed). However, there are some exceptions, since the power of the wind is determined by several parameters that were not investigated in this work, e.g., by the distribution of the wind speed in the 10 minutes interval.

The international standard of wind power measurements also deals with the effect of air density. For pitch regulated wind turbines it specifies the following normalization:

$$v_n = v_{10min} \sqrt[3]{\frac{\rho_{10min}}{\rho_0}}, \quad (9)$$

where  $v_n$  denotes the normalized wind speed,  $v_{10min}$  and  $\rho_{10min}$  are ..... the measured wind speed and air density averaged over 10 minutes, while  $\rho_0$  is the reference air density (IEC 61400-12-1, 2005).

Wind speed forecasts created by OMSZ have 15 minutes temporal resolution. Thus, these data had to be interpolated in order to ensure the same resolution for both datasets. It has to be mentioned that there were no air density data measurements, so the training can only be performed using the forecasted values. However, parameters determining air density (temperature, air pressure, humidity) can be forecasted more precisely than wind speed.

Due to the high computational demand, air density data were only determined for two weeks, one week in June 2010 and one week in February 2011.

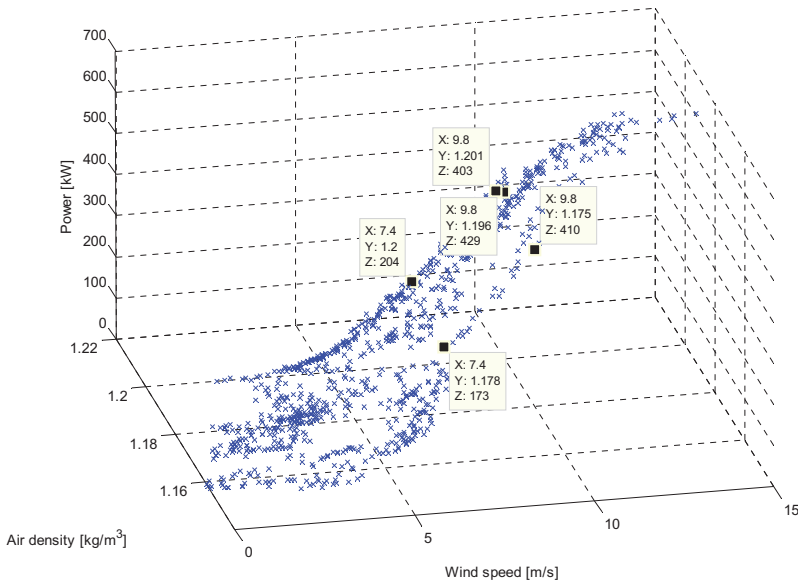


Fig. 7. The effect of air density on the generated power.

### 2.2.3. Autoregressive filtering of wind speed forecast

In this section, wind speed prediction is processed by autoregressive filtering. First of all, the definition of an autoregressive process is given. If  $X_n$  can be calculated as:

$$X_n = a_1 X_{n-1} + a_2 X_{n-2} + \dots + a_p X_{n-p} + \xi_n, \quad (10)$$

where  $a_i$  is real and  $\xi_n$  is white noise, then  $X$  is an autoregressive process of order  $p$ . The autoregressive process is stationary, i.e.,  $a_i$  is constant in time. Consequently, it has to be declared that although the method can model atmospheric processes, it can only describe an ‘average’ behavior. Thus, it will be

unable to follow the unique nature of the atmosphere at a given time. Nevertheless, the algorithm is expected to reduce the mean squared error.

To determine the coefficients  $a_i$ , the output is given as  $y_n = -\sum_{i=1}^p a_i y_{n-i}$ . This formula is similar to Eq. (10), the difference is the sign of the coefficients. This description is useful, because this way an IIR (infinite impulse response) filter can be created with a transfer function of:

$$H(z) = \frac{1}{A(z)} = \frac{1}{1 + a_1 z^{-1} + \dots + a_p z^{-p}}. \quad (11)$$

The other difference is that this description does not contain noise, so the output can only be approximated with an error. The coefficients have to be determined so that the mean squared error is minimal:

$$\sum_{n=-\infty}^{\infty} \left[ y_n - \left( -\sum_{i=1}^p a_i y_{n-i} \right) \right]^2 = \sum_{n=-\infty}^{\infty} \left( y_n + \sum_{i=1}^p a_i y_{n-i} \right)^2. \quad (12)$$

The error is minimal if we solve the following system of equations:

$$\forall j \in [1, k], \sum_{i=1}^k a_i R_{|j-i|} = 0 \quad (13)$$

where  $R$  is the autocorrelation function (Collomb, 2009). This system of equations can be solved using the Levinson-Durbin algorithm that computes the coefficients recursively.

To determine the coefficients of the autoregressive filter, a training set is needed to obtain the correlation coefficients. Furthermore, the order of the model is also to be determined. If the model is high-order, old data distort the output, while if too few number of coefficients are used, important details might not be taken into consideration. Analyzing the data, the model order was chosen so that data from the last 24 hours is used. Considering the 10 minutes resolution, this means that 144 coefficients were to be calculated. The training dataset was the wind speed measurements from April 2011.

### 3. Results and discussion

#### 3.1. Statistical correction of wind power forecast

##### 3.1.1. Simple methods

Test period was chosen from March 12, 2012 to July 31, 2012 to validate the simple lead time BIAS, STT, STB, and COM corrections. As it can be seen in Fig. 8, none of the methods have been able to improve the forecast at a given day significantly. In one case one method was more effective, while in another case the different one. For longer period, all kind of methods resulted in similar statistics (*MAPE, RMSE, BIAS*).

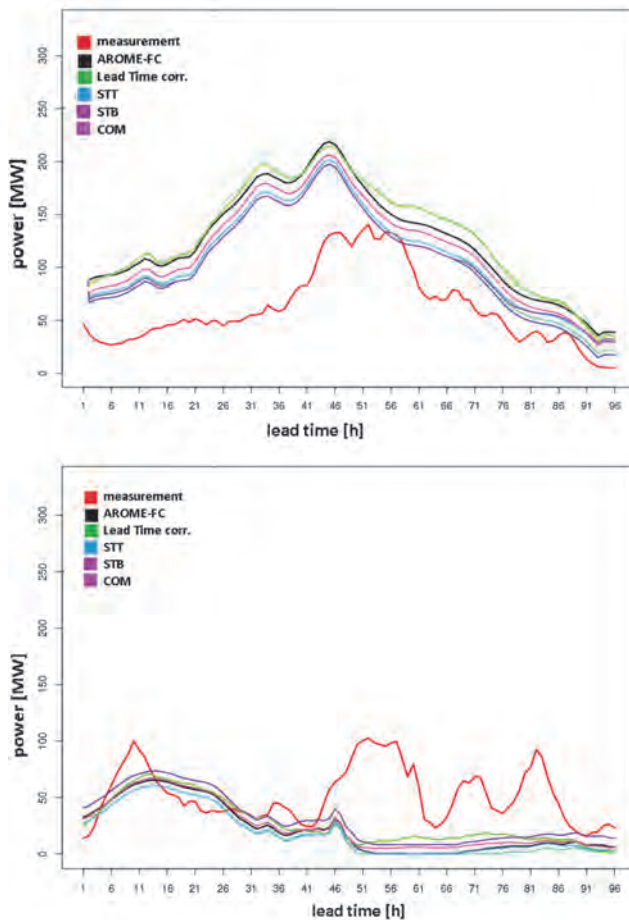


Fig. 8. Wind power measurement, forecast and BIAS corrected forecasts for some selected days.

### 3.1.2. Ensemble based methods

QR and AnEns were applied for the period of July 2012 – August 2013 based on AROME deterministic forecast. During the verification, BIAS and RMSE have been produced. This allows us to compare the results with those obtained by the higher resolution deterministic model, AROME, with the previously mentioned processes (QR and AnEns). These scores are shown for the EPS mean, median, and for AROME, as well as for the standard deviation of EPS members. In order to show, how good a probabilistic forecast is, several scores can be examined, some of them are (Alessandrini *et al.*, 2014):

- reliability diagram,
- rank histogram,
- spread Skill Plot,
- continuous ranked probability score (CRPS).

In the figures of BIAS (*Fig. 9*), basically three things can be observed:

- 1) the AROME's forecast is clearly better than the others,
- 2) the BIAS gets slightly larger when including leadtime as predictor,
- 3) the BIAS of AnEns's is concurrent with the BIAS of AROME (especially that of the median).

Of course that has to be set against RMSE, which may be seen in *Fig. 10*. We can state that:

- 1) There is no concurrence the AROME's forecast. The RMSE of AROME is about half of the others.
- 2) The RMSE of QR is slightly better, when wind speed and leadtime are used as predictors.
- 3) The correlation between the RMSE and the standard deviation of the eps members is high.
- 4) The RMSE of QR and AnEns medians are much worse than QR and AnEns means.

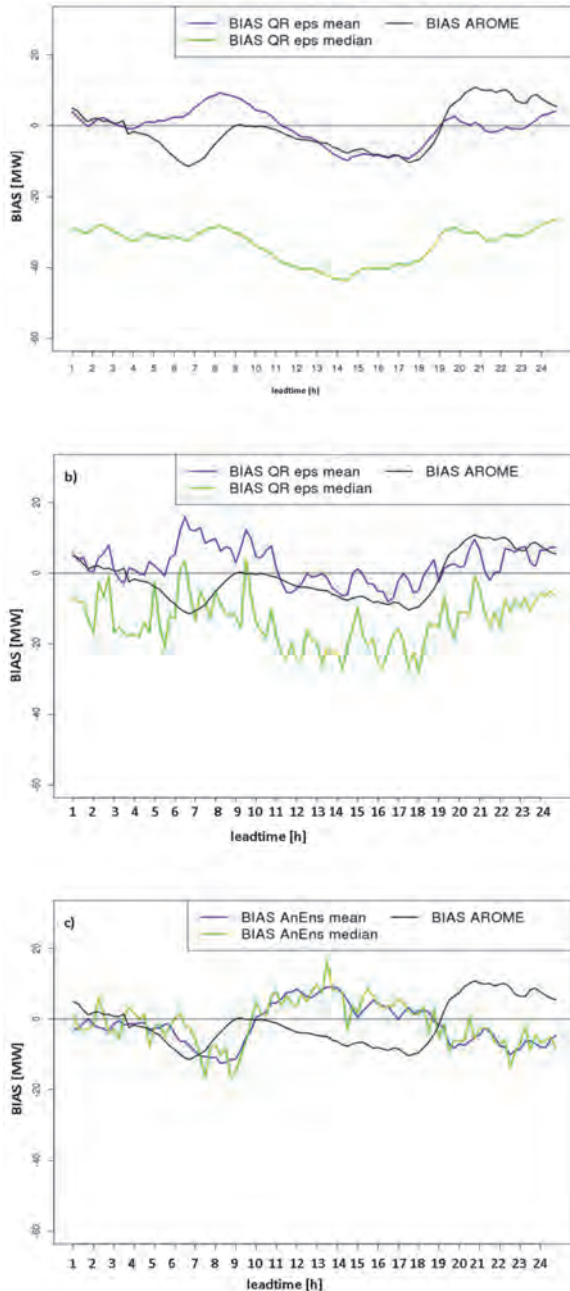


Fig. 9. a) The BIAS of the mean and median of the eps obtained by quantile regression with wind speed as predictor, b) the BIAS of the mean and median of the eps obtained by quantile regression with wind speed and leadtime as predictors, c) the BIAS of the mean and median of the eps obtained by analog ensemble and AROME as the function of leadtime.

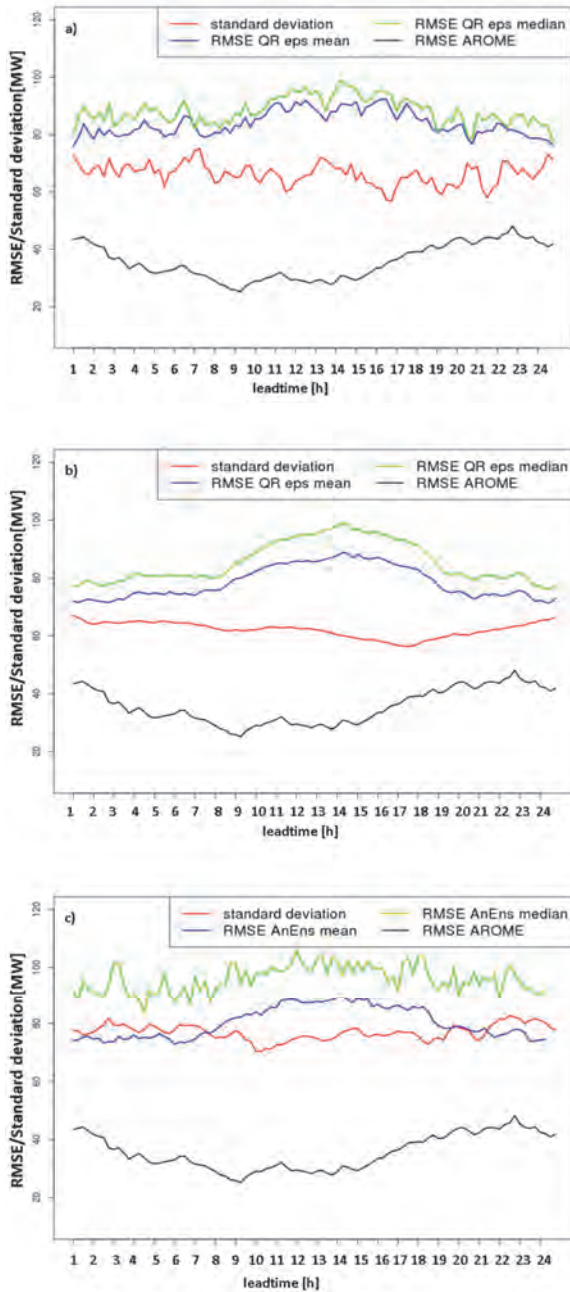


Fig. 10. a) The RMSE of the mean and median of the eps obtained by quantile regression with wind speed as predictor, b) the RMSE of the mean and median of the eps obtained by quantile regression with wind speed and leadtime as predictors, c) the RMSE of the mean and median of the eps obtained by analog ensemble and AROME as the function of leadtime.

In order to get more information about the probabilistic forecast, a number of indicators can be examined, e.g., the rank histogram (*Fig. 11*). This is a diagnostic tool to evaluate the spread of ensemble. The assumption is that all members are distributed with the same probability of occurrence of the observations within each bin. Usually the rank histograms show U-shape, so the spread of the members are not big enough, as it happens on the rank histogram of QR, when only the wind speed was used as predictor (*Fig. 11. a*). Using AnEns gives the best result, because it shows a little less equality between the bins (*Fig. 11. c*).

### 3.2. Corrections of a single wind farm data

#### 3.2.1. Fitting the P-v curve with fuzzy model

The fuzzy model was trained in order to determine the relationship between the wind speed and the generated power. Measured data were available from May 2010 to June 2011. The first training set was a two-month-long data set (May and June 2010).

Fitting the function on all data points would obviously distort the result significantly. However, two simple rules can filter out outliers marked in *Fig. 12*. The first rule prescribes that above the cut-in speed, output values lower than a given value are ignored. For the second rule, it can be observed that at about 5 m/s, zero output was measured many times. A possible reason for that may be the power plant maintenance. This rule filters out data points, at which lower than 3.5 kW power was measured at higher than 3 m/s wind speed. The other rule takes into consideration that beyond the nominal wind speed, the output should be roughly constant. The saturation performance is 619 kW. Thus, according to this rule, above 14 m/s power supply, values lower than 610 kW are outliers.

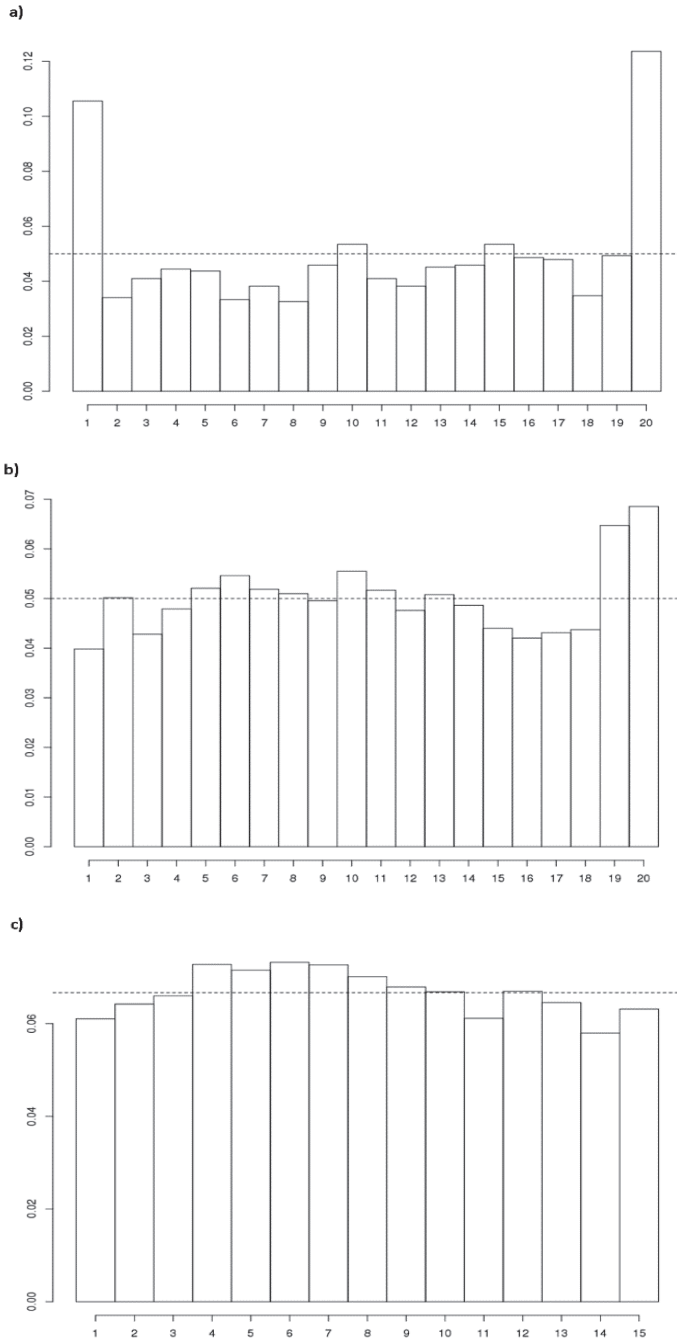
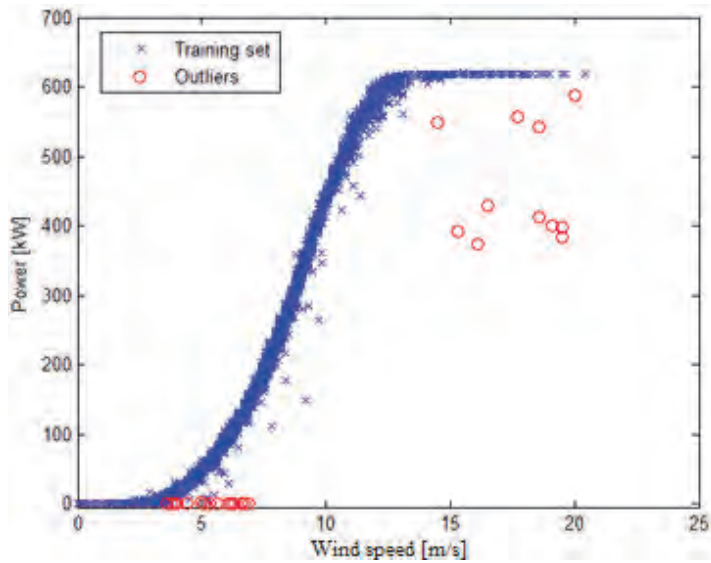


Fig. 11. Rank histograms of QR in case a) when wind speed and b) when wind speed and leadtime were used as predictors. c) Rank histogram of AnEns.

However, *Fig. 12* shows that these rules do not eliminate all of the outliers. In order to filter these points out, a preliminary fit is needed without data points filtered out previously. After that, data points that differ from the model output with more than 10% are to be eliminated. The resulting fitted curve now follows the desired sigmoid-shape.



*Fig. 12.* Training set and the outliers (May and June, 2010).

This fit can be executed for data of different seasons. For both winter and summer, two months were selected as training set. It became evident that the resulting curves are significantly different (see *Fig. 13*). The difference at the two investigated wind speeds is about 5% in both cases. This is problematic, because characteristic curves are mostly considered as static. Furthermore, catalogue data differ from both curves, resulting that they cannot be used for precise forecasting.

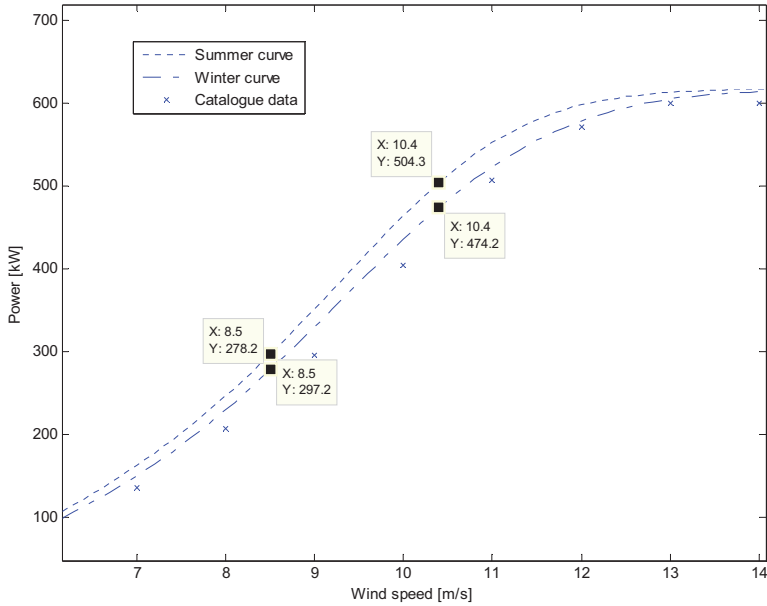


Fig. 13. Fitted curves in summer and winter (2010 and 2011), and catalogue data.

### 3.2.2. Consideration of air density

Curve fitting, using the normalized wind speed data of Section 2.2.2 showed that at low and high wind speeds, there was no significant difference to observe. Contrarily, at medium speeds, the difference is about the 5% of Section 3.2.1. It is obvious again that catalogue data cannot be used for precise forecasting. The difference between the two unnormalized curve is  $108.5 \text{ kW}^2$ , while for normalized curves this value is only  $21.6 \text{ kW}^2$  (Fig. 14), which means that the mean squared error (MSE) is reduced to the fifth of its original value, where MSE is:

$$MSE = \frac{1}{N} \sum_{i=1}^N (P_{summer,i} - P_{winter,i})^2. \quad (14)$$

According to these results, it seems that one of the error sources that cause the difference between the curves is the air density.

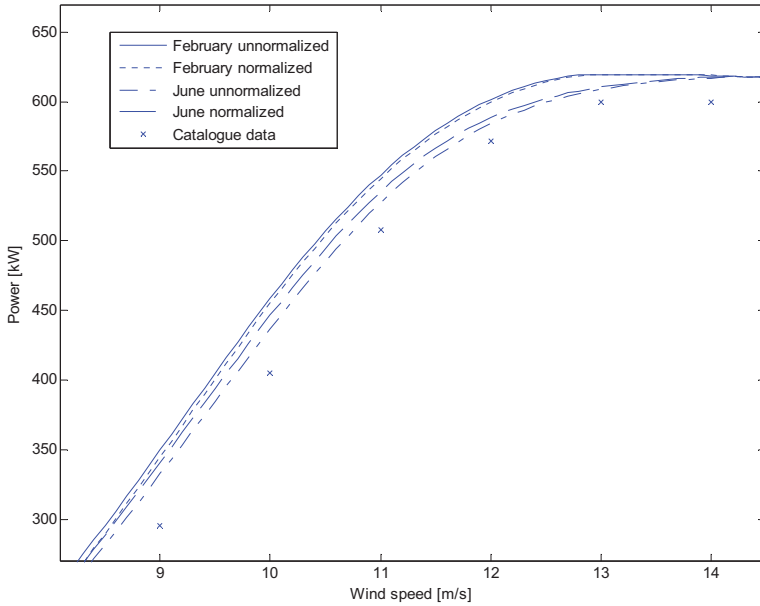


Fig. 14. Fitted power curves and catalogue data.

### 3.2.3. Autoregressive filtering of wind speed forecast

The IIR-filtering on the data given by the OMSZ was performed with the coefficients calculated with the method described in Section 2.2.3. Table 2 contains the results, showing that the MSE of both wind speed and wind power forecasts have been improved by 3–4%. This means that if the filtered data were used as forecast instead of the ‘raw’ meteorological data, these improvements could have been achieved.

Table 1. MSE-improvements using autoregressive filtering

MSE-improvement	June, 2010	February, 2011	April, 2011
Wind speed	3.732%	3.958%	3.015%
Wind power	3.891%	4.387%	3.007%

#### 4. Summary and conclusions

The professionals at MAVIR are responsible for the smooth energy supply of the whole country. Daily plans of the available energies are created for every day with 15 minutes time resolution by the system operator. One segment of this system is the prediction of the generated wind power. The task of meteorologists is to provide the most accurate forecast for the operators and the wind farm owners. The aim of this work was to improve the wind power forecasts.

In this paper, two types of approach were discussed. In the first part, statistical correction of the summarized wind power forecast was shown, which is valid for the whole country. Simple BIAS corrections and more comprehensive ensemble-based methods were applied without real access. None of the methods were able to improve the forecast significantly. Some improvements might be possible in a given day, but the absolute errors became worse for the whole period.

In the second part, we concentrated on the correction of the wind power forecast of a single farm. Investigations showed that the forecasts of the OMSZ follow the real production data well. It was also an important result that the air density should also be taken into account for the calculation of wind power. Namely, this is the parameter that may cause the difference between the characteristic curves in different months.

Another result of this work was that autoregressive filtering may also increase the precision of power forecasting. Using this method, several percent of improvement was achieved, which is significant considering the 5% expectation of the system operator.

Here it was not shown, but it was proven that using meteorological forecasts, much more precise scheduling can be made than by using predictions without physical considerations (data of the previous year, on average production). This would be advantageous for both the system operator and the turbine operators.

This work confirms that the wind energy forecast can be improved in two ways. The first one is to develop the meteorological forecast, so it is very important to create more complex and finer resolution (in horizontal and vertical) NWP models. The second one is using statistical corrections for the individual wind turbines and wind farms, and the sum of corrected values are able to produce more accurate wind power for the operators. This second step seems not realistic, because it is almost impossible to get measurements from all the 172 wind farms, which are necessary for the statistical corrections.

**Acknowledgements:** QR and AnEns were done in the framework of COST Action ES1002 WIRE. The authors would like to thank to the COST STSM host, *Stefano Alessandrini*, for his advices and scripts, to *Simone Sperati* (RSE Spa.) for his loads of help. The 'Improvement of the wind power forecast of a single wind farm' part of the paper is based on MSc thesis 'Study of Wind Turbine Production Forecasting Methods', which was defended at the Budapest University of Technology and Economics in 2013. The authors would like to thank *Professor István Kollár*, *Dr. Bálint Hartmann*, and *Roger Randriamampianina* for their help in writing the thesis. Remarks of the anonymous reviewer which lead to an improvement of the manuscript are greatly acknowledged.

## References

- European Commission, 2016: Proposal for a directive of the European Parliament and of the Council on the promotion of the use of energy from renewable sources (recast). [ec.europa.eu/energy/sites/ener/files/documents/1\\_en\\_act\\_part1\\_v7\\_1.pdf](http://ec.europa.eu/energy/sites/ener/files/documents/1_en_act_part1_v7_1.pdf) (accessed on 8 March 2016)
- Eurostat, 2016: [ec.europa.eu/eurostat/statistics-explained/index.php/Renewable\\_energy\\_statistics](http://ec.europa.eu/eurostat/statistics-explained/index.php/Renewable_energy_statistics) (accessed on 8 March 2016)
- GWEC, 2016: Global wind report. Annual market update 2015. [www.gwec.net/wp-content/uploads/vip/GWEC-Global-Wind-2015-Report\\_April-2016\\_22\\_04.pdf](http://www.gwec.net/wp-content/uploads/vip/GWEC-Global-Wind-2015-Report_April-2016_22_04.pdf) (accessed on 8 March 2016)
- IEC 61400-12-1, 2005: Wind turbines – Part 12-1: Power performance measurements of electricity producing wind turbines.
- MEKH, 2015: Számoló a kötelező átvételi rendszer 2015. évi alakulásáról. [www.mekh.hu/download/1/6a/20000/kotelezo\\_atvetel\\_beszamolo\\_2015.pdf](http://www.mekh.hu/download/1/6a/20000/kotelezo_atvetel_beszamolo_2015.pdf) (accessed on 8 March 2016) (In Hungarian)
- Alessandrini, S., Monache, L.D., Sperati, S., and Niesen, J.N., 2014: A novel application of an analog ensemble for short-term wind power forecasting. *Renew. Energy* 76, pp: 768–781.
- Barbounis, T. G. and J.B. Theocharis, J. B., 2006.: Long-term wind speed and power forecasting using local recurrent neural network models, *IEEE Transactions on Energy Conversion*, 21, 273–284.
- Betz, A. 1966: Introduction to the Theory of Flow Machines. (D. G. Randall, Trans.) Oxford: Pergamon Press.
- Chiu, S.L., 1994: Fuzzy model identification based on cluster estimation. *Intelligent Fuzzy Syst.* 2, 267–278.
- Collomb, C., 2009: Linear prediction and Levinson-Durbin Algorithm, [www.emptyloop.com/technotes/a%20tutorial%20on%20linear%20prediction%20and%20levinson-durbin.pdf](http://www.emptyloop.com/technotes/a%20tutorial%20on%20linear%20prediction%20and%20levinson-durbin.pdf) (accessed on 8 March 2016)
- Farkas, Z., 2011: Considering Air Density in Wind Power Production, *Study*, Eötvös University [arxiv.org/pdf/1103.2198v1.pdf](http://arxiv.org/pdf/1103.2198v1.pdf) (accessed on 8 March 2016)
- Hartmann, B., 2012: Szélérőművek integrálása a villamosenergia-rendszerbe, PhD Thesis Budapest University of Technology and Economics, pp. 110. [repozitorium.omikk.bme.hu/bitstream/handle/10890/1198/tezis\\_eng.pdf?sequence=3&isAllowed=y](http://repozitorium.omikk.bme.hu/bitstream/handle/10890/1198/tezis_eng.pdf?sequence=3&isAllowed=y) (accessed on 8 March 2016) (in Hungarian)
- Hunyár, M., Schmidt, I., Veszprémi K., and Vincze Gy., 2001: A megújuló és környezetbarát energetika villamos gépei és szabályozásuk, Műegyetemi Kiadó, Budapest, 2001
- Kusiak, A., Zheng, H., and Song, Z., 2009: Wind farm power prediction: a data-mining approach. *Wind Energ.* 12, 275–293.
- Llombart, A., Watson, S.J., Llombart, D., J.M. Fandos, J.M., 2005: Power Curve Characterization I: improving the bin method. *Proceedings of the International Conference of Renewable Energies and Power Quality (ICREPQ)*.
- Delle Monache, L., Eckel, F.A., Rife, D.L., Nagarajan, B. and Searight, K., 2012: Probabilistic Weather Prediction with an Analog Ensemble. *Mont. Weather Rev.* 141, 3498–3516.
- Rizwan, M., Saini, S., and Singh, U., 2012: Prediction of wind energy using intelligent approach. *Power Electronics (IICPE), 2012 IEEE 5th India International Conference on.* IEEE
- Sugeno, M. and Tanaka, H., 1992: Successive identification of a fuzzy model and its applications to prediction of a complex system, *Fuzzy Sets Syst.* 42, 315–334.
- Sweeney, C. and Lynch, P., 2011: Adaptive post-processing of short-term wind forecasts for energy applications. *Wind Energ.* 14, 317–325.
- Szintai, B., Szűcs, M., Randriamampianina, R., and Kullmann, L., 2015: Application of the AROME non-hydrostatic model at the Hungarian Meteorological Service: physical parameterizations and ensemble forecasting. *Időjárás* 119, 241–265.

# IDŐJÁRÁS

*Quarterly Journal of the Hungarian Meteorological Service  
Vol. 121, No. 2, April – June, 2017, pp. 161–187*

## **Near-surface wind speed changes in the 21st century based on the results of ALADIN-Climate regional climate model**

**Tamás Illy**

*Hungarian Meteorological Service,  
Kitaibel P. u. 1, H-1024 Budapest, Hungary  
E-mail: illy.t@met.hu*

**Abstract**—This study presents a methodology to assess the climate change impacts on wind conditions and wind energy potential on multiple levels near the surface over the Carpathian Basin and Hungary. The methodology is based on ALADIN-Climate regional climate model results and ERA-Interim re-analysis data.

Since wind energy estimations require wind data in specific hub (turbine) heights, in addition to the 10-meter standard, we evaluate wind speed on 50, 75, 100, 125, and 150 meters above the surface to cover the range of most frequently used hub heights. The main concept of the method is to compute the wind velocity on these levels directly from data on the neighboring model levels instead of extrapolating from the 10-meter wind speed applying a wind profile. Besides giving more accurate velocity values, the use of multiple levels allows us to examine the changes in the vertical profile of near-surface winds as well.

The model results are validated with ERA-Interim re-analysis for the 1981–2000 period. Despite a systematic negative bias, ALADIN-Climate reproduces the main wind characteristics in the Carpathian Basin reasonably. The future projection was carried out considering the RCP8.5 emission scenario and was evaluated for the 2021–2050 and 2071–2100 periods. The projection results show a mild future increase in the average wind speed over most parts of the integration domain. The changes over Hungary are more prominent in 2021–2050 with a slight but statistically significant 7% annual increase. The mean annual change in potential power has similar characteristics, only with higher, 8–13% growth.

As our aim is the demonstration of a methodology, our investigation is based on the outputs of a single climate model simulation, however, to provide some hints about projection uncertainties, we compared our future estimates with further studies which confirmed our main conclusions.

*Key-words:* climate change, ALADIN-Climate, ERA-Interim, regional climate model projections, wind speed, vertical profile, wind energy

Paper is based on the presentation delivered at Meteorological Scientific Days held on 19–20 Nov, 2015 entitled „Meteorological aspects of use of renewable energies”.

## 1. Introduction

To reduce anthropogenic greenhouse gas emissions, the use of renewable energy is highly supported and rapidly growing all around the world. The European Renewable Energy Directive aims at fulfilling 20% of total energy need of the European Union (EU) from renewable sources by 2020 (EU directive, 2009). Wind energy is currently the largest contributor to renewables within the EU with a total installed power capacity of 142 GW and by growing further, it is expected to play a major role in replacing fossil fuels. During 2015, more wind power capacity was installed in the EU than any other form of power generation, and by the end of 2020, the total wind capacity is planned to reach 210 GW which would cover 14% of the total electricity need of the European Union (European Wind Energy Association, 2016). However, due to the high spatial and temporal variability of wind speed, special research and planning must precede investments to assess the potential effectiveness of a given location. For effective future planning, the impacts of climate change must be considered, since it may alter large-scale atmospheric circulations, which can have significant effects on local wind climatology. Numerical models provide a tool for that: Earth-system models simulate the physical processes of the whole climate system (atmosphere, oceans, land surface, cryosphere, and biosphere), while regional climate models (RCMs) serve to downscale the results of global climate models (GCMs) over a specific area of interest. Dynamical downscaling is essential for wind power estimations, because wind speed is heavily influenced by local topography and surface characteristics which are described more precisely in high-resolution regional models.

Researches aiming at exploring the wind climatology of Hungary began based on observational data: in the 1950's, the first National Climate Atlas contained some information about the prevailing winds in our region; shortly after, the first wind tower measurements were launched to assess the available wind energy and the possible options to harness it. In the 1990's, the Department of Meteorology at Eötvös Loránd University started a systematic and detailed analysis of wind-climatological characteristics over Hungary. The WASP software (Wind Atlas Analysis and Application Program, *Mortensen et al.*, 1993) was adapted and used to assess wind speed in different vertical levels above the surface and to determine the modifying effect of the topography and surface roughness to near-surface airflows (*Bartholy and Radics*, 2001). After its validation using tower measurements of Hegyhátsál station, the available wind energy was modeled over the area of Hungary (*Radics*, 2004). The vertical profile of wind velocity was studied by *Varga and Németh* (2004), conducting field measurements with SODAR in four different locations. The frequency distribution and mean value of wind speed were measured in different height levels and used to calculate the average value and diurnal cycle of the Hellmann coefficient. *Szentimrey et al.* (2006) developed a high-resolution gridded wind

dataset of Hungary at 10 m and 75 m height above the surface, using station observations interpolated with the MISH (Meteorological Interpolation based on Surface Homogenized Data Basis, *Szentimrey and Bihari, 2007*) software developed specially for meteorological interpolation. In the framework of an international cooperation, CARPATCLIM project (*Lakatos et al., 2013*), a high resolution ( $0.1^\circ \times 0.1^\circ$  spatial resolution) gridded, homogenized daily observational dataset was produced over the area of the Carpathian Basin including surface wind speed information for 1961–2000. Data from all the available stations were used, the interpolation was performed with MISH and the homogenization was done with MASH (Multiple Analysis of Series for Homogenization, *Szentimrey, 2008*), both methods developed at the Hungarian Meteorological Service (HMS).

Climate re-analyses gave new tools and opportunity to wind power related studies. A 5 km resolution multi-level wind field was produced by *Kertész et al. (2005)* downscaling ERA-40 global re-analyses with ALADIN numerical weather prediction model for the 1957–2002 period. It was performed with three nesting steps, first downscaling the 125 km re-analysis to 45 km, than the 45 km resolution ALADIN fields to a 15 km grid, and finally to the target 5 km spatial resolution. The last step was a short-term model run with a special dynamical adaptation configuration of ALADIN that uses a more detailed topography but simplified parametrization. This method was also applied to refine the results of operational ALADIN wind forecasts to provide more accurate and reliable information required by wind power stations. The results were validated by *Szépszó and Horányi (2010)* against tower observations in 78 m height for a 7-month period. They found that the dynamical adaptation successfully improved the operational forecasts reducing their systematic errors, however, it did not cure the deficiencies in their wind diurnal cycle.

Regional climate model experiments were started in 2005 at the Hungarian Meteorological Service and Eötvös Loránd University in order to assess future climate change in the Carpathian region. Surface wind speed results of ALADIN-Climate, REMO, and PRECIS RCMs were validated by *Szépszó et al. (2007)* finding mainly underestimation of mean wind speed in ALADIN-Climate results and overestimation by the other two models. Evaluation of surface wind data of RegCM RCM was performed by *Péliné (2015)* in an extensive research on wind conditions over Hungary using re-analysis and observational data as reference. Validation and bias correction was performed on the model results using the CARPATCLIM-HU observation dataset. Bias adjusted projection results were also presented focusing on wind extremes and different wind indices. RegCM results showed rather subtle but interesting changes: increasing occurrence of both small and high wind speed extremes with a negligible change of the mean (*Péliné, 2015*). *Illy (2014)* examined the climate change impact on wind conditions and potential wind power in 10 and 100 m height above surface, based on ALADIN-Climate and REMO projection

results considering A1B emission scenario. The 100 m wind speed was extrapolated from the surface using a special wind profile introduced by *Szentimrey et al.* (2006). The changes in wind power were found to be positive but small, under 5 % during all seasons.

The main objective of our study is to present an improved methodological framework (compared to *Illy*, 2014) for assessing near-surface wind speed and wind energy potential in regional climate model results. The method is based on ALADIN-Climate model simulations and ERA-Interim re-analysis data. It aims at evaluating model data in multiple height levels (10, 50, 75, 100, 125 and 150 m) above the surface with minimizing the effects of vertical interpolations and extrapolations. In Section 2, the utilized model and re-analysis datasets are described in addition to the applied vertical interpolation methods. Section 3 contains the validation and projection results regarding wind speed and wind power production on multiple height levels. A brief comparison of projection results with other recent studies can be found in Section 4, and finally, Section 5 closes the article with a short summary and some ideas and future plans that arose while working on the article.

## ***2. Data and method***

### *2.1. Re-analysis data*

Re-analysis datasets contain three-dimensional gridded meteorological information of the atmosphere and the surface, gained from observations and short-term numerical model forecasts. Complex data assimilation methods are used to combine the background model estimation with in-situ and remote sensing observational data, considering the different uncertainties and temporal origins of the different data sources. Re-analyses typically extend over several decades, which makes them a useful tool in climate research and monitoring. Due to the physical consistency of the fields, they are applicable as initial and lateral boundary conditions for limited area numerical models, as well. In our study, ERA-Interim re-analysis was chosen as reference data for the validation of ALADIN-Climate near-surface wind speed results for the period of 1981–2000. ERA-Interim is the current generation of global re-analysis datasets, developed at the European Centre of Medium-Range Weather Forecasts (ECMWF). The observations were compiled with the forecasts of the global model version which was operational in 2006 in ECMWF, applying a 4-dimensional variational data assimilation technique. The temporal coverage of the dataset begins on January 1, 1979, and it is continuously updated in near real-time. Its horizontal resolution is approximately 80 km, and it has 60 vertical levels between 10 m and around 64 km of height above the surface (*Dee et al.*, 2011). In our investigation we applied the following variables:

- $u$  and  $v$  wind components on model levels 56–59 (at 0, 6, 12, and 18 UTC);
- temperature on model levels 56–59 (at 0, 6, 12, and 18 UTC);
- surface pressure (at 0, 6, 12, and 18 UTC).

ERA-Interim model levels are numbered starting from the top of the atmosphere with level 1, and increasing in number towards the surface, which is represented by level 61. The above mentioned levels 56 through 59 are usually located between 220 and 30 meters above the ground with slight temporal variation due to the hybrid vertical levels applied in the forecast model. The use of temperature and surface pressure data was necessary for the interpolation process, by which the wind velocities in given model levels were transformed to specific height levels. The method is presented thoroughly in Section 2.3.1.

## 2.2. Regional climate model data

ALADIN-Climate regional climate model is developed from the ALADIN numerical weather prediction model (Horányi et al., 2006) and the ARPEGE-Climat global climate model (Déqué, 2003). The model dynamics is taken from ALADIN, which is complemented with the physical parameterization schemes of ARPEGE, to be optimized for processes on climate timescales. ALADIN-Climate horizontal coordinate system is designed on Lambert conformal conic projection, and its vertical coordinates are defined by a hybrid pressure-sigma coordinate system. The prognostic variables are the horizontal wind components, the temperature, the surface pressure, and the specific humidity. The model applies hydrostatic approximation, therefore, the vertical velocity is determined diagnostically. The horizontal differential operators are calculated with spectral approximation, and the temporal evolution of prognostic variables is computed with the combination of semi-implicit and semi-Lagrangian schemes. The physical parametrization package is based on that of ARPEGE-Climat. RRTM (Rapid Radiation Transfer Model; Mlawer et al., 1997) scheme is used for calculating the longwave component, and the *Fouquart-Bonnel* scheme (1980) for the shortwave component of radiation. Large-scale precipitation is described by *Smith* (1990), convective processes and precipitation are parameterized with the *Bougeault* method (1985). The atmosphere-surface interactions are handled by the SURFEX scheme (Masson et al., 2013), which is also capable of taking the climatic effects of urban surfaces into account. Anthropogenic greenhouse gas emissions are represented through average yearly concentrations of CO<sub>2</sub>, CH<sub>4</sub>, N<sub>2</sub>O, CFC-11, CFC-12 provided by the RCP8.5 emission scenario in the current simulation. Five types of aerosol particles are considered as well: black carbon, organic carbon, sulphate, desert dust, and sea salt.

ALADIN-Climate was adapted at HMS in 2005 (Csima and Horányi, 2008). Since its adaptation, numerous simulations were performed with different settings in the framework of various downscaling projects (e.g., CECILIA, EURO-

CORDEX). The model version was recently updated to version 5.2, and a new, significantly larger integration domain was chosen for the current experiments in order to improve model performance, especially precipitation bias and extremes. The domain selection was based on the results of a sensitivity study (Szépszó *et al.*, 2015).

In the present research, we evaluate wind data on multiple levels near the surface from the most recent ALADIN-Climate simulations conducted in HMS. One of the examined experiments is driven by ERA-Interim re-analyses (hereafter referred to as ALADIN-ERA), and the other experiment got its initial and lateral boundary conditions from the ARPEGE-Climat/OPA atmosphere-ocean coupled general circulation model (referred to as ALADIN-ARP). The main characteristics of the two simulations are summarized in *Table 1*. In the case of ALADIN-ARP, there was an intermediate downscaling step: the global model results were first downscaled to 50 km spatial resolution, and then further downscaled to 10 km resolution. Both dynamical downscaling processes were performed at HMS with ALADIN-Climate version 5.2 considering the RCP8.5 emission scenario. The applied model domain (*Fig. 1*) covers the Carpathian Basin, the Alpine region, and a part of the Mediterranean coast. It also contains the whole drainage basin of the Danube and Tisza rivers, which is relevant regarding the potential applicability of the results for hydrological impact assessments.

*Table 1.* Characteristics of evaluated model simulations

<b>Name of simulation</b>	<b>ALADIN-ERA</b>	<b>ALADIN-ARP</b>
<b>LBC</b>	ERA-Interim	ALADIN-Climate (downscaled from ARPEGE-Climat)
<b>Spatial resolution</b>	10 km	10 km
<b>Vertical levels</b>	31	31
<b>LBC resolution</b>	80 km	50 km
<b>Time period</b>	1980–2010	1950–2100
<b>Scenario</b>	–	RCP8.5

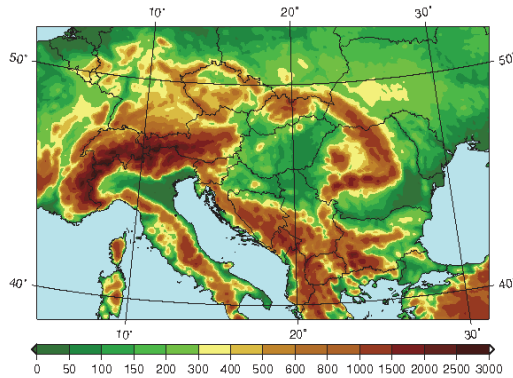


Fig. 1. Integration domain of the analyzed ALADIN-Climate simulations.

The model variables used in the study were the wind components on selected height levels at 0, 6, 12, and 18 UTC. Wind energy estimations require wind data in specific hub (turbine) heights, therefore, besides the 10-meter height, we evaluate the wind speed on 50, 75, 100, 125, and 150 meters above ground level to cover the range of most frequently used hub heights. ALADIN-Climate has a post-processing configuration called FullPos (Yessad, 2015) that allows us to retrieve data on any requested height levels above the surface. The interpolation of wind components from model levels to height levels are calculated by the model itself, so no further transformation is needed. The interpolation method applied by FullPos is described in Section 2.3.2.

### 2.3. Calculation of upper level wind speed

One of the many challenges of wind energy related estimations is the lack of reliable near-surface observational data that can be used to analyze upper level wind climatology and to validate numerical models. Tower measurements exist, but they are rare and scattered in space, therefore, they are not ideal for the validation of gridded model data over a large area. A viable and frequently used way is to extrapolate the observed surface wind velocity to the given height by fitting a wind profile. This method often requires surface parameters (e.g., roughness length) that are difficult to precisely measure and can only be estimated. On the other hand, the impact of surface characteristics on upper level wind conditions diminishes by the height, and they are largely influenced by the atmospheric dynamics. The main goal of our study was to establish a methodology to evaluate the results of ALADIN-Climate model regarding wind speed and wind energy potential on fixed height levels using directly the model level data, thus minimalizing the effects of vertical interpolation. ERA-Interim was chosen as reference because of the availability of upper level wind data. Neither ALADIN-

Climate, nor ERA-Interim uses  $z$ -coordinates in vertical direction, therefore, the first step was to transform all the necessary variables from model levels to the chosen height levels in both cases for easy comparison.

### 2.3.1. Wind speed from ERA-Interim

ERA-Interim vertical coordinates are defined by a hybrid pressure-sigma coordinate system. This consists of pure pressure levels in the upper region (top 24 model levels) of the model atmosphere, with continuous transition into a terrain-following sigma coordinate system at the lower levels. ERA-Interim has 60 hybrid model levels and level 61 represents the surface. The pressure of a given level is the function of surface pressure and two time-independent coefficients that vary in the vertical, but not in the horizontal direction. The pressure of the  $n$ th level can be computed by the formula:

$$P_n(\lambda, \phi, t) = a_n + b_n P_s(\lambda, \phi, t), \quad (1)$$

where  $P_n$  is the pressure of the  $n$ th model level,  $P_s$  is the surface pressure,  $a_n$  and  $b_n$  are the coefficients mentioned above. The actual value of the coefficients for each level can be found in the documentation of ERA-Interim (Berrisford *et al.*, 2011). The method used for transforming the hybrid level wind data to discrete height levels consists of two major steps: (1) first, the height of the model levels is calculated in each gridpoint through all the timesteps; (2) knowing the altitude of model levels in each gridpoint, wind speed is interpolated to the target height by fitting a wind profile to the data at each timestep. For calculating the height of model levels, hydrostatic balance is assumed:

$$P_n = P_s - \rho g h_n, \quad (2)$$

where  $h_n$  is the height of the level to be determined,  $P_n$  can be computed from Eq. (1) using  $P_s$ .  $\rho$  is the average air density which is estimated based on the molar form of the ideal gas law:

$$P_n = \rho R_* T_n, \quad (3)$$

where  $T_n$  is the temperature on the  $n$ th level and  $R_* = 287 \text{ Jkg}^{-1}\text{K}^{-1}$  is the specific gas constant. With these formulas, the height of each model level can be approximated. After determining these heights in each gridcell, wind speed is calculated using the simple power-law wind profile:

$$v = v_n (h/h_n)^\alpha, \quad (4)$$

where  $v_n$  is the wind speed on the  $n$ th model level,  $h_n$  is the height of the model level and  $h$  is the target altitude. The Hellmann exponent was chosen to be  $\alpha = 0.2$  based on international standards for wind turbine design provided by the International Electrotechnical Commission (IEC, 2005).

For every target level (50, 75, 100, 125, and 150 m), this interpolation method was carried out from the two neighboring model levels, resulting in an “upward” and a “downward” fitting of the wind profile (Fig. 2). The final velocity was defined as the weighted average of these two values. The weights were specified inversely proportional to the distances between the target level and the two model levels. The average height of the chosen model levels can be seen in Table 2. The 75 m target level was an exception, because it is close to the model level 58, therefore, in this case, the wind speed was calculated directly from the level 58 data.

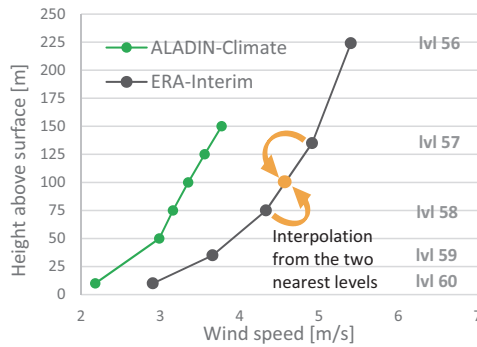


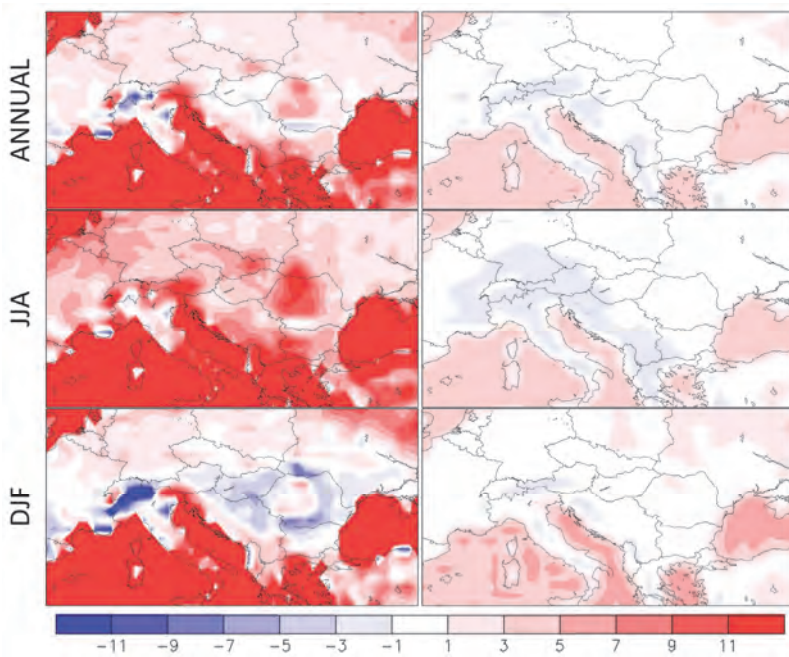
Fig. 2. Interpolation of ERA-Interim wind data to the target (50, 75, 100, 125, 150 m) levels.

Table 2. Average heights of ERA-Interim model levels

Level no.	Average height above surface
56	190–220 m
57	130–140 m
58	70–75 m
59	30–35 m

To evaluate the effectiveness of the presented interpolation process, we compare it side by side with a frequently used method, in which the upper level wind speed is extrapolated using only the near-surface values, i.e., the 10-meter wind speed. The comparison was performed on ERA-Interim data. Wind speed

on level 58 was chosen as reference for the period of 1981–2000. The 75 m wind speed was calculated in two ways: (1) from data on levels 57 and 59 with the methodology presented above, and (2) with extrapolation from the near-surface wind speed, applying the wind profile of Eq. (4) in both cases. The results show that using data from neighboring model levels, the 75 m wind speed is reproduced with significantly less error: the difference of the calculated and reference wind speeds is less than 3% over all the land surface gridpoints in all seasons and less than 1% over Hungary. When extrapolating from the surface, the departures reach 10–15% over mountain areas and exceed 20% over ocean gridpoints (*Fig. 3*).



*Fig. 3.* Comparison of the two applied methods: annual, summer, and winter mean difference (%) between wind speed at level 58 in ERA-Interim and wind speed extrapolated to 75 m using surface data (left) and interpolated using upper level data (right) 1981–2000.

### 2.3.2. ALADIN-Climate

In case of ALADIN-Climate, the upper level wind components were calculated with the FullPos post-processing package. FullPos contains various options to

perform vertical interpolations, making the variables available on any pressure, potential temperature, height, or model level. In the lowest part of the boundary layer, where the wind speed strongly depends on the height above ground level, the vertical profile of wind components is calculated as:

$$v(z) = v_L \cdot C \cdot \ln\left[1 + \frac{z}{z_L}(e^D - 1) - F\right], \quad (5)$$

where  $C$ ,  $D$ , and  $F$  are coefficients depending on the stability of the atmosphere, the height above surface, and the surface roughness;  $z_L$  is the height of the lowest model level, and  $v_L$  is the wind component on that level (Tóth, 2004). The height of the lowest model level varies in time and space but generally is around 30 m above the surface. Consequently, Eq. (5) is applied to determine wind components on 10 meters. Above this altitude, wind components are calculated with linear interpolation between the neighboring vertical levels (Yessad, 2015). The schematic diagram of computation methods used with ALADIN-Climate and ERA-Interim can be seen in Fig. 4.

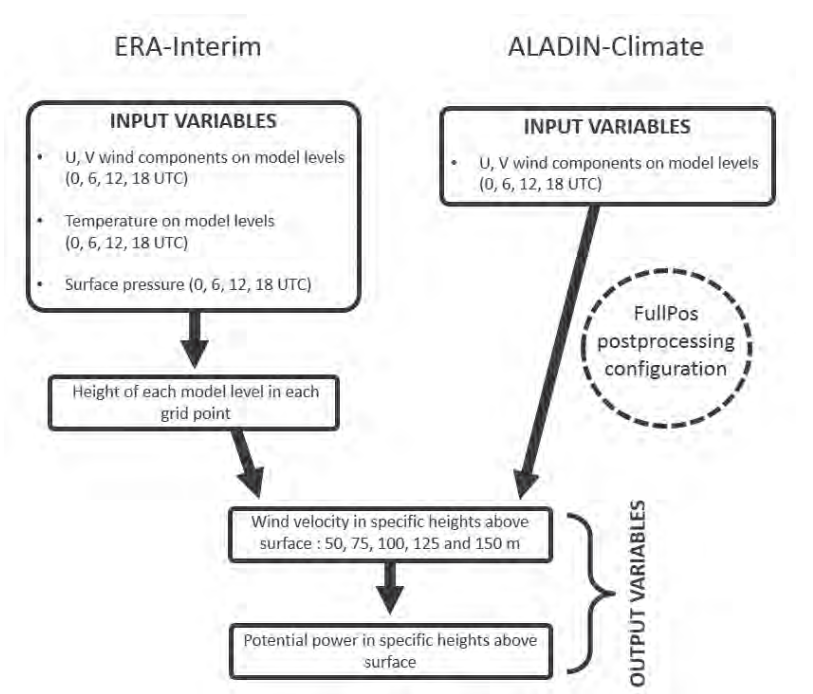


Fig. 4. Schematic overview of the applied interpolation method.

## 2.4. Potential wind power production

In wind power generation, not only the mean wind speed is relevant, but also its distribution. Wind power production was estimated based on the power curve of the Gamesa G90 2 MW rated wind turbine, as it is the most frequently used turbine type in Hungary (Tóth, 2012). The power curve defines the power output of the turbine in function of the wind speed in hub height. All wind turbines have a given cut-in wind speed below which power generation is not possible, and a cut-out wind speed above which the turbine is intentionally stopped due to security reasons. The cut-in wind speed of Gamesa G90 2 MW turbine is 3 m/s, and the cut-out speed is 21 m/s.

## 3. Results

### 3.1. Validation

In this section, validation results of the ALADIN-ERA-Interim and ALADIN-ARP simulations are presented for 1981–2000 using ERA-Interim as reference data. In case of both simulations, the negative bias dominates over the integration domain in all of the chosen height levels. The mean bias of 10-meter wind speed over Hungary is around  $-15\%$  in ALADIN-ERA-Interim, and it gradually decreases with the altitude reaching an average of  $-1\%$  at 150 meters above ground level (Fig. 5, Table 3). ALADIN-ARP underestimates wind speed more strongly, and the decreasing trend is less pronounced in this case with a mean annual bias of  $22\%$  at 150 m (Fig. 5, Table 4). The departure between the ALADIN and ERA-Interim data does not have high spatial variability in either of the simulations. Over Hungary, maximal and minimal errors are found mostly in autumn and summer, respectively (Table 3). Despite the systematic underestimation, the interannual variability of the wind speed is well represented in the re-analysis driven ALADIN-ERA-Interim simulation, i.e., the 20-year time series of ALADIN follows the reference values as it can be seen in Fig. 6, which also illustrates the altitude dependence of systematic error. The annual distribution of 10-meter wind speed, however, is poorly reproduced by both model simulations. ALADIN-ARP produces the maximum and minimum values in the appropriate months, but the shape of the distribution is too flat compared to the reference datasets. ALADIN-ERA-Interim simulation did not reflect the characteristics of the annual cycle despite its smaller average bias (Fig. 7).

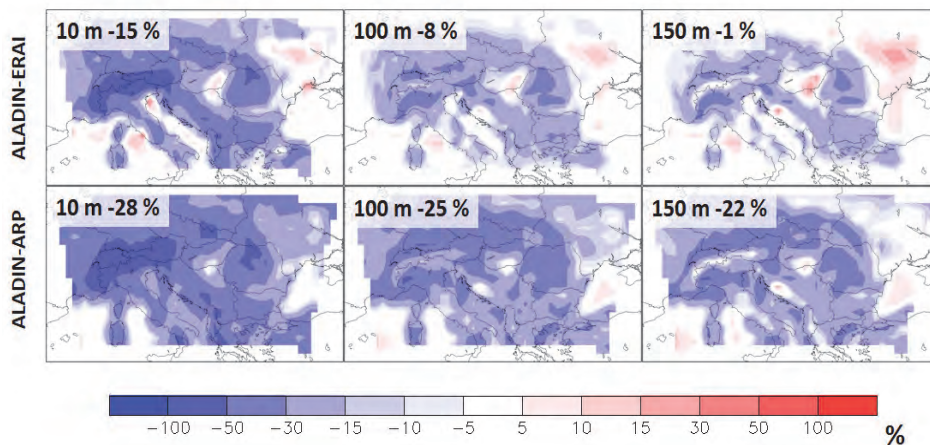


Fig. 5. Annual mean 10 m, 100 m, and 150 m wind speed differences (%) between ALADIN-Climate results and ERA-Interim for 1981–2000. The top left values indicate the average of bias over Hungary.

Table 3. Relative difference (%) between mean wind speeds in ALADIN-ERA results and ERA-Interim (1981–2000).

Height	Annual	MAM	JJA	SON	DJF
10 m	-15	-18	-8	-21	-13
100 m	-8	-9	3	-14	-10

Table 4. Relative difference (%) between mean wind speeds in ALADIN-ARP results and ERA-Interim (1981–2000)

Height	Annual	MAM	JJA	SON	DJF
10 m	-28	-25	-23	-36	-30
100 m	-25	-20	-16	-34	-30

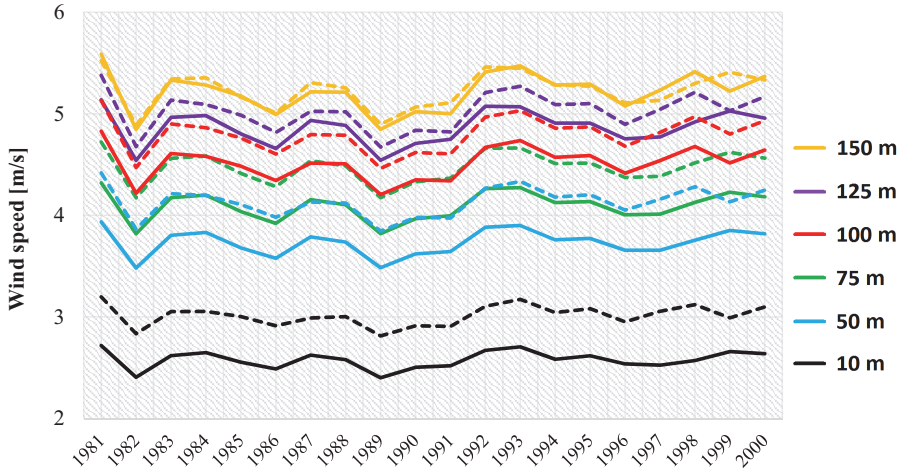


Fig. 6. Annual mean wind speed values (m/s) over Hungary at different heights during 1981–2000. Solid and dashed lines indicate the ALADIN-ERA simulations and re-analyses, respectively.

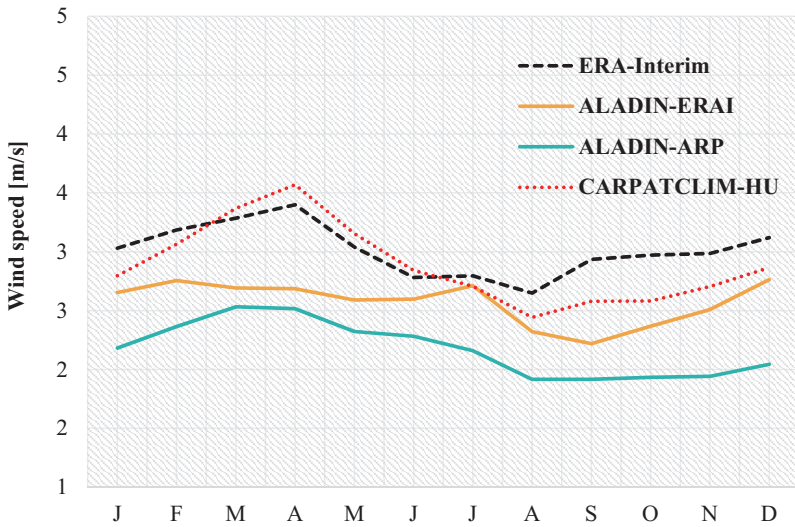


Fig. 7. Monthly mean wind speed (m/s) over Hungary based on CARPATCLIM-HU observational dataset, ERA-Interim re-analysis, and ALADIN-Climate simulation data for 1981–2000.

The vertical wind profile is examined in three gridpoints: two points (A and B) are selected in the territory of Hungary and one (C) over the Mediterranean see (Fig. 8). Points A and B represent the locations of the two greatest wind farms in Hungary, and the C point was chosen to investigate a certain model behavior found in projection results over sea gridpoints (further discussed in Section 3.2). The points are selected as the nearest ERA-Interim gridpoints to the targeted locations: A (48° N, 17.25° E); B (47.25° N, 21° E); C (42.75° N, 15° E). In the case of ALADIN-Climate wind fields, an interpolation was performed before extracting the wind profiles. Model outputs were interpolated to the ERA-Interim grid so that the vertical profiles would be comparable with the ones of the re-analysis. Fig. 8 shows the mean wind profiles at the selected gridpoints. ALADIN-ARP underestimates the wind speed in each location and height level, whereas the sign of ALADIN-ERA1 bias depends more on the location and height. The decreasing mean error with altitude is not valid in these selected locations. Wind profile in point C is clearly different from the ones over land: 10-meter values are higher here due to the lower surface roughness of water compared to mainland, which results in a more neutral vertical structure. This aspect is very well reproduced in both model simulations.

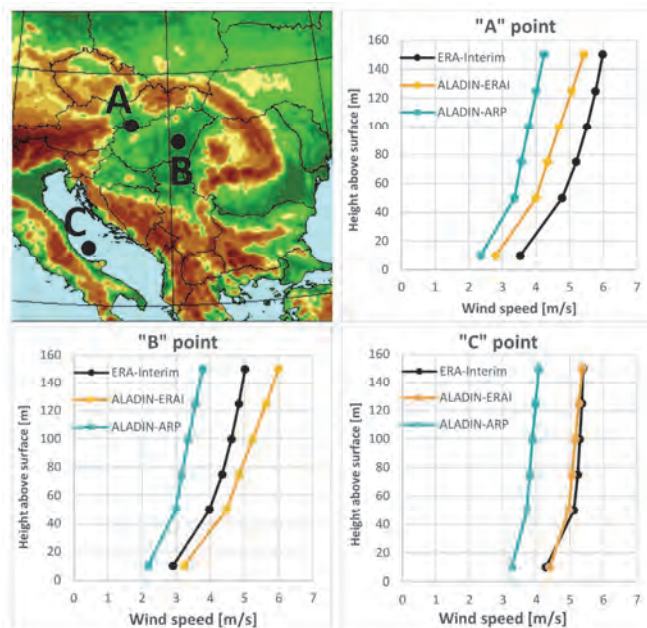
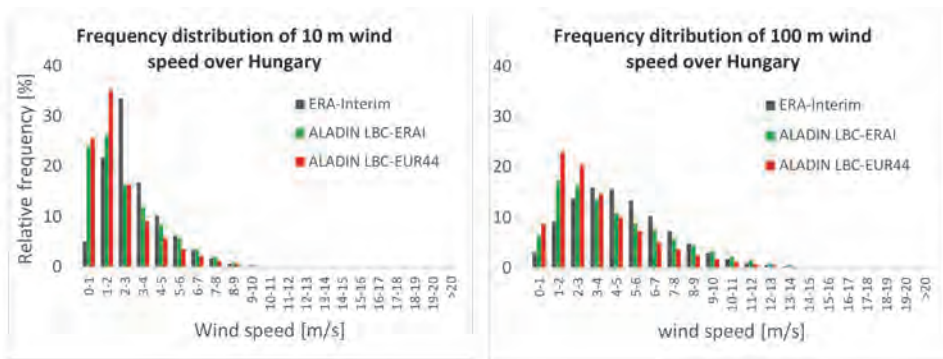


Fig. 8. Average vertical wind speed profiles of ERA-Interim re-analyses (black) and ALADIN-Climate simulations (green and yellow) in three selected gridpoints for 1981–2000. The locations are shown on the map in the top left panel.

Regarding the frequency distribution of 6-hour mean wind speeds at 10 meters, the re-analysis driven simulation overestimates the occurrence of wind speeds smaller than 2 m/s and higher than 9 m/s, while it underestimates the occurrence of wind speeds between 2 and 9 m/s. In the GCM-driven simulation, the frequency of small wind speeds are even more exaggerated, while the values exceeding 2 m/s are underrepresented compared to the reference (*Fig. 9*). With increasing altitude, the difference between the simulated and reference distributions becomes less significant in general, the frequencies of both small and high wind speeds are coming closer to the reference (*Fig. 9*).



*Fig. 9.* Frequency (%) of different wind speed categories at 10 m (left) and 100 m (right) based on ERA-Interim data and ALADIN-Climate simulations. Period: 1981–2000.

### 3.2. Projection results

The changes of future wind conditions are evaluated for two thirty-year periods: 2021–2050 and 2071–2100 with reference to 1971–2000. The projection results are only presented for the near-surface (10 m) and the 100 m height level, although the evaluation was performed for each selected level. The significance of the climate change signals were assessed performing the Welch statistical hypothesis test. The projected changes in near-surface wind speed are mostly below 10% across the whole domain, nonetheless often found to be significant over Hungary during both projection periods. In the mid-century period, the model simulated a slight increase of wind velocity with the exception of the higher mountains and the southwestern part of the domain (*Fig. 10*). The annual mean change over Hungary is around 7 %, and the strongest (9 %) seasonal growth was found in summer and winter (*Table 5*). At the end of the 21st century, the spatial pattern of the climate change signal is similar to that of the first period, but the areas with decreasing wind speed extended. Moving to the 100-meter level, the spatial pattern still remains the same, however, the projected increase of wind

speed is smaller (*Table 6*), and the areas with negative change signal are even more pronounced (*Fig. 11*). As mentioned earlier, an interesting model behavior can be observed in summer: there is a relatively strong, 20–30% (0.5–0.8 m/s) local enhancement of wind speed over the Mediterranean Sea in every height level over water gridpoints near the coastlines. Over the land surface, the summer changes are below 15 % in each gridpoint. Similar local maximums were found in the change signal of an RCM ensemble by *Tobin et al. (2014)* over the Baltic and the Aegean Sea. To investigate the cause of this model behavior, the phenomenon needs further research.

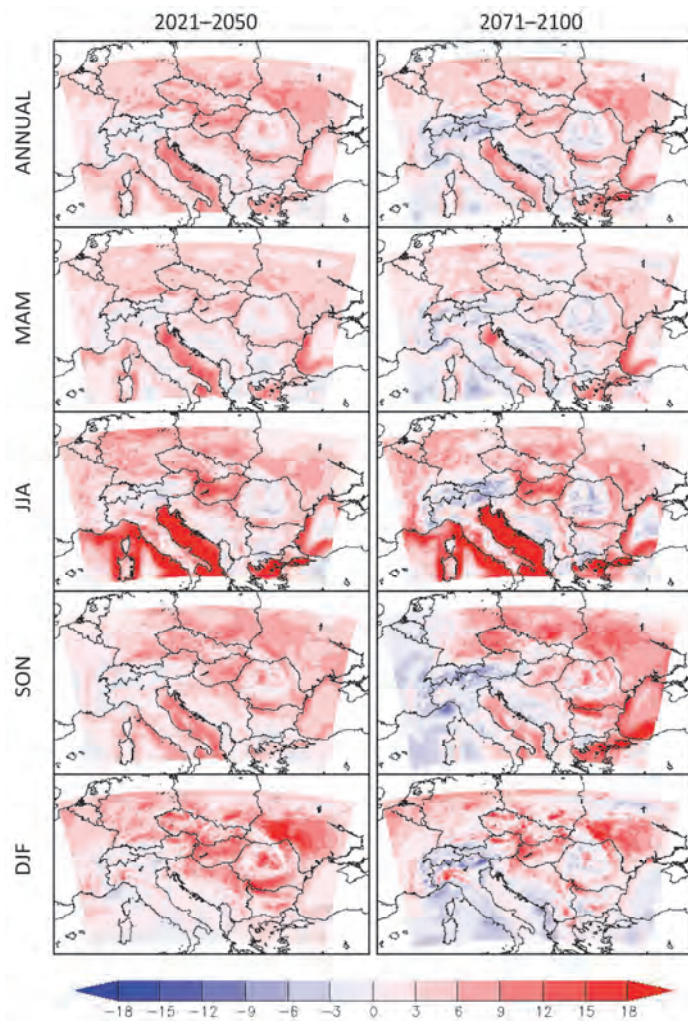


*Fig. 10.* Annual and seasonal mean changes (%) of 10 m wind speed based on ALADIN-ARP simulation results for 2021–2050 (left) and 2071–2100 (right) with respect to 1971–2000.

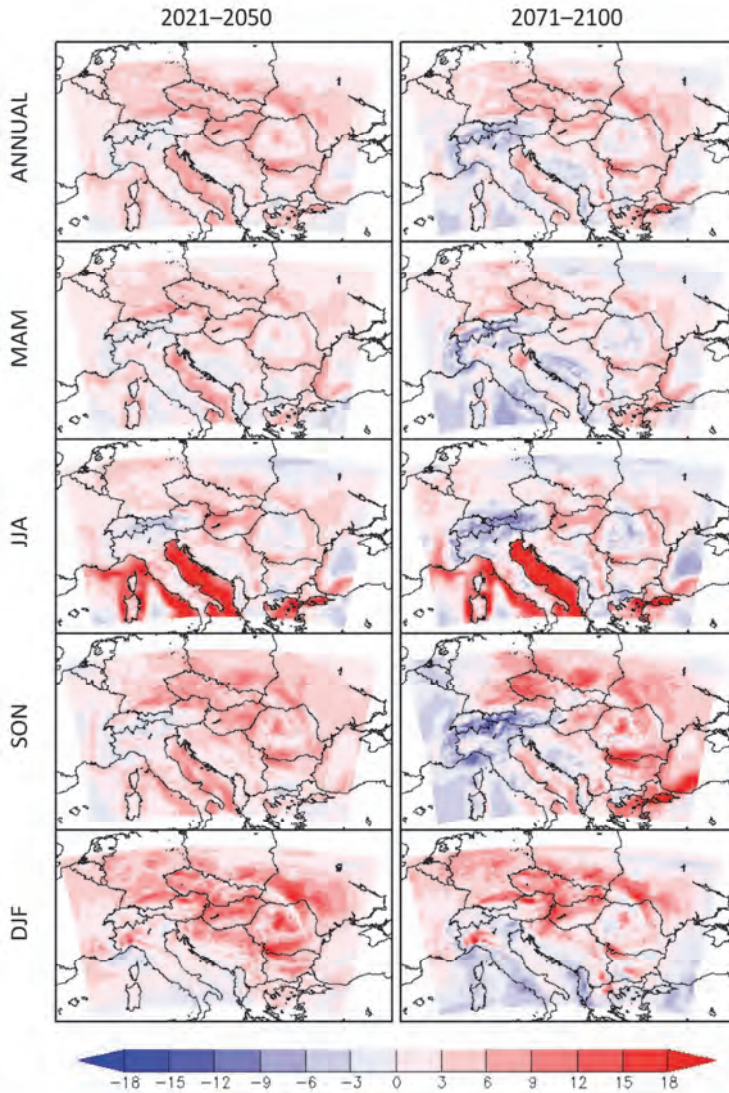


Fig. 11. Annual and seasonal mean changes (%) of 100 m wind speed based on ALADIN-ARP simulation results for 2021–2050 (left) and 2071–2100 (right) with respect to 1971–2000.

Table 5. Annual and seasonal mean change (%) of 10 m wind speeds in ALADIN-ARP simulation results over Hungary with reference to 1971–2000

10 m	Annual	MAM	JJA	SON	DJF
2021–2050	7	5	9	7	9
2071–2100	5	3	9	4	6

Table 6. Annual and seasonal mean change (%) of 100 m wind speeds in ALADIN-ARP simulation results over Hungary with reference to 1971–2000

100 m	Annual	MAM	JJA	SON	DJF
2021–2050	6	4	6	7	9
2071–2100	4	2	5	4	7

The frequency distributions of 10 m and 100 m wind speeds are presented in *Fig. 12* for both the projection and reference periods. To highlight the differences between the distributions, the changes corresponding to each interval are also shown. At the near-surface level, the most frequent wind speed category is between 0 and 2 m/s, and this is where the largest change is projected. Wind speeds below 2 m/s will be less frequent, and the occurrence of values between 2 and 8 m/s will slightly increase in both future periods compared to the reference. At the 100 m height, the peak of the histogram is between 1 and 2 m/s with a frequency around 20%. According to the model results, the number of events with wind speeds under 3 m/s is decreasing, while wind speeds above that limit are slightly more likely to happen in both projection periods.

The mean changes of wind power production are presented for the 100 m level. It shows similar pattern to the 100 m wind speed change, but with more contrast due to its cubic relation to wind velocity. Over Hungary, 13% and 8% mean annual increase is projected in 2021–2050 and 2071–2100, respectively (*Table 7*). In the second period, decreasing tendencies become particularly relevant over the Alps and along the coastline of Southern Europe. The effect of summer wind strengthening over certain parts of the Adriatic Sea is clearly visible causing an increase in potential wind power production of more than 30 % over those gridpoints (*Fig. 13*). Focusing on Hungary, the changes of the given categories of potential wind power production values were analyzed in points A and B. The experienced increasing frequency of wind speeds over 3 m/s has a relatively strong positive effect on the potential power distribution, since the Gamesa G90 turbine, which was used as reference, has a cut-in speed of 3 m/s. *Fig. 14* shows that the number of cases where the output power equals to zero is decreasing by 3–6% in both locations through all seasons.

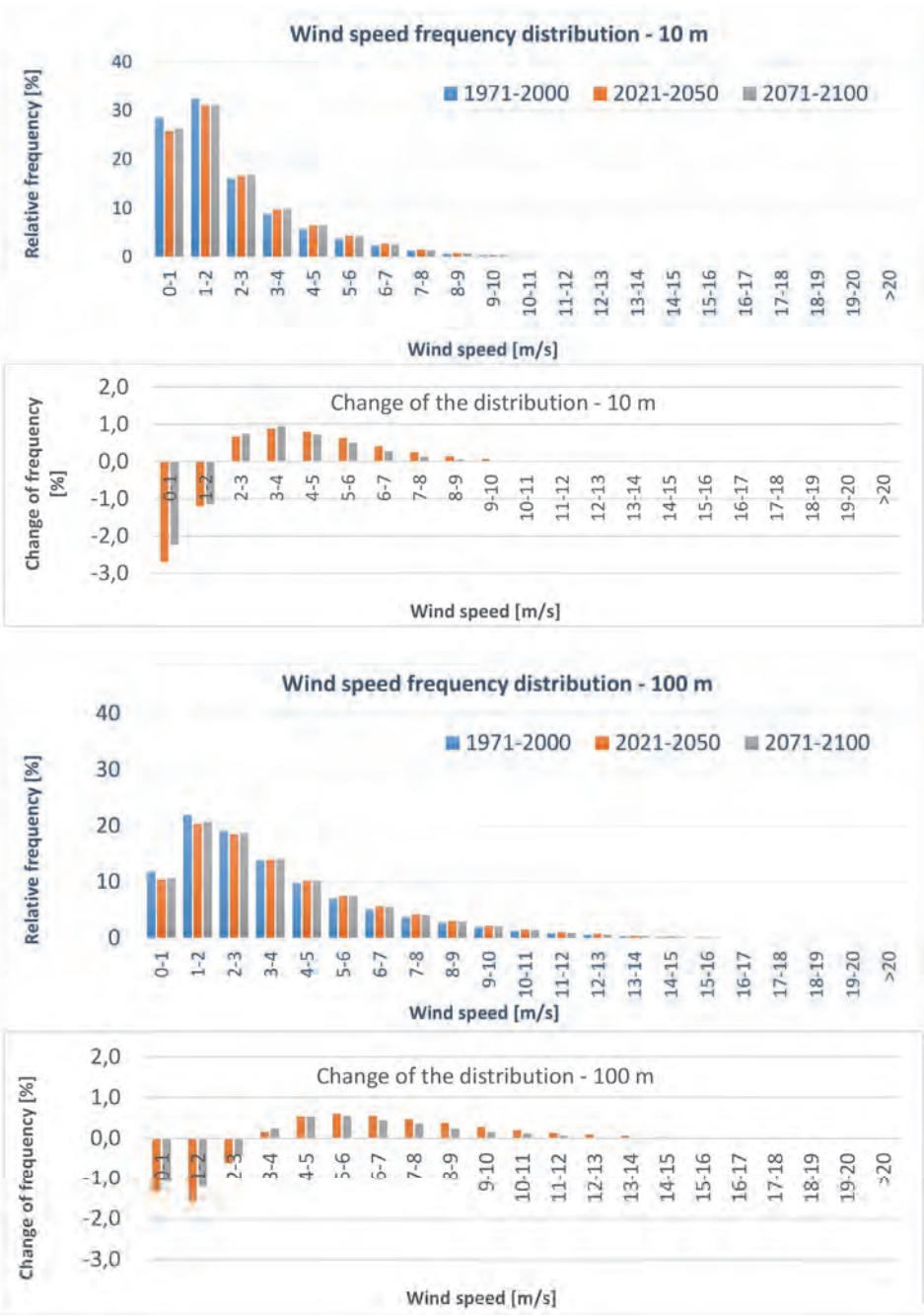


Fig. 12. Average frequency (%) of different 10 m (top) and 100 m (bottom) wind speed categories and projected frequency changes (%) based on ALADIN-ARP simulation results.

Table 7. Annual and seasonal mean change (%) of wind energy production in ALADIN-ARP simulation results over Hungary at 100 m height with reference to 1971–2000

100 m	Annual	MAM	JJA	SON	DJF
2021–2050	13	7	13	13	16
2071–2100	8	3	7	7	14

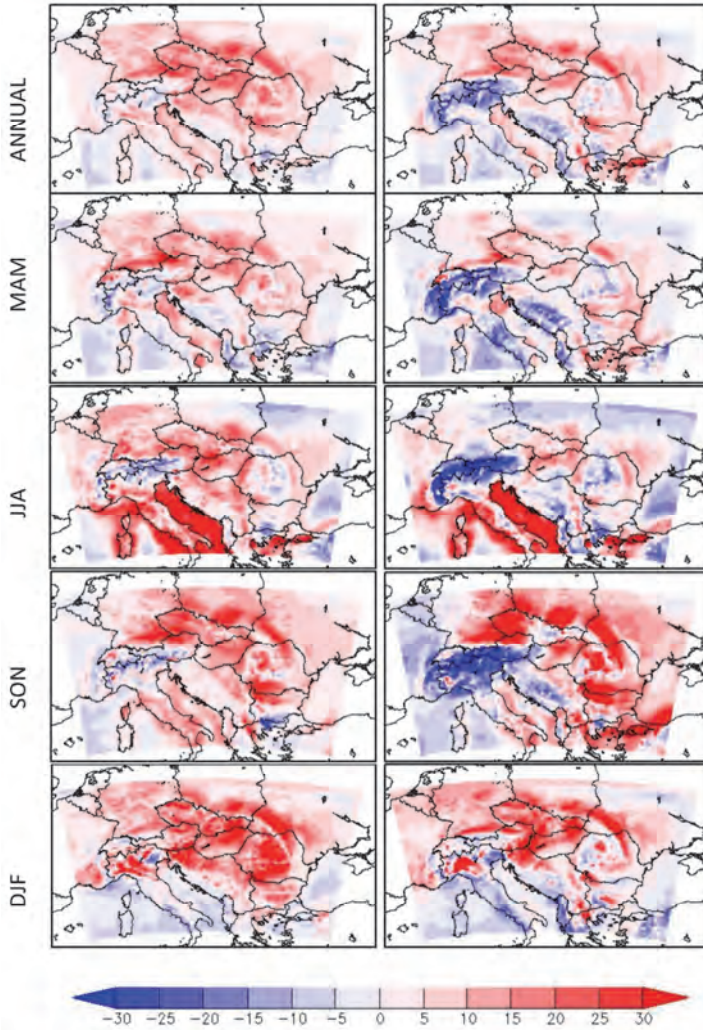


Fig. 13. Annual and seasonal mean changes (%) of potential wind power production at 100 m height based on ALADIN-ARP simulation results for 2021–2050 (left) and 2071–2100 (right) with respect to 1971–2000.

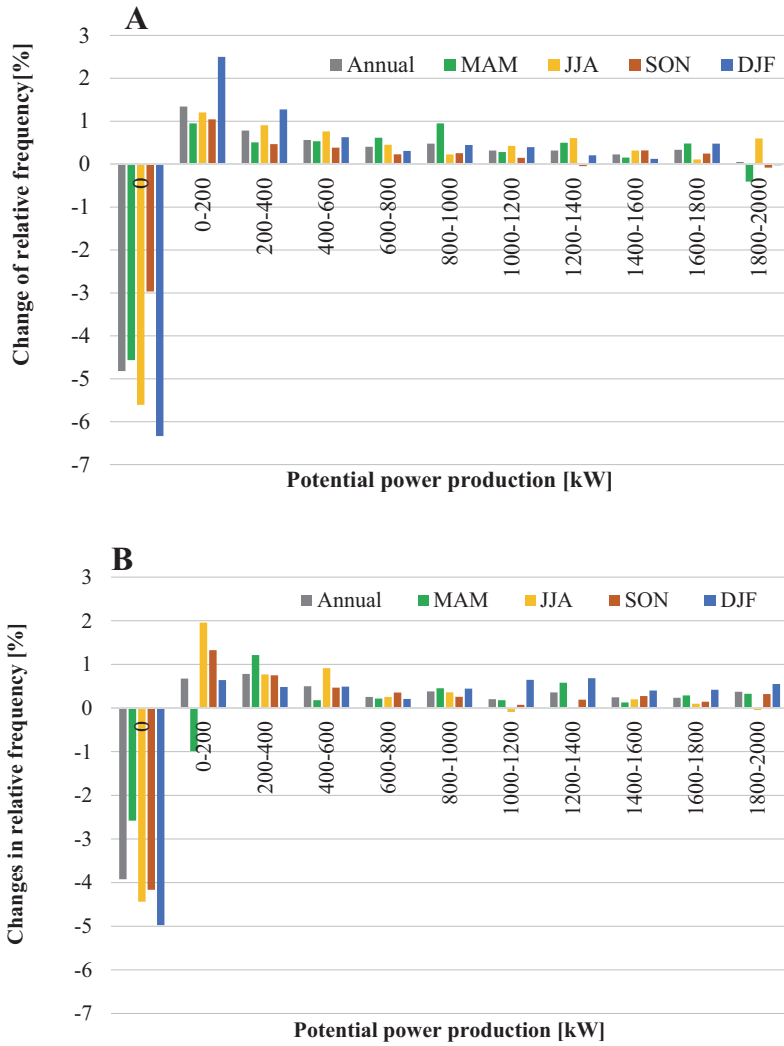


Fig. 14. Annual and seasonal changes (%) in the frequency of potential wind power production categories in point A (top) and B (bottom) based on ALADIN-ARP simulation results for 2021-2050 with respect to 1971-2000.

#### 4. Outlook

Climate model results inherently contain uncertainties originating from the approximations of physical processes, anthropogenic effects, and the natural variability of Earth's climate system. This fact should not be ignored when evaluating simulation results. Ideally, a properly selected ensemble of model projections would be the best basis for future climate estimations. In our case, the focus was on establishing the evaluation methodology for upper-level wind conditions, and it was demonstrated on the outputs of a single climate model. Therefore, our conclusions regarding the climate change effects on near-surface wind climatology do not include information about the projection uncertainties. However, we can compare our results with other assessments of the future changes in wind potential. The comparison is not precise because of the different time periods or emission scenarios considered, nevertheless, it gives a basic overview about the position of ALADIN-Climate results in context of a wider range of climate simulations. As a general statement, it can be said that the expected changes in wind speed and wind energy potential over Europe are rather subtle, but several studies show a slight increasing tendency over Northern Europe and decreasing tendency over Southern Europe (*Pryor et al., 2005; Hueging et al., 2013; Tobin et al., 2014; Reyers et al., 2016*). Two of these studies are discussed here in detail, in which the upper level wind speed was extrapolated from surface data with the power-law wind profile.

*Tobin et al. (2014)* examined the changes in potential wind power generation by evaluating 15 RCM simulations downscaling 6 different GCMs under the SRES A1B emission scenario from the ENSEMBLES project. The ensemble mean showed changes within  $\pm 15\%$  of extractable wind power by the end of the 21st century. There is a decreasing tendency over the Mediterranean areas (except the Aegean Sea) and an increasing trend over Northern Europe. Some relatively strong changes were found over a few sea gridpoints that resemble the summer change signal found in ALADIN-Climate results (*Fig. 15*).

In the research of *Reyers et al. (2016)*, results of the 22 GCM simulations of Coupled Model Intercomparison Project Phase 5 (CMIP5) were downscaled over Europe with a statistical-dynamical method to estimate future changes of potential wind energy under RCP4.5 and RCP8.5 anthropogenic scenarios. A few percent increase of wind energy was found over Northern and Central Europe and a small decrease over Southern Europe and the Mediterranean Sea (*Fig. 16*). More robust changes are projected by the end of the century. The spatial pattern of the ensemble mean change in wind energy production is similar to our results, but its magnitude is smaller ( $\pm 4\%$ ).

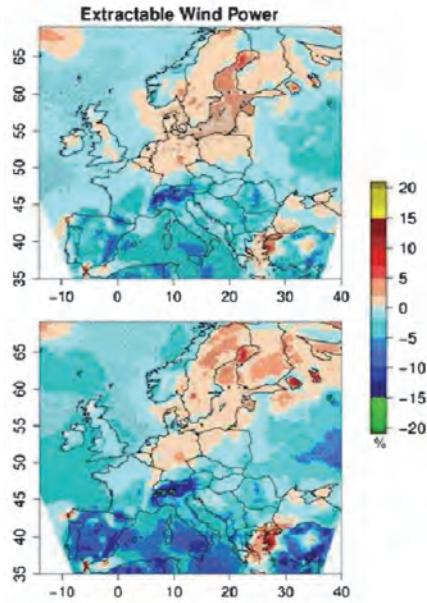


Fig. 15. Ensemble mean of annual changes in extractable wind power (%) for 2031–2060 (top) and 2071–2100 (bottom) with respect to the 1971–2000, based on results of RCM simulations in ENSEMBLES project using A1B emission scenario (Tobin et al., 2014).

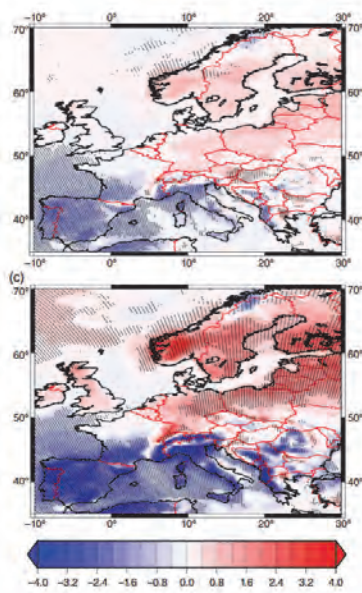


Fig. 16. Ensemble mean of annual change in extractable wind power (%) for 2021–2060 (top) and 2061–2100 (bottom) with respect to the 1961–2000 period, based on RCM simulations using RCP8.5 emission scenario (Reyers et al., 2016).

## 5. Summary

A methodology was developed and presented to assess past and future wind speed and potential wind power production on multiple height levels above the surface based on ALADIN-Climate regional model results. ERA-Interim re-analysis was used to validate the model results for the period of 1981–2000, and the future climate change was evaluated for the near- and far-future, i.e., for 2021–2050 and 2071–2100. The upper level wind velocities were calculated by interpolation of data from hybrid model levels in case of the model and the reference data, as well. It was shown that the applied interpolation method yields more accurate results compared to extrapolation from the 10-meter fields. According to the validation results, both the GCM- and re-analysis, driven simulations reasonably reproduced the near-surface wind climatology over the integration domain with a small underestimation. The interannual wind speed variability and the shape of the vertical profile are well represented in the simulations, however, the annual distribution is not accurate in the model results.

Future projections were carried out considering the RCP8.5 scenario. Results show a slight, 4–7% increase in wind speed over Hungary across the chosen height levels, which is found statistically significant over the majority of the country. Wind speeds under 2–3 m/s are projected to be less frequent in the future, while reduction in occurrence of the moderate wind speeds between 3 and 10 m/s is foreseen. The potential wind power production was produced from the 100-meter wind speed using the power curve of the Games G90 2 MW wind turbine. Projections showed an increase in average potential wind power production over Hungary with a magnitude of 8–13%, and a 3–5 % decrease is indicated in the occurrence of periods with zero power output. To place our findings in broader context, we briefly compared our projection results with outcomes of two recent studies which confirmed our main conclusions.

In the future, we would like to develop and further improve our method by validating model results with higher resolution references (e.g., with regional and new re-analyses) and by involving further regional climate simulations to address the projection uncertainties. Besides mean wind speed characteristics, we also plan to examine future changes in wind extremes.

## References

- Bartholy, J. and Radics, K., 2001: Selected wind characteristics and potential use of wind energy in Hungary. Part I. *Időjárás* 105, 109–126.
- Berrisford, P., Dee, D., Poli, P., Brugge, R., Fielding, K., Fuentes, M., Kallberg, P., Kobayashi, S., Uppala, S., and Simmons, A., 2011: ERA Report series, The ERA-Interim archive.
- Bougeault, P., 1985: A Simple Parameterization of the Large-Scale Effects of Cumulus Convection. *Mon. Weather Rev.* 113, 2108–2121.
- Csima, G. and Horányi, A., 2008: Validation of the ALADIN-Climate regional climate model at the Hungarian Meteorological Service. *Időjárás* 112, 3–4, 155–177.

- Dee, D.P., Uppala, S. M., Simmons, A.J., Berrisford, P., Poli, P., Kobayashi, S., Andrae, U., Balmaseda, M. A., Balsamo, G., Bauer, P., Bechtold, P., Beljaars, A.C.M., van de Berg, L., Bidlot, J., Bormann, N., Delsol, C., Dragani, R., Fuentes, M., Geer, A.J., Haimberger, L., Healy, S.B., Hersbach, H., Hólm, E. V., Isaksen, L., Kållberg, P., Köhler, M., Matricardi, M., McNally, A. P., Monge-Sanz, B.M., Morcrette, J.-J., Park, B.-K., Peubey, C., de Rosnay, P., Tavolato, C., Thépaut, J.-N., and Vitart, F., 2011: The ERA-Interim reanalysis: configuration and performance of the data assimilation system. *Q.J.R. Meteorol. Soc.* 137, 553–597.
- Déqué, M., 2003: ARPEGE-Climate Version 4. Algorithmic Documentation. 365 p.
- EU Directive, 2009: Directive 2009/28/EC of the European Parliament and of the Council of 23 April 2009 on the promotion of the use of energy from renewable sources and amending and subsequently repealing Directives 2001/77/EC and 2003/30/EC.
- European Wind Energy Association, 2016: Wind in power: 2015 European statistics.
- Fouquart, Y. and Bonnel, B., 1980: Computations of solar heating of the Earth's atmosphere: A new parameterization. *Con&B. Atmos. Phys.* 53, 35–62.
- Horányi, A., Kertész, S., Kullmann, L., and Radnóti, G., 2006: The ARPEGE/ALADIN mesoscale numerical modeling system and its application at the Hungarian Meteorological Service. *Időjárás* 110, 3–4, 203–227.
- Hueging, H., Haas, R., Born, K., Jacob, D., and Pinto, J.G., 2013: Regional changes in wind energy potential over Europe using regional climate model ensemble projections. *J. Appl. Meteorol. Climatol.* 52, 903–917.
- IEC, 2005: Wind turbines—Part 1: Design requirements. International Electrotechnical Commission, IEC 61400-1, 179 pp.
- Illy, T., 2014: Szélenergia becslések regionális éghajlati modellek alapján. MSc diplomamunka, ELTE Meteorológiai Tanszék, Budapest. MSc Thesis, Eötvös Loránd Tudományegyetem, Budapest. (in Hungarian)
- Kertész, S., Szépszó, G., Lábó, E., Radnóti, G., and Horányi, A., 2005: Dynamical downscaling of the ECMWF ERA-40 re-analyses with the ALADIN model. ALADIN/ALATNET Newsletter 28, 78–83.
- Lakatos, M., Szentimrey, T., Bihari, Z., and Szalai, S., 2013: Creation of a homogenized climate database for the Carpathian region by applying the MASH procedure and the preliminary analysis of the data. *Időjárás* 117, 143–158.
- Masson, V., Le Moigne, P., Martin, E., Faroux, S., Alias, A., Alkama, R., Belamari, S., Barbu, A., Boone, A., Bouyssel, F., Brousseau, P., Brun, E., Calvet, J.-C., Carrer, D., Decharme, B., Delire, C., Donier, S., Essaouini, K., Gibelin, A.-L., Giordani, H., Habets, F., Jidane, M., Kerdran, G., Kourzeneva, E., Lafaysse, M., Lafont, S., Lebeaupin Brossier, C., Lemonsu, A., Mahfouf, J.-F., Marguinaud, P., Mokhtari, M., Morin, S., Pigeon, G., Salgado, R., Seity, Y., Taillefer, F., Tanguy, G., Tulet, P., Vincendon, B., Vionnet, V., and Voldoire, A., 2013: The SURFEXv7.2 land and ocean surface platform for coupled or offline simulation of earth surface variables and fluxes. *Geosci. Model Dev.* 6, 929–960.
- Mlawer, E.J., Taubman, S.J., Brown, P.D., Iacono, M.J., and Clough, S.A., 1997: Radiative transfer for inhomogeneous atmospheres: RRTM, a validated correlated-k model for the longwave. *J. Geophys. Res.* 102D, 16663–16682.
- Mortensen, N.G., Landsberg, L., Troen, I., and Petersen, E.L., 1993: Wind Atlas Analysis and Application Program (WASP). Ris<sup>-</sup> Nat. Labs, Roskilde, Denmark.
- Péliné, N. Cs., 2015: A regionális szélklíma tendenciáinak elemzése a globális klímaváltozás függvényében. Doktori értekezés, ELTE Meteorológiai Tanszék, Budapest. (in Hungarian)
- Pryor, S.C., Barthelmie, R.J., and Kjellström, E., 2005: Potential climate change impact on wind energy resources in northern Europe: analyses using a regional climate model. *Clim. Dyn.* 25, 815–835.
- Radics, K., 2004: A szélenergia hasznosításának lehetőségei Magyarországon: hazánk szélklímája, a rendelkezésre álló szélenergia becslése és modellezése. Doktori értekezés, ELTE Meteorológiai Tanszék, Budapest. (in Hungarian)
- Reyers, M., Moemken, J. and Pinto, J. G., 2016: Future changes of wind energy potentials over Europe in a large CMIP5 multi-model ensemble. *Int. J. Climatol.* 36, 783–796.
- Smith, R.N.B., 1990: A scheme for predicting layer clouds and their water content in a general circulation model. *Q. J. R. Meteorol. Soc.* 116, 435–460.

- Szentimrey, T., 2008: Development of MASH homogenization procedure for daily data. Proceedings of the Fifth Seminar for Homogenization and Quality Control in Climatological Databases, Budapest, Hungary, 2006, WCDMP-No. 71, WMO/TD-NO. 1493, 123–130.
- Szentimrey, T. and Bihari, Z., 2007: Mathematical background of the spatial interpolation methods and the software MISH (Meteorological Interpolation based on Surface Homogenized Data Basis). Proceedings of the Conference on Spatial Interpolation in Climatology and Meteorology (eds.: S. Szalai, Z. Bihari, T. Szentimrey, M. Lakatos) 2007, COST Office, Luxemburg, ISBN 92-898-0033-X, 17–28.
- Szentimrey, T., Bihari, Z., Birszki, B., 2006: Széltérkép fejlesztés állomások adataiból, statisztikai klimatológiai eljárással. Magyarországi szél és napenergia kutatás eredményei. Országos Meteorológiai Szolgálat, Budapest.
- Szépszó, G., Csima, G., Pieczka, I., 2007: Regionális klímamodellek szisztematikus összehasonlítása. NKFP-3A/082/2004 projekt beszámoló, 2007. december, 32 p.
- Szépszó, G. and Horányi, A., 2010: Validation of the dynamically adapted high-resolution wind forecasts for the wind power stations in Hungary. *Időjárás* 114, 57–77.
- Szépszó, G., Krüszelyi, I., Illy, T., and Sábitz J., 2015: Az ALADIN-Climate regionális klímamodell integrálási tartományának megválasztására vonatkozó érzékenységvizsgálat. RCMTÉR (EEA-C13-10) projekt beszámoló, Országos Meteorológiai Szolgálat, Budapest. (in Hungarian)
- Tobin, I., Vautard, R., Balog, I., Bréon, F.-M., Jerez, S., Ruti, P. M., Thais, F., Vrac, M., Yiou, P., 2014: Assessing climate change impacts on European wind energy from ENSEMBLES high-resolution climate projections. *Climatic Change* 128, 99–112.
- Tóth, H., 2004: A szél előrejelzése és diagnosztizálása az ALADIN modellben. Beszámoló a 2003. évi tevékenységről, Országos Meteorológiai szolgálat, Budapest, 157–163. (in Hungarian)
- Tóth, H., 2012: Szélenergia teljesítmény előrejelzés szélérőművek részére, beszámoló a MAVIR Zrt számára. Kézirat. (in Hungarian)
- Varga, B. and Németh P., 2004: Vertical wind profile analysis from SODAR measurement data, ENERExpo Kiadvány, 173–177.
- Yessad, K., 2015: Full-Pos in the cycle 41T1 of ARPEGE/IFS. Météo France, Toulouse.



# IDŐJÁRÁS

*Quarterly Journal of the Hungarian Meteorological Service  
Vol. 121, No. 2, April – June, 2017, pp. 189–208*

## **Verification of global radiation fluxes forecasted by numerical weather prediction model AROME for Hungary**

**Zoltán Tóth<sup>1\*</sup>, Zoltán Nagy<sup>1</sup>, and Balázs Szintai<sup>2</sup>**

<sup>1</sup>*Hungarian Meteorological Service  
Marczell György Main Observatory  
Gilice tér 39. H-1181 Budapest, Hungary*

<sup>2</sup>*Hungarian Meteorological Service  
Kitaibel P. u. 1. H-1024 Budapest, Hungary*

*\*Corresponding author E-mail: toth.z@met.hu*

*(Manuscript received in final form January 12, 2017)*

**Abstract**— Global radiation output fluxes predicted by numerical weather forecast model AROME were verified by using measured high accuracy global radiation data from the 19 most reliable network stations of the Hungarian Meteorological Service. Three suitably-selected months (April, June, August) from 2013 were used for the study. Differences between observed and forecasted values were analyzed separately for all cases, overcast cases, and cloudless (clear-sky) cases. It was found that AROME performs well for clear cases, and its goodness decreases as cloudiness increases. For cloudless cases, using aerosol optical depth, graybody optical depth, and relative global radiation to represent radiative transmission condition of the atmosphere, it was found that AROME overestimates atmospheric radiation transmission for cases of high turbidity and underestimates it for very clear conditions. It means that radiation transmission scale of the atmosphere produced by the model is more narrow than that of true atmosphere.

*Key-words:* verification, solar radiation, global radiation, observed data, radiative transmission of the atmosphere, optical depth

Paper is based on the presentation delivered at Meteorological Scientific Days held on 19–20 Nov, 2015 entitled „Meteorological aspects of use of renewable energies”.

## 1. Introduction

The aim of this study was to obtain detailed quantitative information about quality of predicted global radiation fluxes of numerical weather forecast model AROME. To know the performance of the predicted global radiation values is of primary importance not only to know how the model itself performs, but because using global radiation prediction starts to become more and more important in the solar energy sector mainly for providing the possible most effective operation of photovoltaics.

In addition to the use of forecasted global irradiance values coming from numerical weather prediction models, there have been developments to produce forecasted global radiation data by empirical models, but very few verification results have been published despite its crucial importance. An example for published results of verification of two empirical models is paper of Foyo-Moreno et al. (*Foyo-Moreno et al.*, 1990).

We have some previous experiences concerning verification of predicted solar radiation fluxes that comes from verification of predicted direct, global, and diffuse radiation fluxes of ALADIN model (*Tóth*, 2002), consequently it was approximately known what the expected strengths and weaknesses can be and where they are mainly found. AROME is a limited-area, high-resolution, non-hydrostatic, mesoscale weather forecast model. It has been developed since 2000 by coordination of MeteoFrance (*Seity et al.*, 2011; *Szintai et al.*, 2015). It contains 59 layers between the surface and the level of 2.7 hPa pressure, while its horizontal spatial resolution is 2.5 km. AROME is run eight times a day at the Hungarian Meteorological Service. It uses the radiative transfer model of the ECMWF. The quantitative background for it is given by both the model of Fouquart and Bonnel (*Fouquart and Bonnel*, 1980) for the short-wave range of the spectrum and the radiative transfer model RRTM for the long-wave range (*Mlawer et al.*, 1997) to produce radiation output quantities. Global radiation and short-wave net radiation are default output quantities of AROME, while some modifications in the code are needed to obtain predicted direct and diffuse radiation fluxes.

## 2. Data and method

### 2.1. Predicted data

Outputs from running of model AROME LAM and measured values from 21 selected stations of the global radiation monitoring network of the Hungarian Meteorological Service (OMSZ) were used for the verification. The study was performed both for daily and half-day (morning and afternoon) totals. The two half-days were separated at 12 h Central European Time (UT+1 h) instead of 12 h true time. It was reasonable, because the forecasted values were available

in UT that means mean time setting similarly to CET. It can result in negligible error in the half-day global radiation values due to equation of time is not significant in magnitude as compared with a half-day interval.

Since predicted global radiation values are not archived in the operational practice, the model was to run again separately for this study. It requires long computer time, and because the re-running could be performed only on the computer of the OMSZ on which the operational forecast is run, the verification could be performed for a limited temporal interval that means three months only.

Due to this obligate limitation, a simple pre-study has been made to select the sufficient months instead of consecutive months. The reason for it was to provide, on the one hand sufficient number of completely clear sky day for the study, on the other, to provide higher diversity of weather conditions: more variable and more stabil periods, more rainy and drier periods, periods being richer in thunderstorms, etc. Suitably-selected months can meet these requirements with far higher reliability than months selected without pre-determined criteria. Considering these facts, April, June, and August of 2013 have been selected for the study, so the re-running of AROME has been done for the months in question.

## *2.2. Measured data as reference values*

Global radiation monitoring network of the OMSZ consists of 40 stations using Kipp&Zonen pyranometers. Operational measurements at the OMSZ are carried out in ISO QA/QC system, so the suitable calibration of the radiometers and routine check of the measured values are continuously operationally provided according to the concerning working instructions of the OMSZ. This fact gives base to use measured data as reference for the verification without any separate study carried out to check reliability of measured data. Still, to obtain the possible highest quality results, and, in the same time, not to considerably enhance the number of data used, a 'sub-network' of stations were selected including approximately half of the total number of the stations. 19 stations have been selected for the study by a method that had developed to determine quantitatively the reliability of each station and so to keep the reliability of the global radiation network continuously on the possible highest level. *Table 1* shows the stations and their coordinates used for the study.

## *2.3. 'Goodness' of the forecast*

'Goodness' of the forecast was represented by the relative error of deviation of forecasted values from the measured value. Forecasted value valid for a given station was taken into consideration as it is usually estimated in the practice to minimize the uncertainty: it is that the forecasted value for a grid quadrat containing the given station is not the value itself forecasted for the given grid quadrat, but is the mean of the forecasted values for the neighboring grid quadrats. It was performed both for four neighboring quadrats and eight neighboring

quadrats, but goodness of the forecast did not show any increase in case of averaging from eight values, so four neighboring values were used for the study.

*Table 1.* Geographical coordinates of the stations used for the study

<b>Station</b>	<b><math>\varphi</math> (°)</b>	<b><math>\lambda</math> (°)</b>
Agárd	47.19	18.58
Budapest-Pestszentlőrinc	47.43	19.18
Debrecen	47.49	21.61
Eger	47.90	20.39
Győr-Likócs	47.71	17.67
Kecskemét K-Puszta	46.97	19.55
Keszthely	46.74	17.27
Kékestető	47.89	20.01
Kunmadaras	47.47	20.89
Nyíregyháza	47.96	21.89
Pápa	47.36	17.50
Pécs-Pogány	46.00	18.24
Püspökszilágy	47.73	19.31
Sopron-Fertőrákos	47.71	17.67
Szeged-külterület	46.26	20.09
Szentkirályszabadja	47.08	17.97
Szolnok	47.12	20.23
Szombathely	47.20	16.65
Tápiószele	47.36	19.89

The verification was performed for (i) all cases, for (ii) totally clear and (iii) overcast cases. To perform the verification for completely cloudless cases is important, because it represents 'purely' the radiative part of the forecast. Due to the very strong effect of cloudiness on the radiative transfer in the atmosphere, verification of the global radiation forecast of the model for cloudy cases becomes, actually, a kind of verification of cloudiness forecast and parametrization of cloud microphysics, except the slightly cloudy cases.

To categorize the cases, the so-called relative global radiation (RELG) was used. RELG for a certain time is defined as the ratio of measured value to the calculated possible maximum value for the time in question. The possible maximum value was taken into consideration as the highest value ever occurred

in a thirty year interval (1967–1996) of our global radiation database for the certain time that has been selected by a statistical method (Nagy, 2005). A study has been performed to obtain empirical relationship between RELG and cloudiness. Cloudiness values for the study have been taken from cloudiness observations operationally carried out in the Marcell György Main Observatory and from satellite cloud estimations performed operationally in the Unit of Remote Sensing of the OMSZ. The results have yielded the following values: RELG values higher than 0.85 correspond completely clear sky and RELG values lower than 0.25 correspond overcast cases, with high reliability. The verification thus was performed for those three RELG categories.

Simple relative error (RE) was used to represent goodness of the forecasted global radiation values, as it was mentioned above. RE was calculated in the usual way:

$$RE = \frac{G_{FOR} - G_M}{G_M} 100, \quad (1)$$

where  $RE$  is the relative error (%),  $G_{FOR}$  is the forecasted global radiation value in  $J/cm^2$ , and  $G_M$  is the measured global radiation value in  $J/cm^2$ .

Relative errors were categorized to intervals of 5%, and their relative frequencies were analyzed.

### 3. Relative error for all cases

#### 3.1. Daily totals

Results for daily totals can be seen in *Fig. 1*. Shape of the relative frequency for April and June is reasonably similar, but differs for August. It reflects the different weather situation in respect of solar radiation. The number at the upper right corner of the figures indicates the percentage rate of the cases when difference relative error was lower than 15% in absolute value. According to this indicator (that can be called as somewhat 'general monthly goodness', it is clear that the model performed, in general, most accurately for August (75.7%) and least accurately for June (68.6%). This behavior can be resulted in by the more frequent occurrence of cloudless or slightly cloudy cases and the small number of thunderstorm situations, while April characterized by very rapidly varying weather. Modality of the frequency distribution that can be produced from the frequencies is somewhat close to the Gaussian curve, but the number of extremely high overestimations (>50%) is big enough to deform it for each month. Assymetry is resulted in by the positive range (0–5 %) both for June and August, while for April it is caused by the negative range (–5–0%). As it is clear from *Fig. 1*, frequency of very high overestimations (>50%) almost equals

for June and August (5 and 6%, respectively), but considerably higher for April (10%). This phenomenon can be resulted in by the fact that the weather has higher and more rapid variability in April than in the other two months, and the model can track it with less reliability. It can seem to be a contradiction that the number of very high overestimation was lower in June, when the general goodness of the forecast was the lowest, than in April. The reason probably is that the model can predict the rainy and showery situations with a bit higher reliability than the rapidly and highly fluctuating ones.

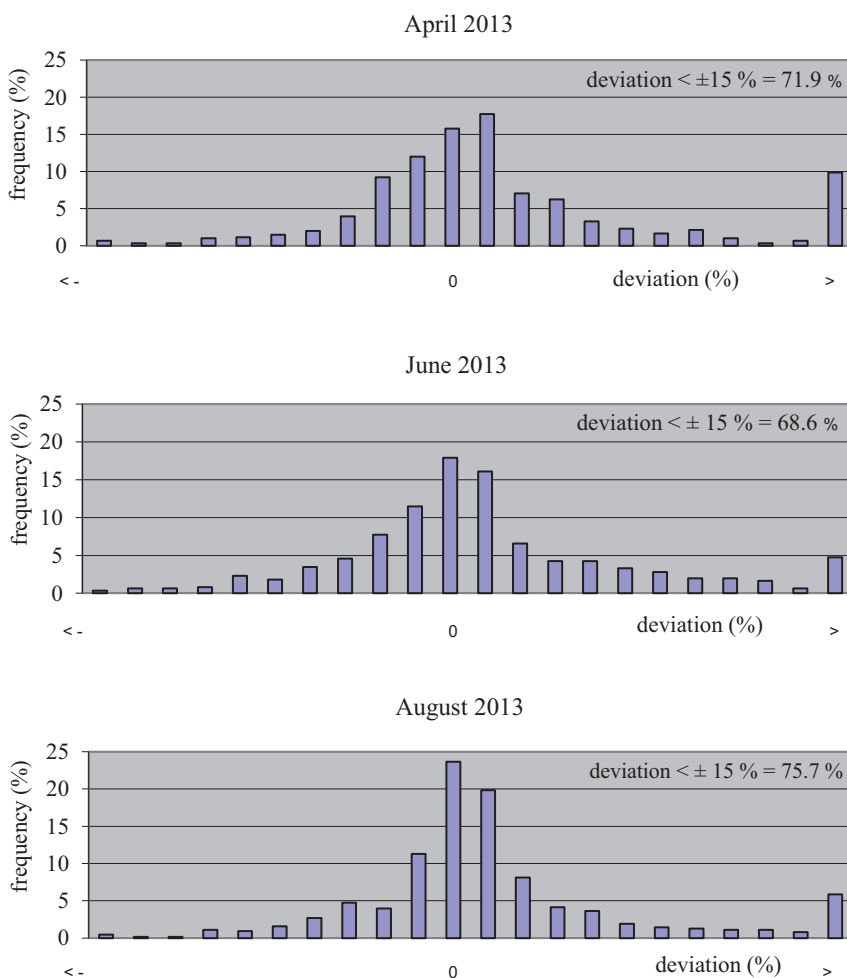


Fig. 1. Frequency of the relative error for daily totals

### 3.2. Half-day totals

Concerning first half-day (morning) totals, characteristics of the errors essentially similar to those obtained for the daily totals, as it can be seen in Fig. 2. April considerably differs from June and August in shape, and the goodness is highest for August (70.6%) and the lowest in June (65.5%). It is clear from the figure that frequency of cases when relative error was higher than 50 % was higher than in case of daily totals.

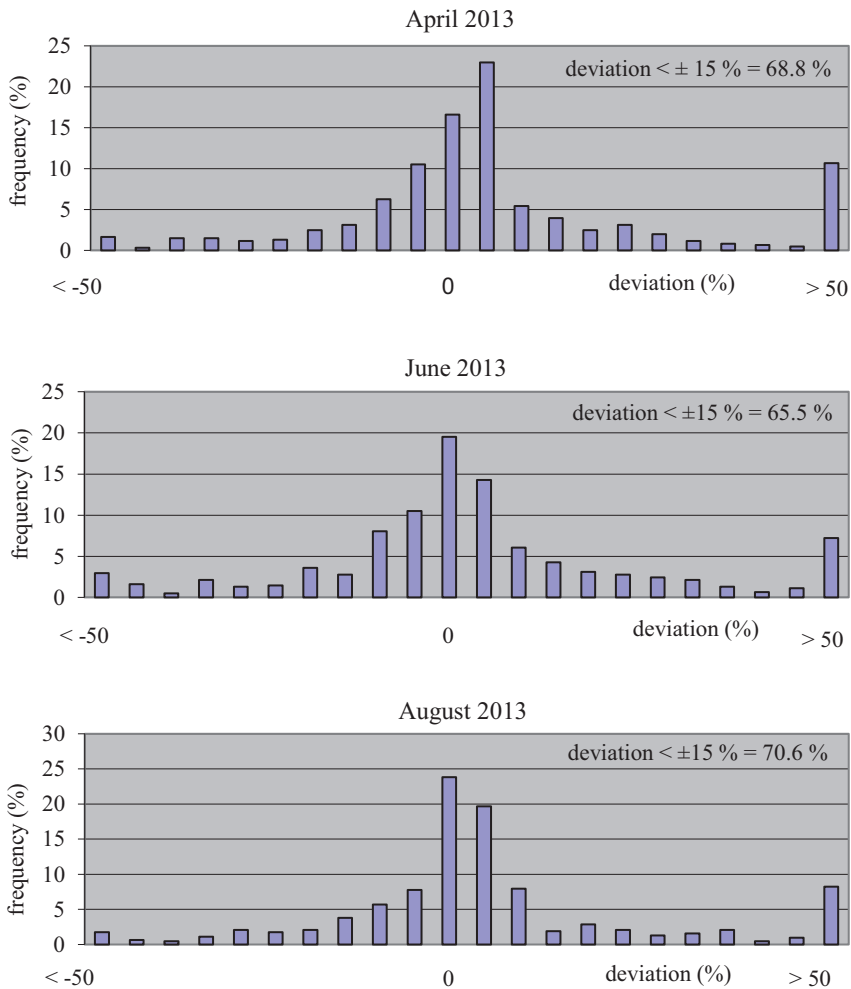


Fig. 2. Frequency of the relative error for first half-day totals

Accuracy of the forecasts was found to be the lowest for the second half-days (*Fig. 3*). Here the shape of the frequency distribution for April does not even approach the Gaussian function, unlike for June and August, and because the skewness is resulted in at the negative part of the  $x$  axis, an inclination for underestimation can be concluded. This effect is stronger for the second half-days, so it can be assumed that either the sky was less cloudy in reality than it has been forecasted or the radiation transmission of the realistic clouds has been higher than that of the model clouds. The general goodness indicator values are considerably lower than those for the first half-day totals for each months: it is 60.6 for April, as against the 68.8 for morning half day totals, and 58.0 for June (65.5 for morning). It is interesting that the two values completely equal for August (69.9). The difference between the goodness values for the two half-days for the corresponding months can be resulted in by the fact that the atmosphere is generally more instable in afternoon, but, at the same time, the differences seem to be too high to be explained solely by the different stability. One can assume that an effect of non-representative sampling can contribute to it: the number of days is presumably not sufficiently high to reduce the effect of special, uncharacteristic weather situations on the statistics, and involving more (at least three or four) of each month in the study can maybe decrease the difference in question.

The relative general stability of weather in August as compared with the two other months involved in this study can be the reason why no goodness difference between the two half-day for August was found.

Different behavior was found for the extremely high range (>50%) of errors. All of these very high errors are overestimations and their frequency is the same for both half-days for April and August, but, however, considerably differs for June: its value is between 7% and 8% for the first half-day totals, as against the value between 10% and 11% for the afternoon totals. It cannot be decided if either real atmospheric physical processes have resulted in these differences completely or also insufficient number of data contribute to the effect, as it was supposed in case of general goodness.

Based on the results shown above, it is, as a general rule, to be concluded that the model more poorly performs on shorter time scales.

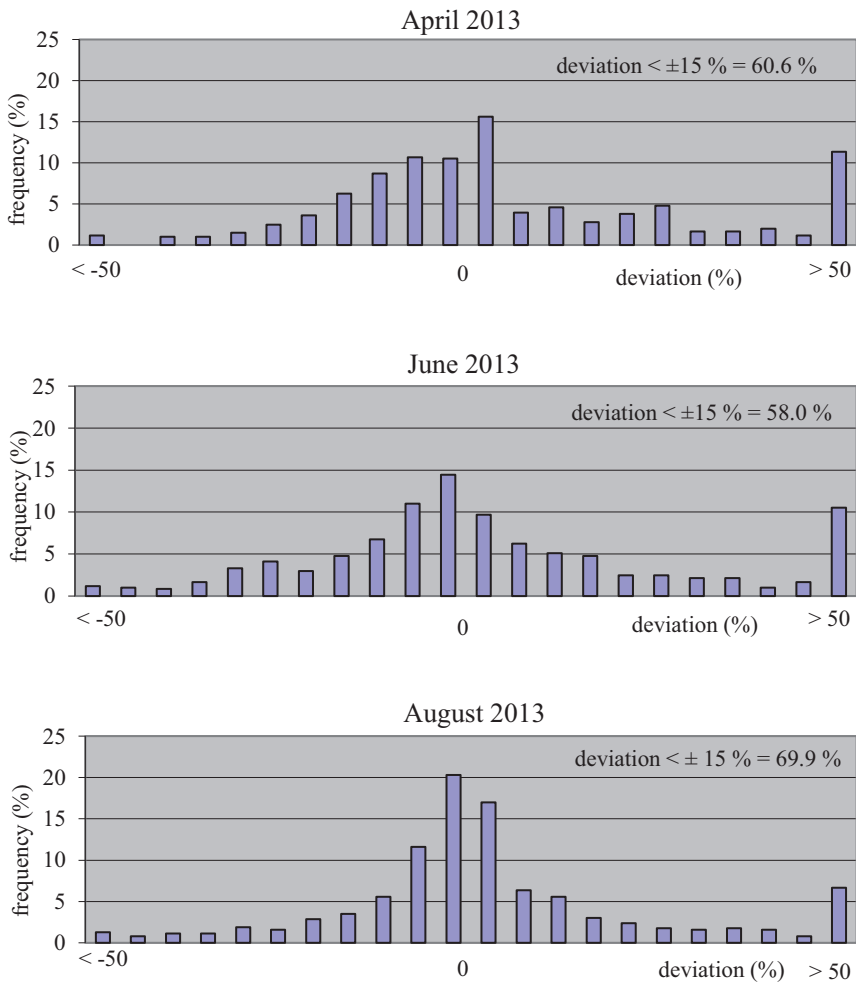


Fig. 3. Frequency of the relative error for second half-day totals

### 3.3. Cloudless and overcast cases

To know the goodness of the model for overcast cases ( $RELG < 0.25$ ) is of primary importance, because it is a well-known fact that the cloud forecast is one of the most unreliable part of the numerical forecast models due to that the basic energetics in cloud microphysics is not completely clear even theoretically. To study completely clear cases ( $RELG < 0.85$ ) is important for the reasons mentioned in Section 2. Results are shown for daily totals.

*Fig. 4a* shows the results of the study in question. As it has been expected, the model can accurately predict daily totals in cloudless cases as the relative error is lower than 5% in approximately half of all cases, and lower than 15% in almost 90% of all cases, with an error distribution approaching the Gaussian function well. The model, however, performs very poorly in overcast cases with a very special error distribution (*Fig. 4b*). Two peaks can be observed in the frequency distribution of error: one falls in one of the 'very good' range (between 0 and +5%) and the other is in the range of extremely high overestimations (> 50%) with a value of 30–30%, which means that errors fall in these two categories in 60 % of the cases. Relative error was lower than 15% in almost 40% of all cases, based on which, one could conclude that the model performs relatively well, if it would not higher than 50% in 30% of all cases. The error is distributed considerably uniformly in the whole error range. This behaviour means almost a two-state system: the forecast was either highly accurate or highly overestimated daily total. The reason supposed is that two types of cases dominates the producing conditions:

- (i) Cases when the sky is uniformly covered by non-fluctuating, permanent, thick cloudiness. In these cases, the global radiation can be precisely forecasted. This type of cloudiness generally exists for longer periods, so neither some temporal inaccuracy in the forecast can result in considerable error in most of the cases.
- (ii) To explain the very high frequency of extreme overestimations is difficult. However, due to the fact that frequency of extreme underestimation is very low, the reason can presumably be that the AROME clouds are more transparent than the realistic clouds in a considerable part of the cases. Considering the fact that these situations occurred at very low global radiation values, these magnitudes of errors do not mean inexplicably high inaccuracy.

Nevertheless, to find out the reasons more precisely, the study should be performed again for higher number of months.

Dependence of relative error on atmospheric radiation transmission were also studied, and the results are described and analyzed separately in Section 4.

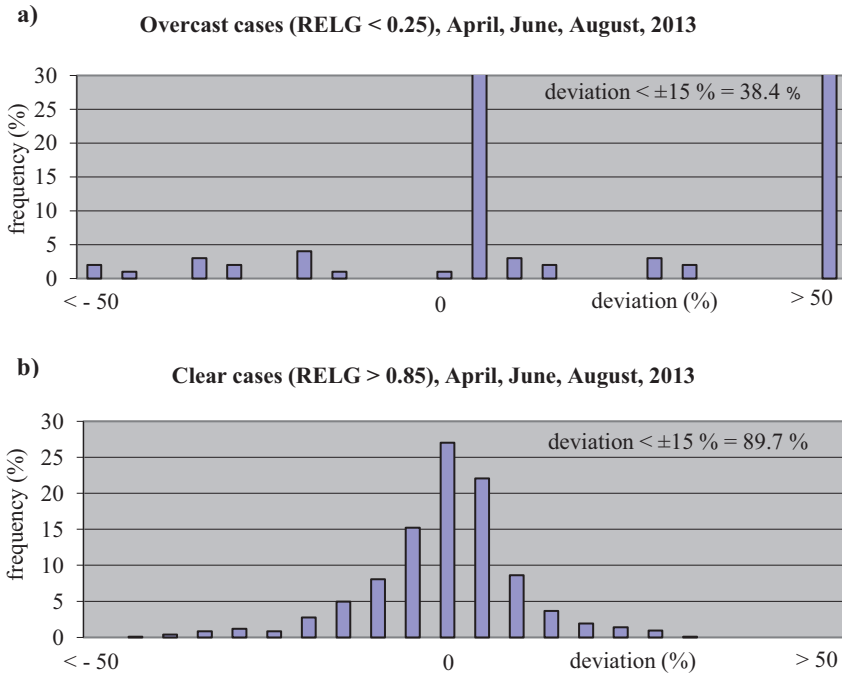


Fig. 4. Frequency of the relative error for daily totals

#### 4. Verification for cloudless cases – dependence of relative error on shortwave radiative transmission of the atmosphere

As it was mentioned in Section 2, it is important to know how accurately the model performs in cloudless cases for different radiative transfer situations, when the relatively high uncertainty of cloud forecast does not affect the modeled radiative transfer. Number of completely clear days was, unfortunately, very low, that means altogether a bit more than 20 on average, during the period studied. But less were suitable to use, because the days that were cloudless, but the model, however, has predicted them cloudy, were to be omitted. This has resulted in about 15–20% decreasing in number of days used. Due to low number of suitable days, to show all precise statistics is not reasonable, so main characteristics of forecast’s behavior are shown only.

Two types of studies were carried out. In the first segment, dependence of relative error on the shortwave radiation transmission was studied. As a second part, temporal course of the relative error was investigated.

To characterize radiative transmission of the air column at the time of the measurement, any optical depth-like quantity is the most suitable, because, due

to its physical definition, it indicates the radiative transmission conditions of any medium (like terrestrial atmosphere) more accurately than any other quantity that can be used for it (Smietana *et al.*, 1984; Tóth, 2008). In our study, aerosol optical depth (AOD), and graybody (broad band) optical depth (GBOD) were used for Budapest, and relative global radiation (RELG) was used for the other (countryside) stations where no spectrophotometric or pyrhelimetric measurements are carried out. Decision concerning in which case which quantity is to be used, depends on the measured quantities available, the effects to be traced, or circumstances affecting the results. Determination of AOD is well-known (Alföldy, 2007; Tóth, 2008, 2013), but, however, because GBOD is rather rarely-used quantity, its definition is shown in details in Section 4.1. It is to be noted that AOD for 500 nm is used for the study. Due to the inevitable high autocorrelation of the AOD values in one AOD spectrum, any AOD can be used without any selection effect, but 500 nm is the generally and widely used to characterize AOD in radiative transfer codes.

AOD is available from operational measurements with sunphotometer SP02 both in Marczell György Main Observatory in Budapest and in Kékestető station, and with sporadic checking measurements in cloudless days with LI-1800 spectroradiometer. In lack of pyrhelimetric and spectrophotometric measurements at the other stations, RELG was used for the other sites involved in the study to characterize atmospheric transparency.

#### 4.1. Determination of graybody (broad band) optical depth

GBOD is a very useful quantity to characterize the general shortwave radiation transmission of the atmosphere. Though it is in close relationship with AOD, they are different and the center of gravity of their sensitivity differs. While AOD is influenced by the absorption and scattering coefficient of aerosol, GBOD is influenced all absorption and scattering occurring in a very broad spectral range, practically in the sensitivity range of the pyrhelimeters. Thus, it gives the rate of spectrally-averaged radiation attenuation for the spectral range in question.

GBOD can be determined if definition of monochromatic optical depth is extended to a wider spectral range if irradiances measured at the surface are available (Tóth, 2008, 2013). Consequently, the GBOD will then be determined in the following way. If  $I_{\lambda_0}$  is the irradiance coming onto the top of the atmosphere at wavelength  $\lambda$  and  $I_{\lambda}$  is the irradiance measured at the surface by a pyrhelimeter in case of relative optical air mass  $m$ , then:

$$\int_{S_{PYR}} I_{\lambda} d\lambda = \left( \int_{S_{PYR}} I_{\lambda_0} d\lambda \right) e^{-m\delta_{GB}}, \quad (2)$$

where  $\delta_{GB}$  is the GBOD and  $S_{PYR}$  is the sensitivity range of the pyrhelimeter.

Thus, GBOD is given by the following equation if direct solar irradiance (denominator of the fractional) is measured:

$$\delta_{GB} = \frac{1}{m} \ln \frac{\int_{S_{PYR}} I_{\lambda_0} d\lambda}{\int_{S_{PYR}} I_{\lambda} d\lambda}. \quad (3)$$

It is clear that dependence of relative error on both optical depths is reasonable to study. To know dependence on AOD is reasonable, because AROME uses AOD in its radiative transfer code, while to know dependence on GBOD is important due to the fact that the verified forecasted quantity is global radiation which is influenced by every circumstance affecting radiative transfer and fine structure of the spectrum, namely each gaseous absorption, aerosol extinction, Rayleigh scattering, etc.

## 4.2. Dependence of relative error on atmospheric transparency

### 4.2.1. Dependence on GBOD and AOD

Results are shown and discussed for daily values only, because in this case there is no real importance to analyze them for the both half-days, too. However, the results are shown and discussed both for Budapest and Kékestető separately, because the latter is a mountain station where model outputs can behave in different way as they do for stations close to the sea level.

*Figs. 5 and 6* show the dependence of the relative error of the forecast on daily mean GBOD for Budapest and Kékestető, respectively. It can be seen in case of both stations, that the model tends to overestimate with higher probability with the increasing GBOD (decreasing atmospheric transparency). This dependence is more stressed and has higher correlation for Kékestető. This means that the model cannot simulate the more extreme radiative transmission situation sufficiently precisely, namely it smooths and averages: it tends to underestimate the incoming radiation in case of extremely transparent (least polluted) cases, while tends to overestimate it in the less transparent (highly polluted) cases. This phenomenon was found for the other stations where RELG was used to characterize transparency of the atmosphere, as it can be seen in *Fig. 9* and discussed in 4.2.2.

During the three months of the present study, forecasted AOD field was not applied in AROME, but an AOD climatology only: it means that monthly AOD fields were used as input AOD field.

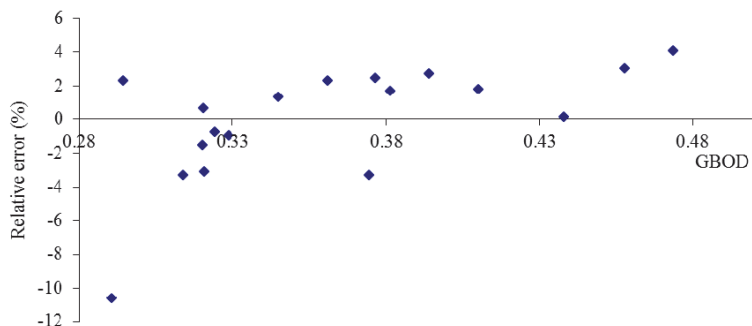


Fig. 5. Dependence of relative error on daily mean GBOD for Budapest

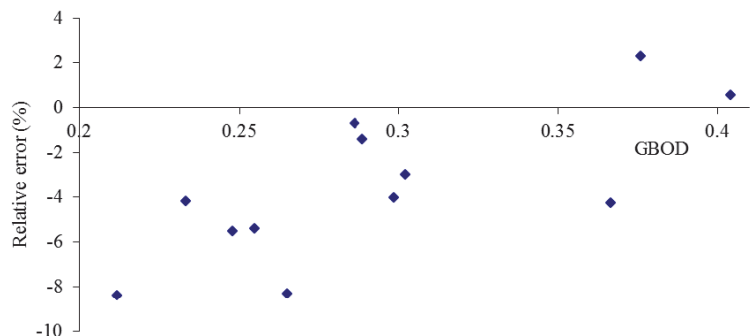


Fig. 6. Dependence of the relative error on daily mean GBOD for Kékestető

Dependence of the relative error of the forecast on daily mean AOD is shown in *Figs. 7 and 8* for Budapest and Kékestető. The relationship differs only a bit from those found for the dependence on GBOD. The correlation is a bit lower here that can be resulted in, on the one hand, by the less number of days used for the study, on the other hand, by the fact that global radiation is a broad spectral band quantity, so its given value that can be measured at the surface at a moment depends on several factors, and aerosol amount is only one of them. The averaging of the model can also be observed for the AOD dependence as it was found for the GBOD dependence. This fact suggests that the model would underestimate global radiation for the very clear cases and would overestimate it for the most polluted cases even in the case when predicted AOD field would be set, but expectably the 'averaging' would be more moderate.

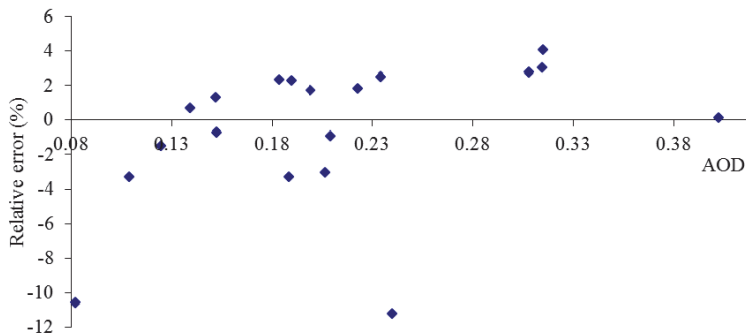


Fig. 7. Dependence of the relative error on daily mean AOD at 500 nm for Budapest

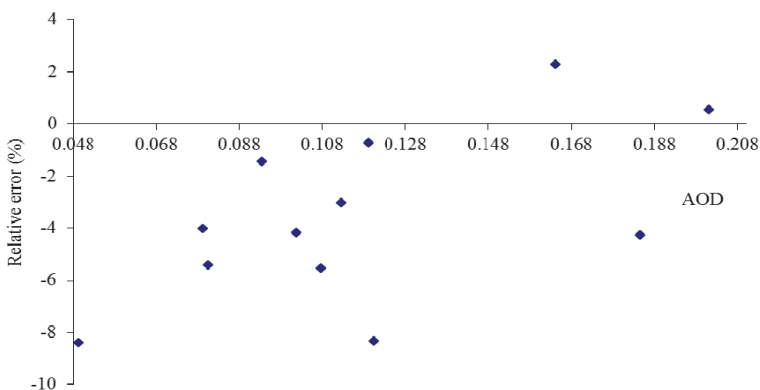


Fig. 8. Dependence of the relative error on daily mean AOD at 500 nm for Kékestető

#### 4.2.2. Dependence on RELG

As it was noted above, RELG was used to characterize atmospheric transparency for the stations where only global radiation is measured and there is no possibility to estimate optical depths.

The result of the study performed for these stations is not shown station-by-station, because it has no high significance and only small differences were found for the different stations. The main shape of the relationship can be seen well if dots obtained for all stations and for all days are shown in one figure (Fig. 9). The pattern is similar to those found for Budapest and Kékestető: the

model tends to underestimate better and better as RELG increases, namely atmospheric transparency increases.

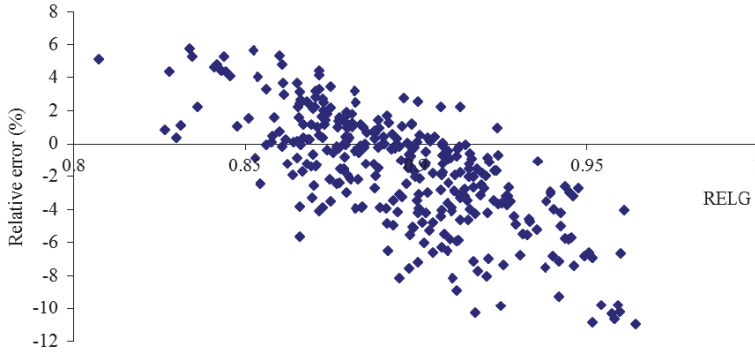


*Fig. 9.* Dependence of the relative error on RELG for all other stations where no spectrophotometric or pyrhelometric measurements are carried out

It can be concluded that the underestimation is typical in general. Because there is necessarily relatively good relationship between RELG and the two optical depth parameters, calculated AOD (AODC) and calculated GBOD (GBODC) can be produced by performing regressions for the two relationships in question. In this way, the dependence of relative errors on atmospheric transparency for the countryside stations, where AOD and GBOD values are not available, can be quantitatively compared with those for Budapest and Kékestető. The correlation coefficient for the relationship with GBODC is higher than that for relationship with AODC due to the different effect of the two optical depths on atmospheric transparency discussed above.

Considering the dependence of relative errors on AODC and GBODC for the countryside stations, this study shows that underestimation characterized the countryside stations, but its measure is lower than its measure for Kékestető. The fact, that overestimation is typical for Budapest, lower underestimation is typical for the countryside stations, and higher underestimation is characteristic for Kékestető, confirms that the model can describe the transparency with decreasing reliability towards the extremes, and it would behave in the same way, though expectably in a lower measure, in case when forecasted AOD field would be applied in the model.

### 4.3. Temporal course of the relative error

Temporal course of error of the forecasted values was also studied. Because data from only three months were available, yearly course could not be produced, while simple comparison of the three months was performed. It was found that standard deviation of the relative error was considerably different for the three months involved in the study for all three time scales. For daily totals, it was the highest for April (3.81), and was the lowest for June (2.58). Its value for August was 3.08. The effect is the same for both half-days, but with different values as it can be seen in *Table 2*. It is to be noted that the standard deviations are considerably higher for the afternoon totals. This can probably be resulted by the convection-caused reliability decrease of the model discussed above.

*Table 2.* Standard deviation of the relative error for the different months

	<b>Apr</b>	<b>Jun</b>	<b>Aug</b>
Daily totals	3.81	2.58	3.08
First half-day totals	3.53	2.20	2.34
Second half-day totals	4.46	3.63	3.98

### 4.4. Areal dependence of the relative error

Areal dependence of the relationship between the relative error of forecasted values and RELG was also investigated. It was performed in the way that, on the one hand, areal dependence of average and standard deviation of the set of dots calculated for the given stations was studied, on the other hand, areal dependence of parameters of linear fitting for the relationship between relative error of forecast and RELG was studied. No significant dependence was found for both daily and half-day totals.

## 5. Conclusions

### 5.1. General conclusions:

- (i) The model performs well both in clear and not highly clouded situations. Relative error is lower than 15% in 89.7% of the completely clear cases, while in 38.4% of the cloudy cases. Its goodness decreases as cloudiness increases.
- (ii) The goodness decreases with decreasing time scale.

### 5.2. Daily totals:

- (i) No difference was found between the results obtained by using methods of 4 neighboring grids and 8 neighboring grids.
- (ii) The model is the most accurate for August and the least accurate for June. The reason can be that more stable situations characterize August, while June is considerably variable, thunderstorms and precipitations can occur more frequently that can result in rapid alternation of clearer and more cloudy skies. April is generally very variable, but thunderstorms can occur very rarely and conditions with very high cloudiness can occur not so frequently.
- (iii) Extremely high overestimations can occur most frequently in April. It can be resulted in by the fact that the unexpected situations are the most frequent in that month.
- (iv) Parameterization of cloud microphysics and thunderstorms is not sufficiently accurate in the model.

### 5.3. Half-day totals:

- (i) Accuracy of the global radiation forecast is a bit lower than in case of the daily totals.
- (ii) The forecast is the most reliable for August and the least reliable for June. The reasons should be the same like those for the daily totals.
- (iii) The model performs significantly better for the first half-day than for afternoon. The reason can be that convection appears and increases in the afternoons and the model cannot describe it sufficiently precisely.
- (iv) Underestimation is the most characteristic for April, and is more stressed for the second half-day than for the first half-day.

The reasons can be as follows: (a) Certain physical processes showing seasonality and being characteristic for April are over-represented in the model that results in clouds in AROME that have higher extinction than realistic clouds have. (b) Effect of convection-caused mixing on radiative transfer is over-represented, and consequently, the AROME clouds appearing in the afternoon have higher optical depth than real ones have.

### 5.4. Dependence of the relative error on the radiative transmission of the atmosphere

- (i) Relationship between relative error and atmospheric transparency has higher correlation for GBOD than for AOD. The reason should be that global radiation is a broad spectral band quantity, so its any given value that can be measured at the surface at a moment depends on several factors, and aerosol amount is only one of them.

- (ii) Reliability decreases at the extreme ends of the radiative transmission scale: it underestimates the global irradiance in the extremely clear cases and overestimates it in the extremely polluted situations. One of the reasons is that the model did not use real AOD during the three months studied, but used AOD climatology varying on monthly base. However, this error should, in some measure, remain in the case of using forecasted AOD field, because dependence of the relative error on the atmospheric radiative transmission was found for GBOD also, which is formed by the forecasted composition of the atmosphere.

#### 5.5. *Temporal course and areal dependence of the relative error*

- (i) Though three months are not sufficient to study seasonality, it is clear that considerable difference can be observed for those months, however, it cannot be ascertained if there is any regularity in the yearly course.
- (ii) Standard deviations of relative error are typically the highest for April, which suggests that the model smooths: it describes the higher variability with less reliability.
- (iii) Concerning daily and afternoon totals, lowest standard deviations are found for June. It is surprising at first, but it can result in by the fact that despite June is characterized by frequently cloudy and rainy cases, the circumstances have been considerably similar for clear cases.
- (iv) Concerning areal dependence of the relative error, no significant dependence was found for both daily and half-day totals.

#### 5.6. *Comparison of dependence of relative error on transparency for countryside measuring sites with those for Budapest and Kékestető*

Concerning dependence of relative error on atmospheric transparency (indicated by calculated optical depth from relative global radiation) for the countryside measuring sites, it can be established that countryside stations are characterized by underestimation as it was found for Kékestető, but in a lower measure. Knowing that countryside stations, considering pollution circumstances, should fall statistically somewhere between Budapest and Kékestető, it should mean that the model pull the extremes towards the average situations. Consequently, applying forecasted AOD field instead of the monthly-based AOD climatology that has been used during the time of the study, would solve the problem of transparency-dependent reliability only partly.

## 6. Possible future studies

Though several basic properties of the forecast were studied in details, and the used three month were carefully selected by preconception set by reasonable and practical respects, a possible yearly course was not to detect. To ascertain if there is seasonality in the goodness of the forecast, at least twelve months would be needed for the study. However, because it can occur that weather circumstances of some months considerably differ from the usual behavior characterizing the certain months, rather three complete years would be preferred for a study.

To know sufficiently deeply the behavior of predicted global irradiance fluxes and to ascertain the reasons causing variability of its reliability, verification of direct and diffuse irradiances would be also very useful in the future.

As the results show, relative error of the forecast depends on the atmospheric transparency, and that dependence differs a bit for the two optical depths used to indicate transparency, as it can be expected due to the facts discussed above. Recently, developments are in progress to produce predicted AOD field. When it will be applied in the operational use in the future, it would expectably improve the ability of the model to produce more realistic values for both most polluted and least polluted 'end' of the transparency scale in clear sky cases. It means that repeating the study is worth in the future for this reason also.

## References

- Alföldy B., Osán, J., Tóth, Z., Török, Sz., Harbusch, A., Jahn, C., Emeis, S. and Schäfer, K., 2007: Aerosol optical depth, aerosol composition and air pollution during summer and winter conditions in Budapest. *Sci. Total Environ.* 383, 141–163.
- Fouquart, Y. and B. Bonnel, 1980: Computations of solar heating of the earth's atmosphere: A new parameterization. *Beitr. Phys. Atmos.* 53, 35–62.
- Foyo-Moreno, I., Y. Castro-Diez, F.J. Olmo and J.I. Jimenez, 1990: Verification of two models to predict global radiation on a horizontal surface. *Solar Wind Techn.* 7, 707–711.
- Mlawer, E.J., S.J. Taubman, P. Brown, M.J. Iacono, and S.A. Clough, 1997: Radiative transfer for inhomogeneous atmospheres: RRTM, a validated correlated-k model for the longwave. *J. Geophys. Res.* 102, 663–682.
- Nagy, Z., 2005: Budapest globálsugárzási adatai. *Léggör* 50 (4), 2-7. (in Hungarian)
- Seity, Y., P. Brousseau, S. Malardel, G. Hello, P. Benard, F. Bouttier, C. Lac, and V. Masson, 2011: The AROME-France convective-scale operational model. *Mon. Weather Rev.* 139, 976–991.
- Smietana, Jr. P.J., Flocchini, R.G., Kennedy, R.L. and Hatfield, J.L., 1984: Comparison of diffuse global ratios calculated from one-minute, hourly and daily solar radiation data. *Solar Energy* 32, 417–423.
- Szintai B., Szűcs M., Randriamampianina R., and Kullmann L., 2015: Application of the AROME non-hydrostatic model at the Hungarian Meteorological Service: physical parametrizations and ensemble forecasting. *Időjárás* 119, 241–265.
- Tóth, Z., 2002: Verification of surface solar radiation fluxes predicted by ALADIN. *ALADIN Newsletter* 21, 80–92.
- Tóth, Z., 2008: Long-term variation of atmospheric shortwave radiation transmission above Budapest, Hungary. Proceedings of the 4th International Conference on Solar Radiation & Daylighting SOLARIS 2008 (Hong Kong, China), 27–35.
- Tóth, Z., 2013: High resolution solar spectrophotometry and narrow range solar radiation measurements at the Hungarian Meteorological Service. *Időjárás* 117, 403–433.

## INSTRUCTIONS TO AUTHORS OF *IDŐJÁRÁS*

The purpose of the journal is to publish papers in any field of meteorology and atmosphere related scientific areas. These may be

- research papers on new results of scientific investigations,
- critical review articles summarizing the current state of art of a certain topic,
- short contributions dealing with a particular question.

Some issues contain “News” and “Book review”, therefore, such contributions are also welcome. The papers must be in American English and should be checked by a native speaker if necessary.

Authors are requested to send their manuscripts to

*Editor-in Chief of IDŐJÁRÁS*  
P.O. Box 38, H-1525 Budapest, Hungary  
E-mail: [journal.idojaras@met.hu](mailto:journal.idojaras@met.hu)

including all illustrations. MS Word format is preferred in electronic submission. Papers will then be reviewed normally by two independent referees, who remain unidentified for the author(s). The Editor-in-Chief will inform the author(s) whether or not the paper is acceptable for publication, and what modifications, if any, are necessary.

Please, follow the order given below when typing manuscripts.

*Title page:* should consist of the title, the name(s) of the author(s), their affiliation(s) including full postal and e-mail address(es). In case of more than one author, the corresponding author must be identified.

*Abstract:* should contain the purpose, the applied data and methods as well as the basic conclusion(s) of the paper.

*Key-words:* must be included (from 5 to 10) to help to classify the topic.

*Text:* has to be typed in single spacing on an A4 size paper using 14 pt Times New Roman font if possible. Use of S.I.

units are expected, and the use of negative exponent is preferred to fractional sign. Mathematical formulae are expected to be as simple as possible and numbered in parentheses at the right margin.

All publications cited in the text should be presented in the *list of references*, arranged in alphabetical order. For an article: name(s) of author(s) in Italics, year, title of article, name of journal, volume, number (the latter two in Italics) and pages. E.g., *Nathan, K.K., 1986: A note on the relationship between photo-synthetically active radiation and cloud amount. Időjárás 90, 10-13.* For a book: name(s) of author(s), year, title of the book (all in Italics except the year), publisher and place of publication. E.g., *Junge, C.E., 1963: Air Chemistry and Radioactivity.* Academic Press, New York and London. Reference in the text should contain the name(s) of the author(s) in Italics and year of publication. E.g., in the case of one author: *Miller (1989)*; in the case of two authors: *Gamov and Cleveland (1973)*; and if there are more than two authors: *Smith et al. (1990)*. If the name of the author cannot be fitted into the text: (*Miller, 1989*); etc. When referring papers published in the same year by the same author, letters a, b, c, etc. should follow the year of publication.

*Tables* should be marked by Arabic numbers and printed in separate sheets with their numbers and legends given below them. Avoid too lengthy or complicated tables, or tables duplicating results given in other form in the manuscript (e.g., graphs).

*Figures* should also be marked with Arabic numbers and printed in black and white or color (under special arrangement) in separate sheets with their numbers and captions given below them. JPG, TIF, GIF, BMP or PNG formats should be used for electronic artwork submission.

*More information* for authors is available: [journal.idojaras@met.hu](mailto:journal.idojaras@met.hu)

Published by the Hungarian Meteorological Service

---

Budapest, Hungary

**INDEX 26 361**

**HU ISSN 0324-6329**